8-2021

Analysis of Large Embankment Dam in Case of Rapid Drawdown and Earthquake Aftershock

Pothikul Vivithkeyoonvong
Utah State University

ANALYSIS OF LARGE EMBANKMENT DAM IN CASE OF RAPID DRAWDOWN AND EARTHQUAKE AFTERSHOCK

by

Pothikul Vivithkeyoonvong

A thesis submitted in partial fulfillment
of the requirements for the degree

of

MASTER OF SCIENCE

in

Civil and Environmental Engineering

Approved:

_____	_____
James Bay, Ph.D. Major Professor	John Rice, Ph.D. Committee Member
_____	_____
Brian Crookston, Ph.D. Committee Member	D. Richard Cutler, Ph.D. Interim Vice Provost of Graduate Studies

UTAH STATE UNIVERSITY
Logan, Utah

2021

ABSTRACT

Analysis of Large Embankment Dam in Case of Rapid Drawdown and Earthquake Aftershock

by

Pothikul Vivithkeyoonvong, Master of Science

Utah State University, 2021

Major Professor: Dr. James A. Bay
Department: Civil and Environmental Engineering

Dams and reservoirs are important as a source of freshwater as well as for regulating flooding and producing hydroelectricity. The same as with any other manmade structure, dams need to monitored and maintained to prevent disastrous failure.

One of the events that can reduce the stability of an embankment dam is rapid drawdown. Rapid drawdown is when the water level decreases at such a rapid rate that the dam material(s) cannot drain and adjust to the equilibrium in time. Without the buttressing effect of the water, the upstream slope of the dam becomes less stable. Another threat to dam stability is earthquake shakings. Strong seismic events can cause damage to dams and appurtenant structures.

The main objective of this thesis is to analyze the stability of large embankment dam in the event of rapid drawdown and aftershock loading at the same time. The slope

stability analysis is run in the program GeoStudio 2020. Sirikit Dam is used for the analyses. The dam geometry and materials properties used are a combination of existing data, reasonable estimation, Stark and Hussain's (2013) empirical correlation for drained fully softened secant friction angle, and engineering judgment.

The method for analyzing slope stability during rapid drawdown in this research is the multi-stage rapid drawdown analysis proposed by Duncan, Wright, and Wong (1990).

Seismicity data for the two active faults in the area are from a U.S. Geological Survey report, Thailand's Department of Mineral Resources, and Thailand's Meteorological Department. Maximum moment magnitude of each earthquake source is estimated from these data. Using Bath's Law, the largest aftershock magnitude is estimated. Maximum peak ground acceleration (PGA) is estimated from the NGA-West2 ground motion prediction equations (GMPEs) model. Horizontal seismic coefficients (k_h) are determined from PGA and applied in the SLOPE/W slope analysis in GeoStudio.

The results of this study show that this mode of failure should be considered for embankment dams. The analyses results shows that Sirikit Dam outperforms the required factors of safety in the largest possible event of rapid drawdown and aftershock. This method of analysis can be extended to other embankment dams. Further research could estimate the probability of this event.

(119 pages)

PUBLIC ABSTRACT

Analysis of Large Embankment Dam in Case of Rapid Drawdown and Earthquake Aftershock

Pothikul Vivithkeyoonvong

Dams and reservoirs are important as a source of freshwater as well as for regulating flooding and producing hydroelectricity. The same as with any other manmade structure, dams need to monitored and maintained to prevent disastrous failure.

One of the events that can reduce the stability of an embankment dam is rapid drawdown. Rapid drawdown is when the water level decreases at such a rapid rate that the dam material(s) cannot drain and adjust to the change in time. Without the buttressing effect of the water, the upstream slope of the dam becomes less stable. Another threat to dam stability is earthquake shakings. Strong seismic event can cause damage to dams and appurtenant structures.

The analysis is run in the program GeoStudio 2020 using existing data, reasonable estimation, well-accepted theories, and engineering judgment.

The results of this study show that this mode of failure should be considered for embankment dams. The analyses results shows that Sirikit Dam outperforms the required factors of safety in the largest possible event of rapid drawdown and aftershock. This method of analysis can be extended to other embankment dams. Further research could estimate the probability of this event.

ACKNOWLEDGMENTS

I would like to thank Dr. James Bay for his guidance and support throughout my course of study and this research. Furthermore, I am deeply thankful for Dr. Bay for looking out for me outside of class, especially when the pandemic made already stressful graduate student life even harder. I would like to express my gratitude to my committee members, Dr. John Rice and Dr. Brian Crookston for their insights. I would like to thank Dr. Loren Anderson for sharing his expertise.

I would like to thank Ariel Blair for always providing solutions for my problems. I would like to express my appreciation to my classmate and office mates that not only helping me with my study but also being a delightful part of my college life. I would like to thank USU's Counseling and Psychological Services (CAPS) for providing mental wellness resources and helping combat my imposter's syndrome and anxiety.

I would like to thank Electricity Authority of Thailand (EGAT) for sponsoring me. I am thankful for the Civil Maintenance Division and its officers that provide their information and knowledge for this research.

Lastly, I would like to thank my family and friends in Thailand who may not be with me in person but provide continuous support and encouragement throughout the process. I would like to thank the Universe for always having my back and guiding me in the right direction.

Pothikul Vivithkeyoonvong

Disclaimer

The purpose of this research was to assess the viability of a dam failure mode involving the combination of rapid drawdown and seismic loading due to an earthquake aftershock, and to determine methods and procedures to evaluate this failure mode. The analyses required to assess this failure mode were performed on Sirikit (SRK) Dam. To perform these analyses, we relied on data and material properties developed and published by others, that we could not verify. Furthermore, there is no record of other material properties required for these analyses. Lacking actual measurements of material properties, reasonable assumptions were made, that would be consistent with typical properties of materials used in a well-constructed earth dam.

While this research did not raise any concerns about the safety of SRK Dam, it should not be construed as being specific to SRK Dam. Applying these analyses to SRK Dam, or any other dam would require a laboratory and field investigation of geometry and material properties of that specific dam. Lacking these investigations, this research should be viewed a general evaluation of the failure mode, and the development of procedures to evaluate the failure mode.

CONTENTS

Page

LIST OF TABLES

Page

LIST OF FIGURES

Page

CHAPTER 1

INTRODUCTION

Dams and reservoirs play a vital role in providing usable water for humanity. They regulate flooding, can be used for recreation, and produce clean hydroelectric power. A dam is a manmade structure that needs to be designed, built, and maintained thoroughly as the failure of a dam can cause major loss of life and property damage.

One phenomenon that can threaten the stability of a dam is rapid drawdown. This occurs when the water level on the upstream face of a dam decreases at such a rate that the dam's fine-grained materials do not have enough time to drain and adjust. Without the buttressing effect of the water, the upstream slope becomes less stable. Rapid drawdown may lead to slope failure, which may develop into dam breach.

Another threat to a dam's stability is earthquake shakings. Earthquakes can cause such damage to a dam as cracks, crest settlement, and slope failure. They can lead to overtopping or internal erosion that develops into a dam breach. Earthquakes may cause seiches and large waves in the reservoir that may overtop the dam. Damage to a water-releasing structure such as a spillway, river outlet, or penstock can impede controlled water release and may lead to overtopping.

An aftershock is a smaller earthquake that follows the larger main shock. An aftershock that follows a large earthquake can be quite large itself and may cause more damage to the already weakened structures. If a reservoir were to being drawn down

after exhibiting damage from a main shock, it is very likely that it would also experience aftershocks.

Rapid drawdown and aftershocks may seem unrelated. However, under certain circumstances, they may contribute to a dam breach. One possible sequence starts when a large earthquake occurs and causes consequential damage to a fine-grained embankment dam. The dam operators, in an attempt to lessen the load on the dam, may decide to draw down the reservoir. As a result, the upstream slope will be in a rapid-drawdown condition. An aftershock may occur within that time period and may cause slope failure, which in turn may lead to dam breach. This sequence is shown in Fig 1.1.

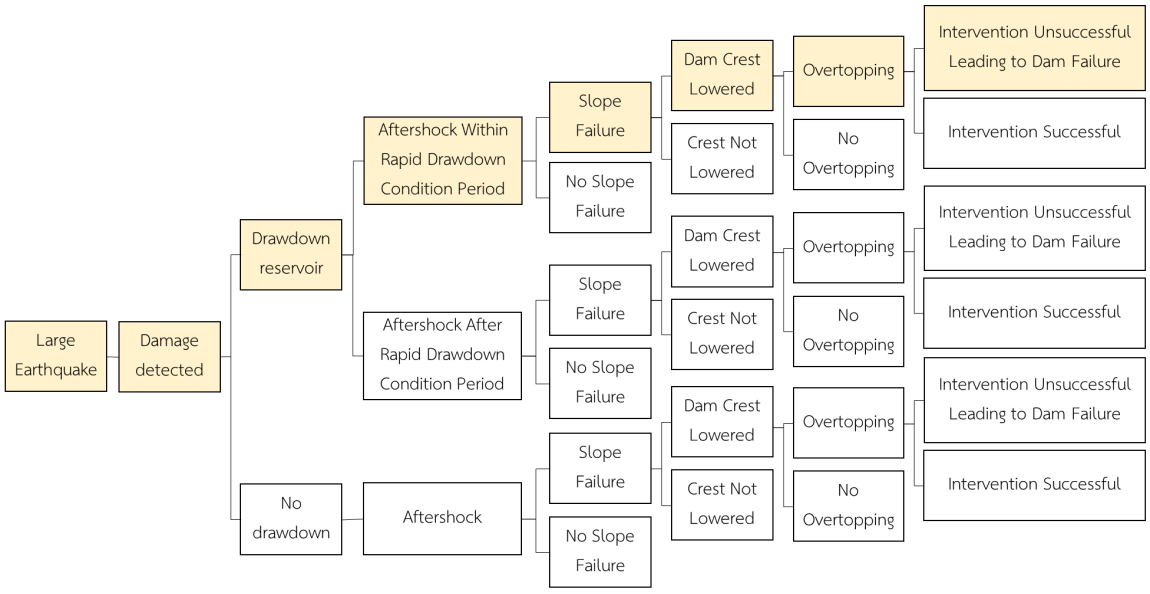

Fig. 1.1 Simplified event tree for possible dam breach event due to rapid drawdown and aftershock loading.

This research investigates the failure mode of rapid drawdown with earthquake aftershocks, leading to a dam breach. The Dam used in the analyses is Sirikit Dam (SRK

Dam). SRK Dam is a 113.6 m tall earth dam located in Uttaradit Province, Thailand. Its large reservoir and powerhouse have a vital role in providing fresh water, preventing flooding, and generating electricity for the northern region of Thailand. There are two known active faults located within a 200 km radius of the dam.

SRK Dam has a very large reservoir and thus cannot be drawn down very rapidly. It is also in a region with moderate seismicity. To make this research applicable to other dams, the analyses include larger drawdown rates and larger earthquake aftershocks than SRK Dam could experience.

The objectives of this research are as follows:

- To identify if this new mode of failure should be included in risk assessment for embankment dams.
- To analyze the stability of SRK Dam in the event of rapid drawdown coupled with aftershock loading.
- To determine whether to modify the current large earthquake emergency plan.

To perform this research, SRK Dam is modeled in GeoStudio 2020. The initial water level is at normal full pool for the reservoir (+162m MSL). The embankment material properties are determined from existing data, literature, and engineering judgment. The two analyses in GeoStudio are SEEP/W and SLOPE/W. SEEP/W analyzes the steady-state seepage conditions for a water level from +162m MSL to +112m MSL at 5m intervals. The levels of drawdown in meters are 0, 5, 10, 15, 20, 25, 30, 35, 40, 45, and 50. These levels include the practical and impractical drawdown for SRK Dam.

SLOPE/W uses the pore water pressure condition from SEEP/W analyses and various seismic coefficients to determine the critical factor of safety for each scenario. From then on, scenarios with practical drawdown levels and aftershock seismic coefficients are analyzed to determine if the factors of safety meet the minimum requirement.

This thesis consists of five chapters. Chapter 1 is the research introduction of the subject and objectives. Chapter 2 presents a summary of literature materials relevant to understanding and selecting suitable data and parameters in soil strengths, rapid drawdown analysis, seismic hazard analysis, and aftershocks. Chapter 3 is a description of data used in the analysis of SRK Dam in case of rapid drawdown and aftershock loading. Chapter 4 describes the development of SRK Dam model in the GeoStudio program. Chapter 5 discusses the analysis procedure and presents the results. Lastly, Chapter 6 contains the summary and conclusions of this research.

CHAPTER 2

LITERATURE REVIEW

2.1 Introduction

Although there is extensive research on the topic of rapid drawdown and seismic loading on dams, there is little research that include the two events happening simultaneously. The effects both phenomena have on slope stability are still little known.

The following topics are related to strength parameters for an existing dam, rapid drawdown, ground motion prediction, and aftershocks.

2.2 Fully Softened Shear Strength

2.2.1 Stress-Strain Behavior in Fine-Grained Soils

Overconsolidated and compacted clays have brittle stress-strain characteristics. After the peak in the stress-strain curve has been reached, the shearing resistance of the brittle soils decrease with further strain. Skempton (1977) concluded that overconsolidated clays undergo a softening process which results in the fully softened strength and not the peak shear strength of the intact or unsoftened overconsolidated clay. Fully softened strengths are used for slopes that have not undergone previous sliding (first-time slides).

The source of the fully softened strength of fine-grained soil is achieved when clay structure is destroyed during straining. With further strain, clay particles align with the failure surface forming slickensides, and strength is further reduced to a residual shear strength. Both fully softened and residual shear strength depend on mineral composition, which is related to plasticity and grain-size characteristics.

Fully softened strength is numerically equivalent to the drained peak strength of a normally consolidated specimen given that there is no preexisting slickensided failure surface as shown in Fig. 2.1. It corresponds with the back-calculated strengths of first-time slides. Once a failure has occurred and a continuous slickensided failure surface has developed, only the residual shear strength is available to resist sliding.

This type of stress-strain behavior makes progressive failure possible, and makes it impossible to mobilize the peak strength simultaneously at all points around a potential shear surface.

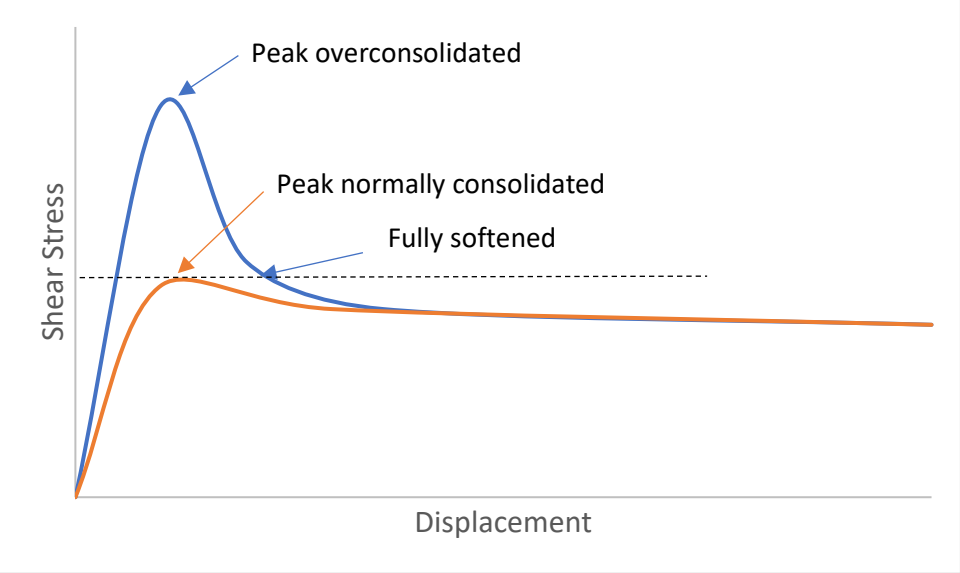

Fig. 2.1 Shear strengths of fine-grained soil.

2.2.2 Progressive Failure

Duncan, Wright, and Brandon (2014)

Progressive failure is an effect of soil brittleness. Field observations indicate that the fully softened strength can be mobilized around excavations in fissured clays and compacted clay embankments subjected to cycles of desiccation and weathering.

A non-uniform ratio of stress to strength along the potential slip surface results in different points reaching the peak strength and fully softened strength at different times. Duncan et al. (2014) stated that in the case of excavated slopes in overconsolidated clay and shales, particularly stiff-fissured clays and shales, there is a strong possibility of progressive failure. Immediately after excavation of the slope (at time t_1), only the stresses at point A might have reached the peak of the stress-displacement curve as shown in Fig. 2.2. The slope would rebound into the cut as a result of delayed response to the unloading from the excavation, and possibly also due to swelling of the clay as its water content increases following the reduction in stress.

With time (t_2), the displacements at A, B, and C would all be larger. The shear stress at point A would decrease as it moves beyond the peak, and the shear stresses at points B and C would move toward the peak.

At some later time (t_3), the shear stress at point B would also pass the peak and decrease the average shear strength. Through this process, progressively, failure would spread around the slip surface, without ever mobilizing the peak shear strength simultaneously at all points along the slip surface.

In conclusion, it would be an overestimation to assume that the entire slope is at peak strength when mobilized. Therefore, in slope stability analysis where slickensides have not developed, fully softened strength is used to model progressive failure.

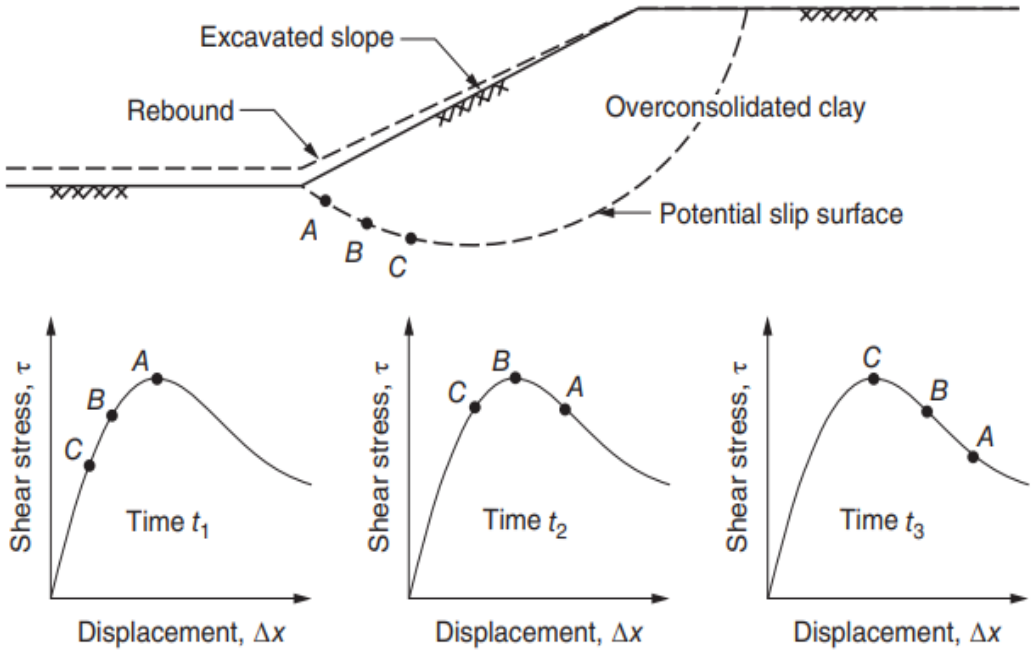

Fig 2.2. Mechanism of progressive failure on an excavated slope in overconsolidated clay (Duncan et al. 2014).

2.2.3 Drained Fully Softened Friction Angle for Fine-Grained Soil

Stark and Hussain (2013)

The fully softened strength of fine-grained soil corresponds to a random arrangement of clay particles and is stress dependent. Therefore, an empirical correlation incorporating effective normal stress (σ'_n), liquid limit (LL), and clay fraction (CF) provides a good estimate of the friction angles. These empirical correlations were

developed using torsional ring shear test results and verified using back-analysis of landslide case histories.

Stark and Hussain (2013) stated that the empirical correlation for drained fully softened secant friction angle requires only LL and CF to estimate the drained ϕ'_{fs}. Thus, the fully softened strength correlation suggested by Stark, Choi, and McCone (2005) provides a reliable estimate of ϕ'_{fs} for use in preliminary design, verification of laboratory test results, and confirmation of back analysis of first-time slides.

The fully softened strength empirical correlation uses three different CF groups (CF ≤ 20%, 25% ≤ CF ≤ 45%, and CF ≤ 50%) and accounts for the effect of CF and σ'_n on ϕ'_{fs} values, as shown in Fig. 2.3.

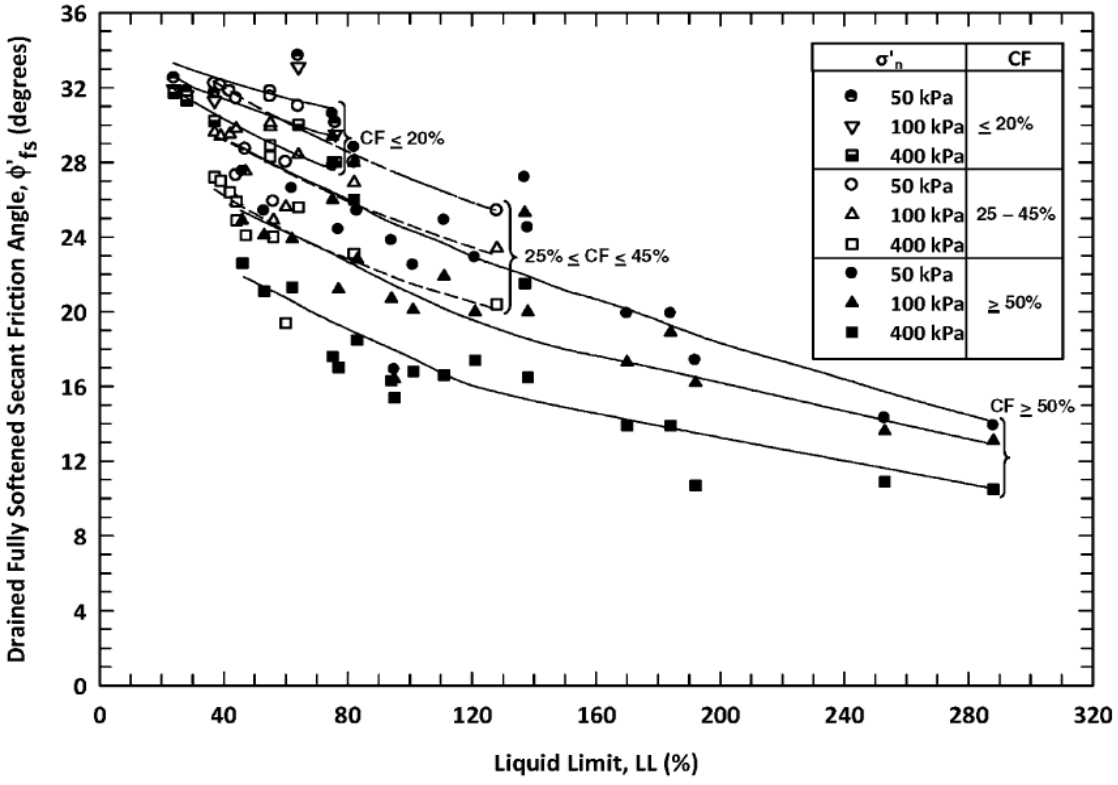

Fig 2.3 Empirical correlation for drained fully softened secant friction angle based on LL, CF, and σ'_n for 39 natural soils (Stark and Hussain 2013).

The current study suggests a separate mathematical expression for each trend line of the correlation in Fig. 2.3 that can be used to estimate values of ϕ'_{fs} and a stress-dependent strength envelope using values of LL and CF measured using disaggregated samples.

2.2.4 Effective Cohesion

The fully softened shear strength corresponds to the drained peak strength of a normally consolidated specimen, and this suggests that the value of effective stress cohesion (c') should be set to zero, i.e., the value of cohesion measured in shear tests on normally consolidated clay (Holtz et al. 2013; Terzaghi et al. 1996) for the analysis of first-time slides in overconsolidated clays. This is important because even small values of c' can result in significant differences in calculated factors of safety, especially in shallow slides, such as levee or embankment slopes. However, back-analysis of first-time slides in London clay indicates that small values of c', approximately 0.96 kPa (20 psf), can be mobilized (Chandler and Skempton 1974). Skempton (1977) also suggested a c' of 0.96 kPa (20 psf) and a ϕ'_{fs} of 20 degrees for London clay. Mesri and Abdel-Ghaffar (1993) back-analyzed 45 case histories and concluded that c' can range from zero to 24 kPa. In summary, the fully softened value of cohesion should be zero unless back-analysis of local case histories suggests a value greater than zero.

2.3 Slope Stability During Rapid Drawdown

The upstream slope stability of an embankment dam or a levee is influenced by water pressure. The water has a buttressing effect that increases the stability of the upstream slope. If the water level drops at such a rapid rate that the pore pressures within the slope do not have enough time to adjust in equilibrium with the drop in external water level, the slope becomes less stable (Duncan et al. 1990). Rapid drawdown failure can and does happen on river bank slopes and other slopes subject to submersion.

Rapid drawdown is frequently the design condition that controls the steepness of the upstream slopes of dams. Factors of safety for this condition vary from case to case. For dams with an extremely large storage capacity, rapid drawdown from a high reservoir level is an improbable event. Therefore, the factor of safety for the rapid drawdown condition may be lower. On the other hand, pumped-storage reservoirs experience drastic water level changes as a regular operating condition. Therefore, they require a higher factor of safety for the drawdown condition. The minimum required factor of safety for rapid drawdown from USACE Slope Stability manual (2003a) is 1.1–1.3.

The permeability of the embankment material dictates the rate at which an embankment will drain. The higher the permeability, the faster the material drains. In some cases, it may be difficult to decisively determine if the material will drain or not. Thus, it must be assumed that drainage will or will not occur, whichever will result in the lower shear strength within the particular zone, and the lowest factor of safety for the slope (Duncan et al. 1990).

There are a number of methods for analyzing slope stability during rapid drawdown. These include the effective stress method, the Corps of Engineers method (U.S. Army 2003), and the Lowe and Karafiath method. In 1990, Duncan, Wright, and Wong proposed the "multi-stage rapid drawdown analysis," also known as "staged undrained strength," that combines the best features of previous methods. The three steps are as follows:

1. Determine whether drainage will occur during rapid drawdown. This must be performed for every soil layer in the cross-section. The dimensionless time factor T is estimated by the following equation:

$$T = c_v t / D^2 \qquad \text{(Eq. 2.1)}$$

where c_v = coefficient of consolidation, t = time for drawdown, and D (or H) = length of drainage path.

Values of c_v can be calculated using data for the time rate of consolidation during consolidation tests. Approximate values for various types of compacted soils are listed in table 2.1.

If the calculated value of T is equal to or greater than 0.848, the dissipation of excess pore pressures during drawdown will be 90 percent or more, and it is reasonable to consider the material fully drained. If the value of T is less than 0.848, undrained strength should be considered. The following steps assure that the undrained strength used in the stability analyses will not be larger than the drained strength. If there is doubt whether or not complete drainage will occur, the material should be assumed to be undrained.

2. Establish the strength envelopes required for the analyses. If the materials drain during drawdown, only the drained strength envelope is required. If low-permeability materials are undrained during drawdown, both the drained envelope and the undrained envelope from an isotopically consolidated CU test are required. The required envelopes for values of K_c between 1.0 and K_f can be determined by linear interpolation.

   K_c is the effective principal stress ratio during consolidation, $\sigma'_{1c}/\sigma'_{3c}$. In the earlier rapid drawdown method presented by Lowe and Karafiath in 1960, the undrained stress of soils, when plotted as τ_{ff} vs σ'_{fc} , varies with K_c. The value of this ratio can vary from unity (for consolidation under isotropic stresses) to K_f, the value $\sigma'_{1c}/\sigma'_{3c}$ at failure. For any material there is a family of undrained strength envelopes corresponding to different values of K_c varying from 1.0 to K_f. This multistage analysis uses this τ_{ff} vs. σ'_{fc} envelope as shown in Fig. 2.4.

Table 2.1 Approximate value of c_v for various soils (after Duncan et al.,1990).

Type of Soil	Values of c_v	
	ft^2/day	m^2/day
Coarse sand	>10,000	> 929
Fine sand	100 to 10,000	9.3 to 929
Silty sand	10 to 1000	0.93 to 92.9
Silt	0.5 to 100	4.6×10^{-2} to 9.3
Compacted clay	0.05 to 5	4.6×10^{-3} to 0.46
Soft clay	< 0.2	$< 1.86 \times 10^{-2}$

3. Calculate the factor of safety after drawdown for a slip surface using a 3-step procedure:

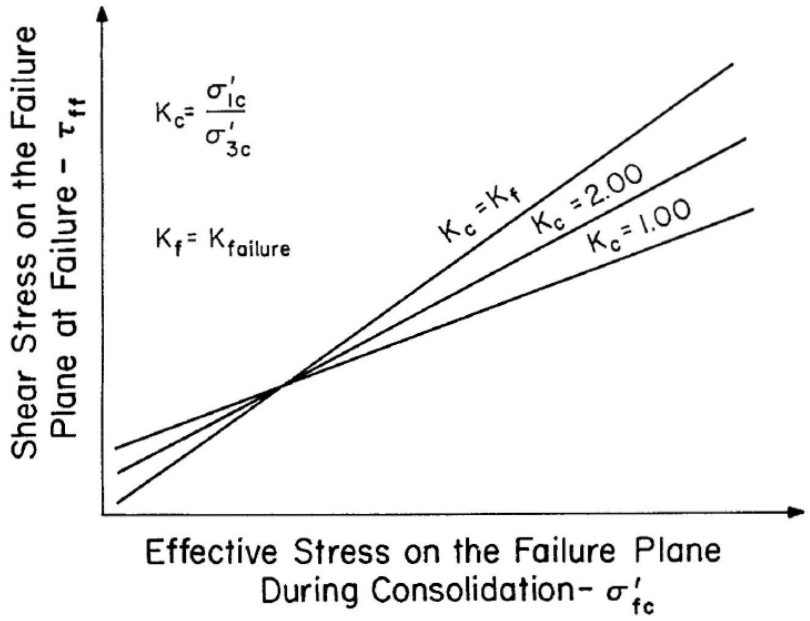

Fig. 2.4 Undrained strength envelope (Duncan et al. 1990).

i. Perform a stability analysis before drawdown using drained strength parameters for all materials in the slope. The pore-water pressure condition uses the piezometric line before drawdown. This step is to determine the effective normal stress (σ'_{fc}) and shear stress (τ_{ff}) on the base of each slice and the value of K_c for each slice.

ii. Perform an analysis of stability after drawdown using piezometric line after drawdown as pore-water pressure condition. For materials that drain during drawdown, use effective strength parameters. For materials that do not drain freely, use the interpolated strengths determined in stage i.

iii. Compute drained strength for all slices along the slip surface using the effective normal stress from stage ii and the effective strength

parameters. For materials that do not drain freely, compute the undrained strength at the base of the slice and compare with the drained strength. Choose the smaller strength to compute factor of safety.

4. Repeat the 3-step procedure for other slip surfaces to locate the critical slip surface (the one with the lowest factor of safety) following drawdown.

2.4 Ground Motion Prediction

The Pacific Earthquake Engineering Research Center (PEER), in collaboration with international multidisciplinary experts, has developed the "Next Generation of Ground-Motion Attenuation Models" (NGA, also known as NGA-West1) project. The main objective is to develop ground-motion prediction relations for shallow crustal earthquakes in the western United States and similar active tectonic regions. Five teams of experts developed the ground motion prediction equations (GMPEs) to be used in earthquake hazard analysis at the global and regional levels (Power 2019). The developer teams are as follows:

- Abrahamson, Silva, and Kamai (ASK)
- Boore, Stewart, Seyhan, and Atkinson (BSSA)
- Campbell and Bozorgnia (CB)
- Chiou and Youngs (CY)
- Idriss (I)

These teams worked independently on their models but had frequent interactions. NGA-West2 is the follow-up project which is the current version.

Ground Motion Prediction Equations (GMPEs), or “attenuation” relationships, provide a means of predicting the level of ground shaking and its associated uncertainty at any given site or location, based on an earthquake magnitude, source-to-site distance, local soil conditions, fault mechanism, etc. GMPEs are efficiently used to estimate ground motions for use in both deterministic and probabilistic seismic hazard analyses.

Bozorgnia et al., 2014

The NGA-West2 database includes 21,332 (mostly) three-component recordings, after excluding the recordings with missing important metadata (like magnitude) and/or missing ground motion data (like PGA). The database includes a moment magnitude range of 3.0 to 7.9. The range of distances from the recording site to the rupture plane is from 0.05 to 1533 km. However, the database is well populated up to around the 400 km range.

The horizontal GMPEs address: horizontal components of peak ground acceleration (PGA), peak ground velocity (PGV), and pseudo-absolute response spectral acceleration (PSA) for at least 21 oscillator periods (T) ranging from 0.01 to 10 s. The general applicable limits of the NGA-West2 GMPEs are: $M \leq 8.5$ for strikeslip faults, $M \leq 8.0$ for reverse faults, and $M \leq 7.5$ for normal faults; and rupture distance, R_{RUP}, or Joyner and Boore distance, R_{JB}, ranging from 0 to 300 km.

The NGA-West1 and NGA-West2 spectral acceleration ground motion models were developed for a reference damping ratio of 5%. As part of the NGA-West2 project, PEER researchers developed a new damping model that can be used to adjust the 5%

damped GMPEs for damping values ranging from 0.5% to 30%. The new damping model was developed directly from the NGA-West2 database and is independent of any specific GMPE.

NGA-West2 GMPEs include terms for local site amplification, and all five NGA-West2 GMPEs use the average shear-wave velocity in the upper 30 m of sediments, V_{S30}, as the site parameter.

Additionally, there are a number of supporting research projects assisting in defining and constraining the GMPEs. The NGA database and models are updated and adjust when new data is available.

Models of the NGA research programs are adopted by the earthquake community in a wide spectrum of application such as: (1) site-specific seismic analysis and design of structures and facilities; (2) development of regional seismic hazard maps for use in building codes, financial estimation, etc.; and (3) social and financial loss estimation.

2.5 Deterministic Seismic Hazard Analysis

Kramer (1996)

Deterministic seismic hazard analysis (DSHA) is a four-step seismic hazard evaluation at a particular site. The steps can be simply described as follows:

1. Identify all earthquake sources capable of producing significant ground motion at the site. Characterize their geometry and earthquake potential.

2. Select a distance parameter from source to site for each source zone. Typically, the shortest distance is selected. It can be the distance from the earthquake epicenter or hypocenter.
3. Select the earthquake expected to produce the largest level of shaking at the site (the controlling earthquake). The selection is made by comparing the levels of shaking caused by the earthquake potential from step 1 occurring at the distance of step 2.
4. Define the hazard at the site, normally in terms of the ground motion parameters of the controlling earthquake. Peak acceleration, peak velocity, and response spectrum ordinates are commonly used to characterize the seismic hazard.

This procedure does not provide information on the likelihood of occurrence. DSHA is a worst-case-scenario evaluation. However, it is still a suitable hazard analysis for critical structure such as large dams which may cause disastrous consequences upon failure.

2.6 Aftershock Magnitude

Båth, 1965

Båth's law states that for shallow shocks, there is a finite difference between the magnitude of the earthquake main shock (M) and the largest aftershock (M_1). The difference is 1.2 and it is independent of magnitude. Båth's law can be expressed as follows:

$$M - M_1 = 1.2 \quad \text{(Eq. 2.2)}$$

The magnitudes are based on the surface wave scale. Equation 2.2 implies that the seismic energy of the main shock is on average about 53 times as large as the energy of the largest aftershock. Båth stated that there are exceptions to this law but it still has a remarkable range of validity nonetheless.

Båth (1965) presents one example of an aftershock sequence that did not strictly follow Båth's law was that of the 8.5 Alaska earthquake in March 28, 1964. There was no definitive largest aftershock, but there were five shocks within the range of 6.5–6.8 magnitude. Together these five shocks yielded the same energy as one shock of magnitude 7.2 would do. If this is taken to be the largest aftershock (M_1), 8.5 – 7.2 = 1.3, in close agreement with Båth's law. Assuming that similar circumstances hold in the case of several equally large main shocks, Båth presented the energy–magnitude relation as follows:

$$M - M_1 = 1.2 + \frac{\log\left(\frac{N_1}{N}\right)}{1.2} \quad \text{(Eq. 2.3)}$$

where N = number of equally large main shocks, N_1 = number of largest aftershocks, and the logarithm is to base 10.

Båth also suggested that the depth of focal depth can affect the largest aftershock magnitude. The difference between the main shock and the largest aftershock increases with increasing focal point which can be express as follows:

$$M - M_1 = \frac{2}{3}h + 1 \quad \text{(Eq. 2.4)}$$

Where h = focal depth in units of 100 km. However, Båth stated that little data existed from deeper aftershock sequences to test and it would need more investigation.

There have been more studies on the variability of the difference between the main shock and the largest aftershock, as well as earthquakes and aftershocks data that show differences slightly less than 1.2. Shcherbakov and Turcotte (2005) proposed a modified version of Båth's law based on an extrapolation of the Gutenberg-Richter statistics. From their study, the scatter in the modified Båth's law is less than the scatter in the original Båth's Law.

CHAPTER 3

DATA DESCRIPTION

3.1 SRK Dam

3.1.1 SRK Dam General Characteristics

Sirikit Dam or SRK Dam is the largest zoned earth dam in Thailand. It is located in Tha Pla District, Uttaradit Province. SRK Dam was constructed as a part of the Development of the Nan River Basin Project to prevent flooding in the southern area of Uttaradit Province. Previously known as the Phasom Dam, SRK Dam was buit by the Royal Irrigation Department. Construction started in 1963 and was completed in 1972, while the construction of Sirikit Hydropower Plant by the Electricity Generating Authority of Thailand (EGAT) started in 1968 and was completed in 1972.

SRK Dam construction project comprises the main embankment dam and eight saddle dams. The main dam height is 113.60 m. The crest level is at +169 m above mean sea level (MSL) without camber. The crest is 810 m in length and 12 m in width. The maximum width at the base of the dam is 630 m. SRK Dam is an earth dam with an impervious clay core, filter drain, and riprap covering part of the upstream slope.

On the upstream side, the slope from elevation +60 to +120 m MSL is 1:3 and the slope from elevation +120 to crest is 1:2.5. On the downstream side, the slope from elevation +60 to +150 m MSL is 1:2.5 and the slope from elevation +150 to crest is

1:2.25 as shown in Fig 3.1 from the Royal Irrigation Department (RID) *Sirikit Dam Report* (1975).

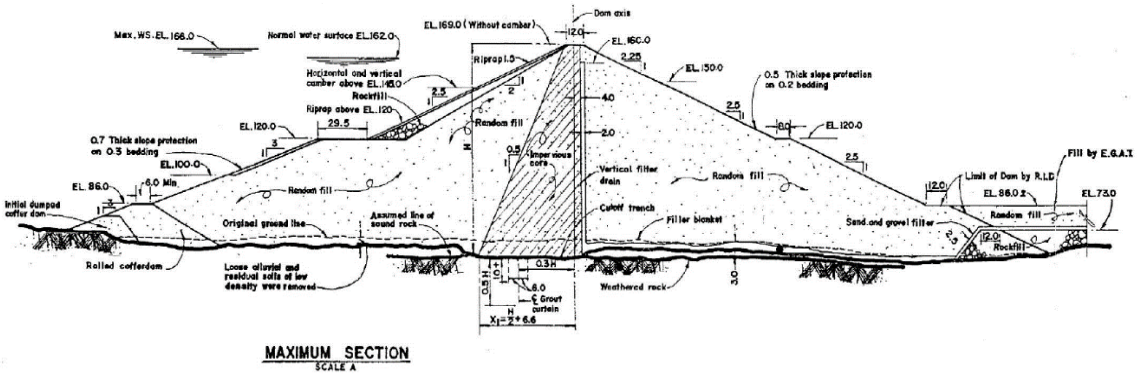

Fig 3.1 Maximum section of SRK Dam (Royal Irrigation Department 1975).

Eight saddle dams (or dikes) located 20 km northeast of the main dam have a total length of 5.3 km. The crest is 8 m wide and the dams' lengths range from 40 to 1,450 m. The crest level is at +168 m MSL except Dike 2 which stands at +169 m MSL. The heights of the dikes vary from 1 to 30 m. On the upstream side, the slope from elevation crest to +160 m MSL is 1:2 and the slope below elevation +160 m MSL is 1:3. Downstream slope is 1:2. Dike 2 is the only one with an irrigation outlet. The typical as-built section of saddle dams is shown in Fig. 3.2.

Fig. 3.3 and 3.4 show a plan view of SRK Dam and saddle dams.

The catchment area of the reservoir is 13,130 km^2 with a length of 129 km. The normal retention level is at +162 m MSL. Maximum retention level is at +166 m MSL. Tailrace water level is at +76 m MSL. Total storage capacity is 9,510 million m^3. Dead

storage capacity is 4,819 million m^3. Average annual inflow (for 10 years return period) is 2,850 million m^3. Average annual loss is 342.20 million m^3.

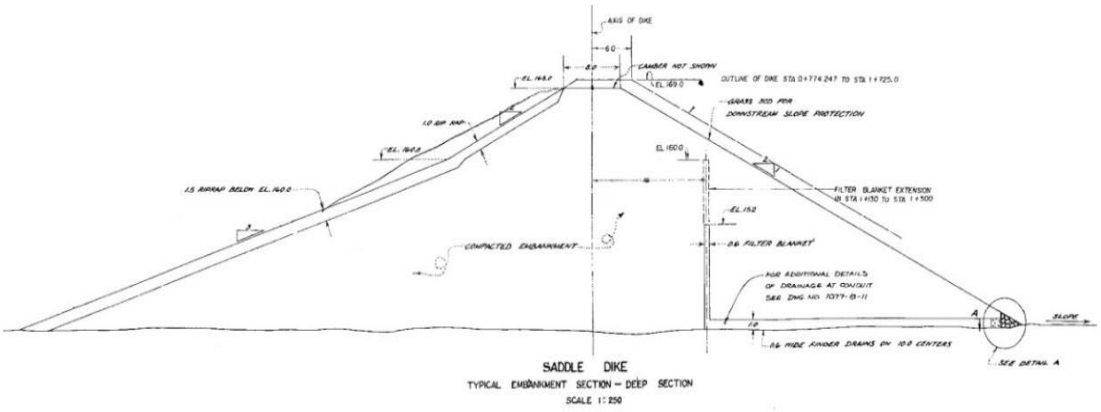

Fig. 3.2 Typical as-built section of a saddle dam (Royal Irrigation Department 1975).

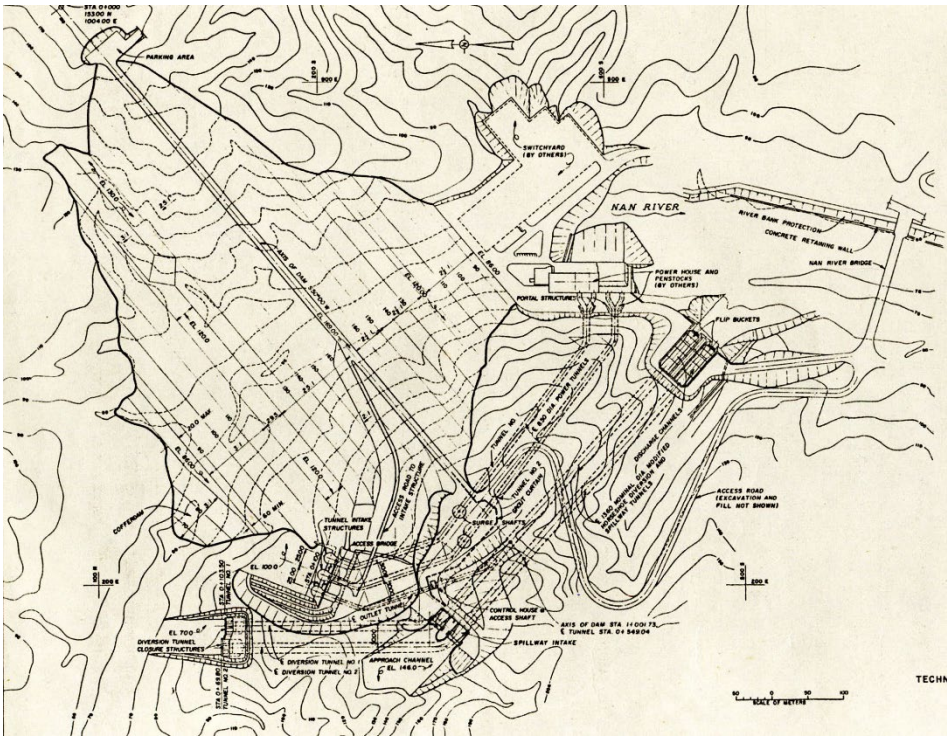

Fig. 3.3 Plan view of SRK Dam (Royal Irrigation Department 1975).

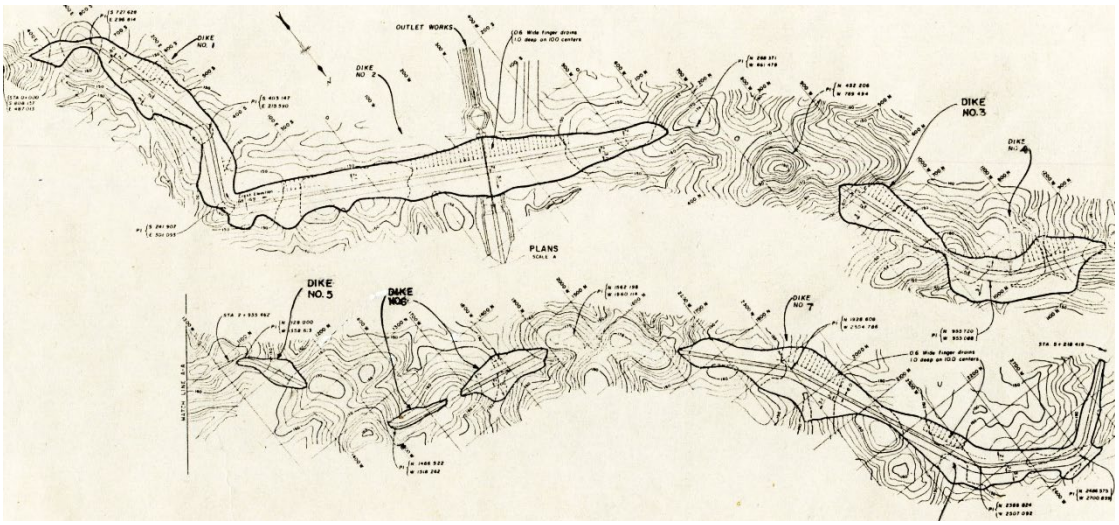

Fig 3.4 Plan view of saddle dams (Royal Irrigation Department 1975).

SRK Dam has three water-releasing structures: river outlet, penstocks (release through turbines to produce electricity in the power plant), and spillway, with maximum releasing capacity of 400 cubic meters per second (CMS), 732 CMS, and 3,250 CMS respectively.

3.1.2 Site Geology

3.1.2.1 Main Dam

Geologically the main dam site consists of metamorphic rocks from the Silurian-Devonian Period. The dam's foundation is mostly made of quartz-mica schist, talcose schist, and graphitic schist. Originally, the geological profile consisted of an about 1 m thick residual soil layer followed by a weathered rock layer and a strong fresh rock layer. The rocks are highly fractured in a mostly even pattern throughout the site.

A fault zone consisting of clay and crushed rock was found at station 0+600 m as shown in Fig. 3.5. There was no evidence to indicate that it was an active fault.

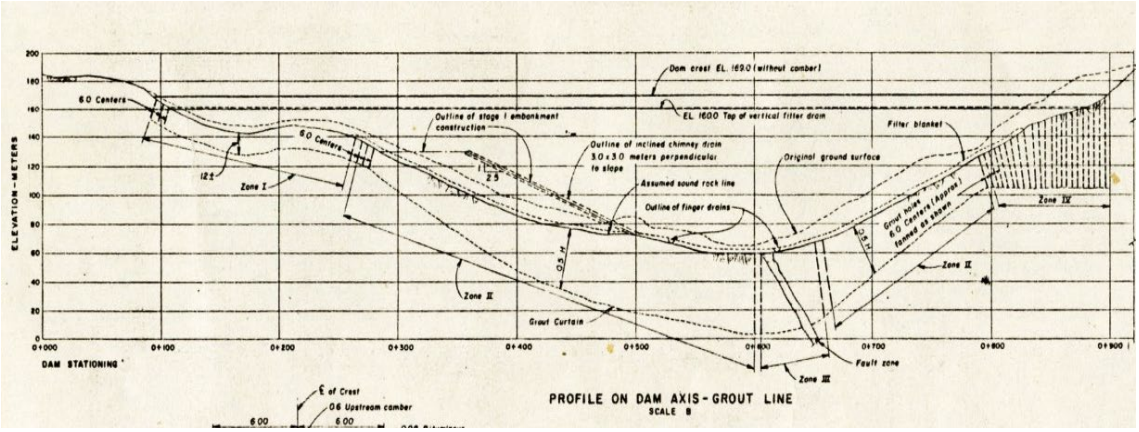

Fig. 3.5 SRK Dam profile (Royal Irrigation Department 1975).

3.1.2.2 Saddle Dams

Geological feature of the saddle dams site consists of phyllite, phyllitic-shale, and slaty shale. Originally, the geological profile consisted of an about 4 m thick residual soil layer followed by a weathered rock layer and a strong fresh rock layer. The rocks are highly fractured, especially at a depth of 2 to 10 m.

3.1.3 Excavation and Foundation Improvement

3.1.3.1 Main Dam

The excavation was down to the top of the sound rock layer. There was a large amount of good quality river sand and gravel. They were subsequently used as fill on the downstream side of the dam. Three rows of grout curtains were constructed to prevent

seepage through the foundation as shown in Fig. 3.1. The foundation rocks on the right abutment are highly fractured and discontinuous. Furthermore, there was a rock slide incident that was the result of constructing intake tunnels. Therefore, the slope was adjusted to 1:2 and rock anchors and shotcrete were installed.

The inactive fault at station 0+600 m was remediated by removing residual soil and fractured rocks from the fault and filling with dental concrete.

3.1.3.2 Saddle Dams

Only 1 m of the residual soil layer was removed. The designer believed that to be sufficient because the saddle dams had low height, low water pressure, and low overburden.

3.1.4 Material Properties

3.1.4.1 Existing Data

Data for material properties are from *Stability Analysis of SRK Dam under Seismic Loading Report* by Geotechnical Engineering Research and Development Center, Department of Civil Engineering, Faculty of Engineering, Kasetsart University (GERD) in 2012. Table 3.1 shows the designed material properties for SRK main dam.

Table 3.2 shows and compares material properties during construction (1963–1972) and after the dam has been in operation (2012). The report from the construction period stated that the properties of the random fill material were substantially

Table 3.1. Designed SRK Dam material properties (Geotechnical Engineering Research and Development Center, 2012).

Material	USCS	Net Weight (t/m^3)	Saturated Weight (t/m^3)	ø (Degree)	c (kg/m^2)
Core Zone	SC	2.00	2.12	27.0	0.5
Random Fill	GM, GM-GC	2.00	2.12	28.5	0.2
Sand Filter	*	1.80	1.90	33.0	0.0
Rock Fill	*	1.80	1.90	37.0	0.0
Foundation (Earth)	*	1.90	2.00	27.0	0.0
Foundation (Rock)	Quartzitic Schist	2.60	2.00	30.0	0.5

consistent (Geotechnical Engineering Research and Development Center 2012). Therefore, the random fill and the core will be treated as the same material in this research (clayey sand) but with different levels of compaction and permeability.

There are inconsistency and uncertainty in the recorded data. Therefore, the material properties used in the analysis will be estimated from a combination of existing data, typical properties of materials, and engineering judgment.

3.1.4.2 Hydraulic Conductivity (k)

Hydraulic conductivity or permeability of soil represents how quickly water passes through soil. The value can vary greatly depending on types of soil, void ratio, turbulence of flow, fines content, clay types, soil density, and compaction.

The value of hydraulic conductivity can be determined in laboratory tests. Table 3.3 provides the general range for the values of hydraulic conductivity (k) for various soils.

Table 3.2. Main Dam material properties during construction and after use (after Geotechnical Engineering Research and Development Center 2012).

Property	Unit	During Construction (RID, 1975)		After use (GERD, 2012)
		Clay Core	Random Fill	
USCS	-	SC	GM	SC, CL
Liquid Limit	%	31.5	30.1	30.81 – 39.55
Plastic Limit	%	-	-	22.04 – 26.58
Plastic Index	%	12.9	7.8	7.41 - 16.86
Maximum Dry Density	(t/m^3)	1.73	2.01	1.31 – 1.90
Optimum Moisture Content	%	14.7	8.7	15.25 - 18.62
Compaction Dry Density	%	99.1	98.9	
Compaction Moisture Content	%	1.0 dry of optimum	0.9 dry of optimum	
Hydraulic Conductivity (k)	cm/s	$4x10^{-8}$		$6.5x10^{-8}$ - $5.7x10^{-10}$
Cc	-	-	-	0.078 - 0.260
Effective Cohesion (c')	kN/m^2	-	-	14.87 - 25.66
Effective Friction Angle (Ø')	degree	-	-	24.74 - 35.52
Total Cohesion (c)	kN/m^2	0.5 (design)	-	11.26 - 12.92
Total Friction Angle (Ø)	degree	27 (design)	-	12.92 - 16.34

The impervious sections of earth dam have a k range of 10^{-6}–10^{-11} m/s (Holtz et al. 2013). There is no reliable present data for the k value of SRK dam. Combining the available information with typical values and standards, k values of SRK Dam core and fill estimated at $4x10^{-7}$ m/s and $1.6x10^{-6}$ respectively. The significance of the two values is that the core has one-fourth the permeability of the fill. The estimated k for sand filter drain is $5x10^{-4}$ m/s. For rock riprap, the k value is 0.01 m/s. The exact values of the hydraulic conductivity of these materials are not as important as the ratios among them. These estimated values produce a reasonable pore water condition in the dam model which is vital for analyzing slope stability.

Table 3.3. Range of the hydraulic conductivity for various soil (after Das and Sivakugan 2019).

Type of Soil	Hydraulic Conductivity, k (m/s)
Medium to coarse gravel	Greater than 10^{-3}
Coarse to fine sand	10^{-3}–10^{-5}
Fine sand, silty sand	10^{-5}–10^{-7}
Silt, clayey silt, silty clay	10^{-6}–10^{-8}
Clays	10^{-9} or less

The embankment dam is deposited in layers, which results in the difference between horizontal and vertical permeability. This produces standard anisotropy ratios (k_H/k_V) in the embankment as shown in table 3.4.

Table 3.4. Anisotropy of embankment materials according to USBR standard placement (after U.S. Department of Interior, Bureau of Reclamation 2014).

Material	k_H/k_V range
Embankment core	4 to 9
Embankment shell	4 to 9
Embankment drains	1 to 4

From the construction report and the downstream piezometers data, it is reasonable to assume that the k_H/k_V ratio of SRK core is 4. There was no report on the effectiveness of compaction of the fill. In order to be on the safe side, a k_H/k_V ratio of the shell in this research is 10 to account for the higher level of soil variation. For the sand drain, rockfill, and riprap layers, the k_H/k_V ratio is 1 (U.S. Department of Interior, Bureau of Reclamation 2014).

3.1.4.3 Cohesions and Friction Angles

More than 45% of rockfill material is 0.03–0.4 m sized rocks with less than 5% fine material (Geotechnical Engineering Research and Development Center 2012). The typical effective friction angle for cohesionless rockfill is 45°. Rockfill embankment is an easily drained material and therefore will go through the cycle of saturation–unsaturation frequently. When most of the water drains, the moisture film surrounding the individual grains of material creates an "apparent cohesion." This phenomenon is caused by the water surface tension occurring between the surfaces of water, mineral grains, and air (Holtz et al. 2013). This apparent cohesion should not be relied on for strengths of the materials as it can vanish when more water is introduced (e.g., rain, flood) or water evaporates.

As mentioned in section 3.1.4.1, the core and fill layers of the dam were built with the same material. The typical cohesion of clayey sand and saturated compacted clayey sand are 5 kPa and 11 kPa respectively (Geotechdata n.d.). This research selected 7.5 kPa as the appropriate effective cohesion value for core and fill material.

In order to determine the drained fully softened friction angle, values of clay size fraction and liquid limit of the material are required. From the available grain size analysis data (table 3.5), the core material has an average clay size fraction of 22%. From Atterberg's limit data (table 3.6), the core material has an average liquid limit of 35.5%.

Therefore, a reasonable estimation of the drained fully softened friction angle is 32° as shown in Fig. 3.6. The undrained friction angle is estimated to be 17°.

Table 3.5. Grain size analysis of SRK Dam core sample (Geotechnical Engineering Research and Development Center 2012).

Boring No.	Depth, m.	Sieve Analysis Test (% Passing)									Hydrometer Test (mm)					
		1/2"	3/8"	# 4	# 8	# 10	# 20	# 40	# 100	# 200	0.037	0.019	0.009	0.005	0.002	0.001
OPP-61	6.00-6.50	100	94.65	85.53	76.61	74.7	67.69	63.05	56.06	53.52	51.61	49.51	46.21	37.87	29.31	28.53
	27.00-27.50	100	91.48	82	70.43	67.77	57.88	52.36	45.37	42.29	40.01	37.66	32.92	27.8	19.77	18.49
	39.00-39.50	100	91.75	79.31	66.19	63.02	51.29	44.99	37.67	34.62	31.62	30.06	27.79	22.7	15.9	15.28
	48.50-49.00	100	95.33	89.39	80.27	77.94	68.13	62	53.84	50.58	48.29	46	41.5	34.13	25.63	24.68
	63.00-63.50	100	95.6	82.25	69.73	66.9	56.04	49.95	41.37	38.23	37.36	35.48	32	25.03	19.14	18.38

Table 3.6. Atterberg's limit of SRK Dam core sample (Geotechnical Engineering Research and Development Center 2012).

Boring No.	Depth, m.	Atterberg's Limit Test		
		LL%	PL%	PI%
OPP-61	6.00-6.50	36.16	23.91	12.25
	27.00-27.50	39.55	22.66	16.89
	39.00-39.50	32.40	23.41	8.99
	48.50-49.00	37.30	26.58	10.72

There are no data on the cohesions and friction angles of the sand drain layer therefore they are assumed to be the same as fill to be on the conservative side.

3.1.4.4 Unit Weights

From the GERD 2012 report, the unit weight (ɣ) of the core zone is 20 kN/m^2. The same unit weight will be used for the fill and drain layer. The rock riprap unit weight is 22 kN/m^2.

The material properties used in this research are shown in table 3.7.

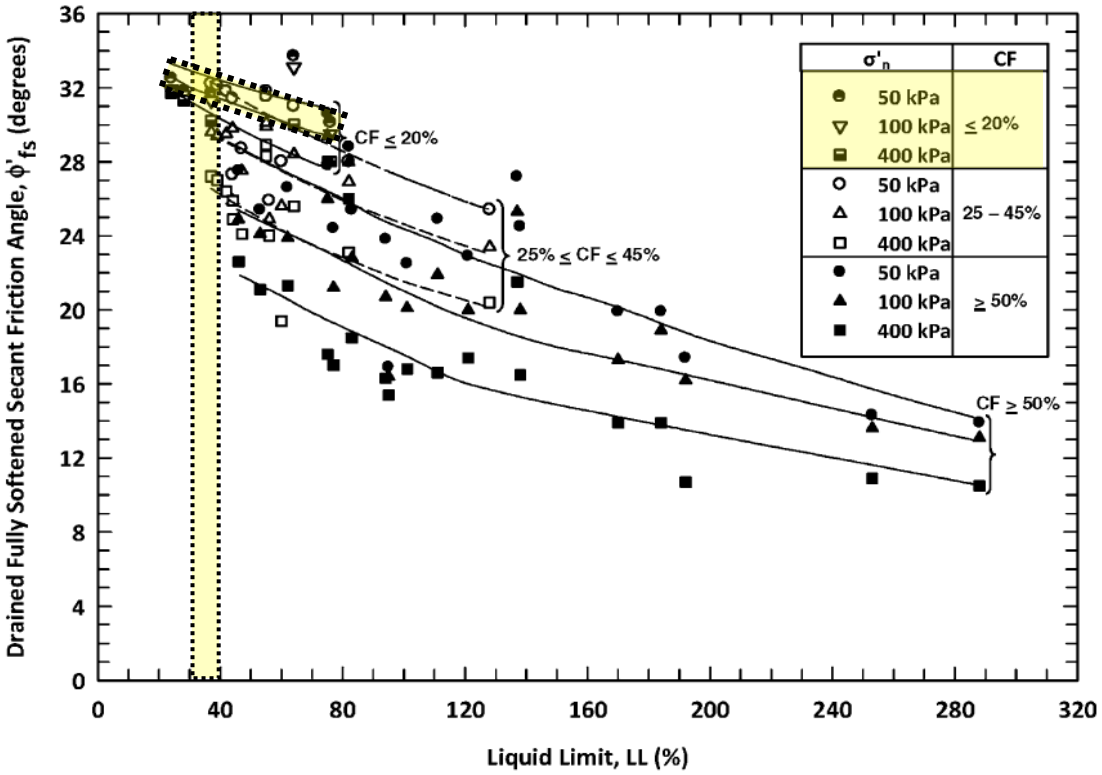

Fig. 3.6 Drained fully softened friction angle for SRK Dam's clayey sand material (after Stark and Hussain 2013).

Table 3.7. Material properties of SRK Dam used in this research.

Material Zone	K (m/s)	k_H/k_V	c'	ϕ'	c	ϕ	γ (kN/m^2)
Riprap, Rockfill	0.01	1	0	45	0	45	22
Fill	$1.6x10^{-6}$	10	7.5	32	35	17	20
Core	$4.0x10^{-7}$	4	7.5	32	35	17	20
Drain	$5.0x10^{-4}$	1	7.5	32	35	17	20

3.2 Rapid Drawdown

3.2.1 Drawdown Plot

The maximum rate of drawdown is calculated by the maximum capacity of all water-releasing structures at SRK Dam (i.e., spillway, power plant turbines, and river outlet) along with the lowest rate of inflow.

The spillway or service spillway is a two-tunnel horseshoe-section concrete spillway. The tunnels are 90 m long and each has a diameter of 11 m. The crest elevation is at +150.5 m MSL. There are 2 radial control gates of the dimensions 11.85 x 15 m. The maximum water-releasing capacity is 3,250 CMS with the maximum gate opening of 9.2 m.

SRK power plant has 4 generators capable of generating 125 MW each. The maximum flow through these generator turbines is 732 CMS. The intake sill sits at +104 m MSL.

The river outlet is a 6 m diameter tunnel. The inlet level is at +104 m MSL. The river outlet has maximum capacity of 400 CMS.

To estimate the quickest possible drawdown, this analysis will use the reservoir inflow during dry season. From the recorded average of inflow during the three driest months of the year, the inflow is estimated to be 30 CMS (Civil Maintenance Division 2003).

From SRK Dam Spillway Manual, the reservoir water level (RWL) can be plotted against the reservoir storage volume in million cubic meters (MCM) as shown in Fig. 3.7.

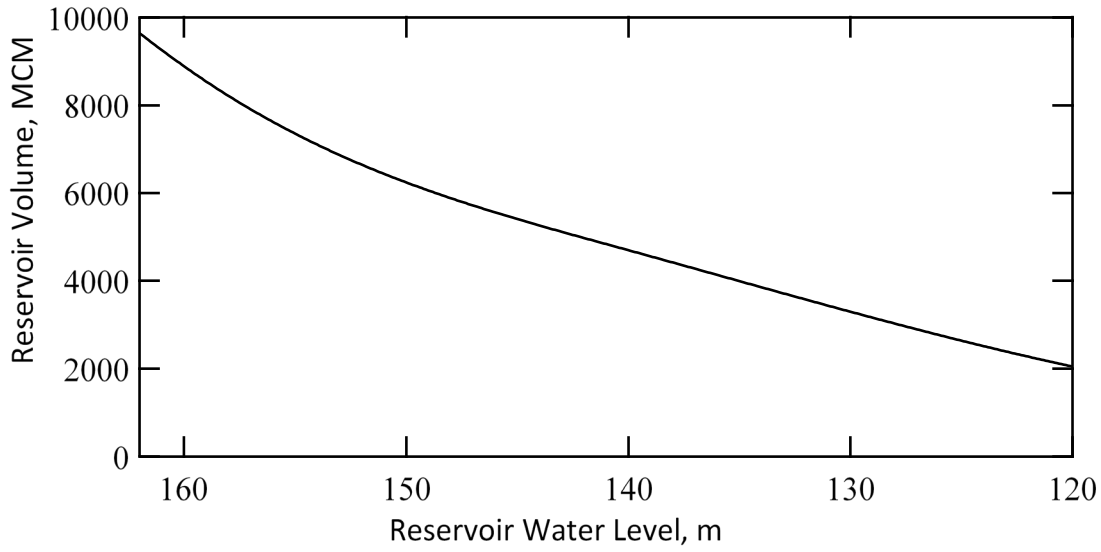

Fig. 3.7 Reservoir water level vs. reservoir volume.

The rate of maximum outflow is calculated by subtracting the minimum inflow from the combined maximum capacity of all releasing structures. Fig. 3.8 shows the rate of outflow at each RWL in the range of +162 m MSL to +120 m MSL. Fig. 3.9 shows the decrease of RWL as the result of the continuous maximum outflow rate.

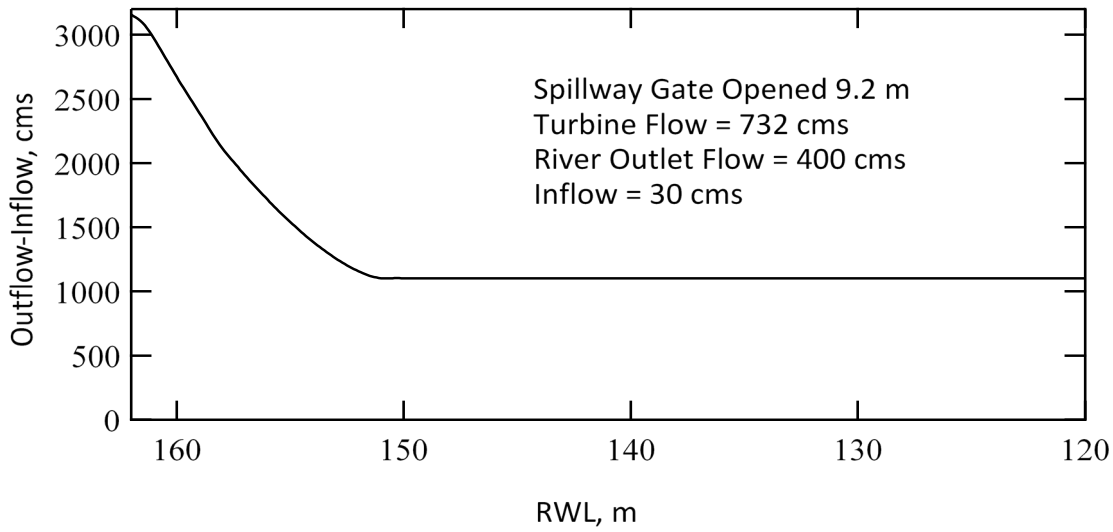

Fig. 3.8 Reservoir water level vs. maximum outflow rate.

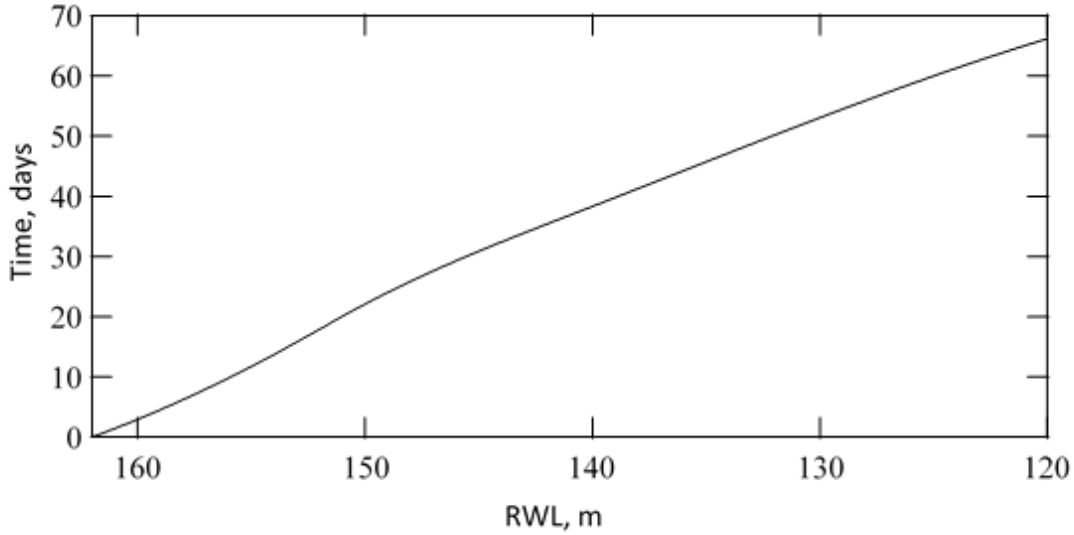

Fig. 3.9 Reservoir water level vs. time.

This graph represents the quickest possible time that the reservoir can be drawn down. It is important to note that in practice, there are a number of factors that will prevent this drastic scenario such as the safety of the downstream community, possible damage to downstream lands and properties, the higher rate of inflow, and the stoppage of turbine flow due to a high tailrace water level.

3.2.2 Drawdown Time for SRK Dam

The equation for drawdown time (equation 2.1 in section 2.3) can be used to calculate the number of days that SRK dam materials will drain after drawdown.

$$t = TD^2/c_v \qquad \text{(Eq. 3.1)}$$

The average degree of consolidation, U, as a percentage can express the degree of pore water pressure dissipation. In the multistage rapid drawdown analysis method by

Duncan, Wright, and Wong (1990), it is stated that for material to be considered drained, 90% of excess pore pressure needs to be dissipated. This value is considered highly conservative since this method considered the material fully undrained up until that point. In reality, some drainage would have occurred before the dissipation reached 90%. In this research, setting the value of U at 50% is considered to be appropriate to calculate drawdown time. This is still somewhat conservative for this analysis since there is a layer of rockfill riprap which is an easily drained material. The time factor, T, for U = 50% is 0.197 and for U = 90% is 0.848 (Das and Sivakugan 2019).

Length of drainage path, D, is considered in two cases. Given the geometry of the dam, failure on the upstream face may occur in two modes. First, the slip surfaces may be controlled by both a decrease in water level and the +120 m MSL berm and result in relatively shallow failures as shown in Fig. 3.10. In this case, the average depth from the base of the slice to the surface is approximately 10 m. Secondly, the failure surface may extend beyond the berm and include the whole face of the upstream slope as shown in Fig. 3.11. In this case the average estimated drainage depth is 30 m, which is deeper than the first case.

The range coefficient of consolidation, c_v, is estimated from the typical value for clayey sand because of the limited existing data. This research uses a c_v of 1–5 m^2/day.

Table 3.8 shows the result of equation 3.1 using the T, D, and c_v values selected.

3.2.3 Drawdown History

A maximum drawdown event at SRK Dam occurred in January to March of 1983. The

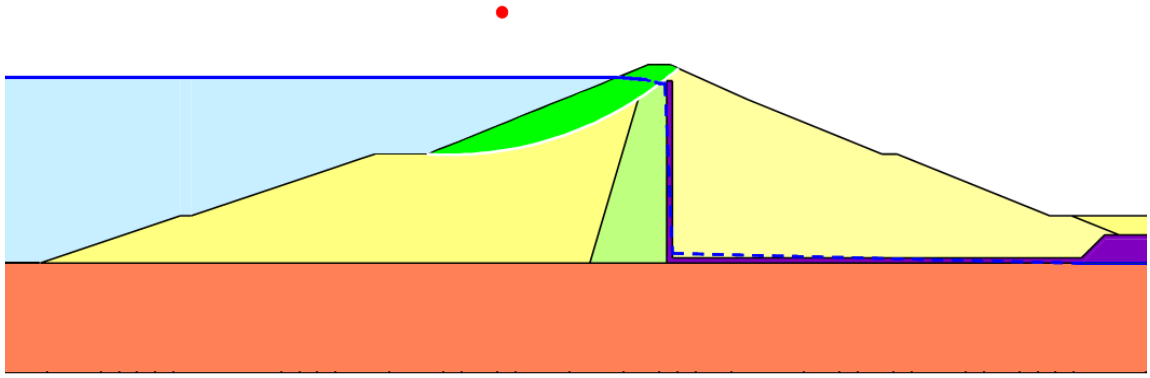

Fig. 3.10 An example of a shallow failure surface in the upstream slope of SRK Dam.

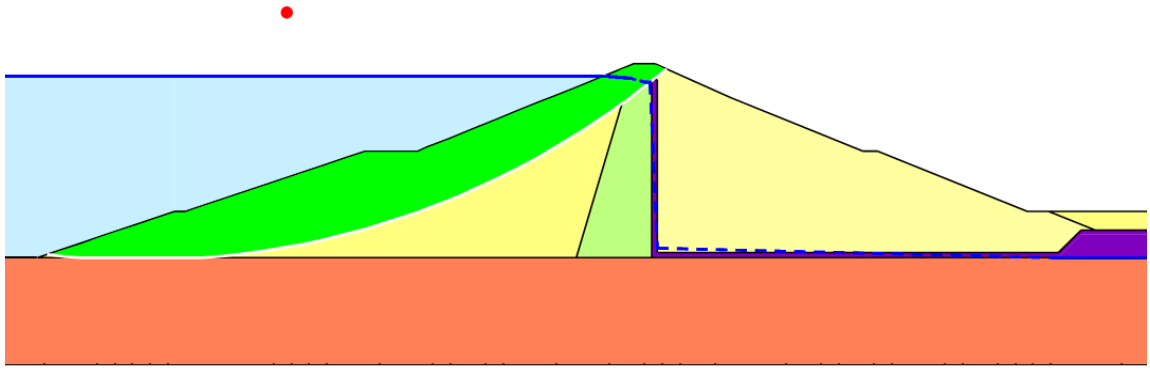

Fig. 3.11 An example of a deep failure surface in the upstream slope of SRK Dam.

Table 3.8. Time for drawdown of SRK Dam.

Length of drainage path		U = 50 %		U = 90%	
		c_v (m^2/day)		c_v (m^2/day)	
		5	1	5	1
Shallow (m)	10	4 days	20 days	17 days	85 days
Deep (m)	30	35 days	177 days	153 days	763 days

water level decreased from +163 m MSL to +143 m MSL in approximately 60 days. This level of drawdown has happened only once since SRK Dam has been in operation. Therefore, it is reasonable to state that in the practice, maximum drawdown of SRK Dam reservoir is 20 m.

3.3 Seismicity

3.3.1 Earthquake Sources Identification and Characterization

3.3.1.1 Active Faults in The Area

The two active fault zones nearest SRK Dam are the Uttaradit Fault and the Thoen Fault, as shown in Fig. 3.12. Both faults orientate along a northeast–southwest direction. The Uttaradit Fault is the closer of the two. The distance from the main dam to the Uttaradit Fault is in the range of 8 to 62 km. The minimum distance from SRK main dam to the Thoen Fault is 52 km.

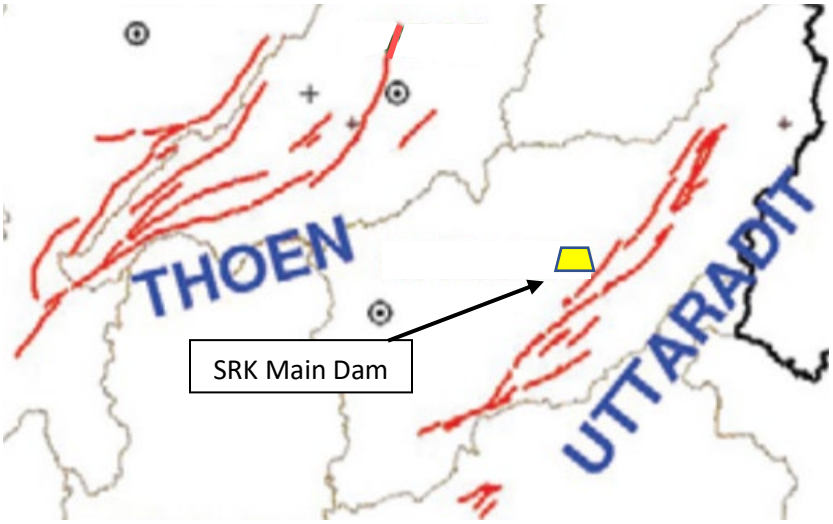

Fig. 3.12 Faults near SRK main dam and saddle dams.

The Earthquake Observation Division, Thai Meteorological Department (n.d.) has records of earthquake events from the two faults since 2007. The magnitude ranges from 1.3 to 3.5 with a depth between 1 and 10 km.

USGS (Petersen et al. 2007) reported the Uttaradit Fault to be a normal fault with a length of 38 km and the Thoen Fault to be a normal fault with a length of 107 km. The moment magnitude of each fault can be estimated using the empirical relationship for normal fault movement presented by Wells and Coppersmith (1994) as follows:

$$M_w = 4.86 + 1.32 \log L \quad \text{(Eq. 3.2)}$$

Where M_w is the moment magnitude Mw and L is surface rupture length in km.

From equation 3.2, the largest earthquake magnitude of the Uttaradit Fault and Thoen Fault are 6.95 and 7.55 respectively.

3.3.1.2 Background Earthquake

In addition to the two known faults, there is a possibility of an undiscovered earthquake source. In a tropical area like Thailand, the precipitation and vegetation often hinder a thorough exploration and discovery of earthquake faults. Therefore, another potential earthquake source should be considered. A background earthquake is an earthquake not linked to identified sources. The maximum background earthquake (MBE) typically has a magnitude of 6. Because of the uncertainties of the area source, the source-to-site distance for the background earthquake in this case is 0 km.

The characteristics of the Uttaradit Fault, Thoen Fault, and background earthquake are presented in table 3.9. The fault mechanism of the two known faults are summarized from the USGS documentation (Petersen et al. 2007) as well as data from Thailand's Department of Mineral Resources (2016).

Table 3.9. Characteristics of earthquake sources of SRK Dam site.

Source	Mw	Distance (km)	Fault mechanism		Dip
Background	6	0	normal	hanging	50
Thoen Fault	7.55	52	normal	foot	50
Uttaradit Fault	6.95	8	normal	hanging	50

3.3.2 Peak Ground Acceleration and Horizontal Seismic Coefficient

The maximum peak ground acceleration (PGA) can be estimated from the NGA-West2 Ground Motion Prediction Equations (GMPEs) as mentioned in chapter 2. The GMPEs spreadsheet is available from the PEER Center (n.d.) website. The input variables for a maximum earthquake event from a background earthquake, the Thoen Fault, and the Uttaradit Fault are as shown in table 3.10.

Table 3.10. NGA-West2 GMPEs input variables for a maximum earthquake event from the three SRK Dam earthquake sources.

Variable	Description	Background	Thoen fault	Uttaradit fault
M_w	Moment magnitude	6	7.55	6.95
R_{JB} (km)	Source to site distance	0	52	8
R_X (km)	Horizontal distance from top of rupture measure perpendicular to fault strike	0	-52*	8*
V_{S30} (m/s)	The average shear-wave velocity	760**	760**	760**
U	Unspecified-mechanism factor	0	0	0
F_{RV}	Reverse-faulting factor	0	0	0
F_{NM}	Normal-faulting factor	1	1	1
F_{HW}	Hanging-wall factor	1	0	1
Dip (deg)	Average dip of rupture plane	50	50	50
Z_{TOR} (km)	Depth to top of rupture	2,5,10	2,5,10	2,5,10
$V_{s30flag}$	1 for measured, 0 for inferred	measured	measured	measured
F_{AS}	Aftershock effect	No	No	No
Region	Regions considered in the models	California***	California***	California***

*For a hanging wall, R_x is equal to R_{JB}. For a foot wall, R_x is equal to negative R_{JB}.

** Soil site class B: Rock

*** From the available region in the spreadsheet, California is the closest to SRK Dam area

The depths of 2, 5, and 10 km are considered based on the recorded seismic events in the area.

Each of five models is applied and the resulting PGA are averaged as presented in table 3.11.

Table 3.11. Peak ground acceleration of maximum earthquake from each source.

Source	Z_{TOR} (km)	PGA					
		ASK14	BSSA14	CB14	CY14	I14	Average
Background earthquake	2	0.3675	0.3203	0.3778	0.3161	0.3652	0.35
	5	0.3048	0.3203	0.2992	0.2414	0.2523	0.28
	10	0.2218	0.3203	0.1858	0.1762	0.1561	0.21
Thoen fault	2	0.0871	0.0837	0.0729	0.0723	0.0768	0.08
	5	0.1024	0.0837	0.0726	0.0800	0.0764	0.08
	10	0.1331	0.0837	0.0718	0.0943	0.0752	0.09
Uttaradit fault	2	0.3860	0.2157	0.2857	0.2532	0.3132	0.29
	5	0.3873	0.2157	0.2748	0.2575	0.2857	0.28
	10	0.3146	0.2157	0.2247	0.2447	0.2262	0.25

The controlling earthquake in this case is the background earthquake. However, this research is interested in the aftershock. According to Båth's law, the largest aftershock is 1.2 magnitude smaller than the main shock. Subtracting 1.2 from the moment magnitudes from table 3.9 results in the aftershock moment magnitudes that can be entered in the GMPEs spreadsheet to calculate PGA. The focal depth range of earthquake events from both faults is 2 – 10 km. From equation 2.4, the magnitude difference is between 1.01 and 1.07. Furthermore, there are records of aftershocks that do not strictly follow Båth's law. Therefore, 1 and 0.8 magnitude differences are also

considered. PGA values of each aftershock magnitude are as shown in tables 3.12, 3.13, and 3.14.

Table 3.12. Peak ground acceleration of the largest aftershock according to Båth's Law from each source.

-1.2 Magnitude Difference	Z_{tor} (km)	PGA					
		ASK14	BSSA14	CB14	CY14	I14	Average
Background earthquake M_W = 4.8	2	0.1728	0.0927	0.1114	0.1240	-*	0.13
	5	0.1230	0.0927	0.0845	0.0889	-*	0.10
	10	0.0794	0.0927	0.0479	0.0644	-*	0.07
Thoen M_W = 6.35	2	0.0323	0.0336	0.0376	0.0261	0.0302	0.03
	5	0.0379	0.0336	0.0374	0.0291	0.0300	0.03
	10	0.0490	0.0336	0.0368	0.0345	0.0295	0.04
Uttaradit M_W = 5.75	2	0.1591	0.1581	0.1878	0.1344	0.1582	0.16
	5	0.1628	0.1581	0.1678	0.1346	0.1419	0.15
	10	0.1477	0.1581	0.1250	0.1211	0.1075	0.13

* I14 model is applicable for $M_W \geq 5.0$

Table 3.13. Peak ground acceleration of 1 magnitude difference aftershock from each source.

-1 Magnitude Difference	Z_{tor} (km)	PGA					
		ASK14	BSSA14	CB14	CY14	I14	Average
Background earthquake M_W = 5	2	0.2189	0.1292	0.1474	0.1642	0.2398	0.18
	5	0.1700	0.1292	0.1129	0.1177	0.1574	0.14
	10	0.1160	0.1292	0.0651	0.0838	0.0912	0.10
Thoen M_W = 6.55	2	0.0398	0.0379	0.0440	0.0317	0.0362	0.04
	5	0.0467	0.0379	0.0438	0.0353	0.0360	0.04
	10	0.0605	0.0379	0.0431	0.0417	0.0354	0.04
Uttaradit M_W = 5.95	2	0.1974	0.1665	0.2077	0.1537	0.1769	0.18
	5	0.1989	0.1665	0.1901	0.1537	0.1591	0.17
	10	0.1698	0.1665	0.1447	0.1387	0.1214	0.15

The controlling aftershock earthquake from tables 3.12 and 3.13 is from the Uttaradit Fault while the controlling aftershock earthquake from table 3.14 is from the background earthquake. Marcuson (1981) suggested that the appropriate seismic

pseudo-static coefficient for dams should correspond to one-third to one-half of the acceleration, including amplification or deamplification effects. From the PGA of all controlling earthquakes, horizontal seismic coefficients (k_h) can be determined as shown in table 3.15.

Table 3.14. Peak ground acceleration of 0.8 magnitude difference aftershock from each source.

-0.8 Magnitude Difference	Z_{tor} (km)	PGA					
		ASK14	BSSA14	CB14	CY14	I14	Average
Background earthquake M_W = 5.2	2	0.2391	0.1807	0.1948	0.2034	0.2584	0.22
	5	0.1888	0.1807	0.1506	0.1463	0.1713	0.17
	10	0.1323	0.1807	0.0886	0.1028	0.1006	0.12
Thoen M_W = 6.75	2	0.0490	0.0426	0.0486	0.0381	0.0437	0.04
	5	0.0576	0.0426	0.0484	0.0423	0.0434	0.05
	10	0.0746	0.0426	0.0477	0.0499	0.0426	0.05
Uttaradit M_W = 6.15	2	0.2444	0.1753	0.2291	0.1734	0.1987	0.20
	5	0.2427	0.1753	0.2129	0.1737	0.1792	0.20
	10	0.1949	0.1753	0.1650	0.1578	0.1377	0.17

Table 3.15. Horizontal seismic coefficients of each controlling aftershock earthquake in the range of one-third to one-half peak ground acceleration.

Controlling Aftershock PGA	k_h	
	One-third	One-half
0.16	0.05	0.08
0.18	0.06	0.09
0.22	0.07	0.11

To account for the amplification effect, Anderson et al. (2008) recommended the following equations:

$$k_{av} = \alpha k_{max} \quad \text{(Eq. 3.3)}$$

where k_{max} = peak seismic coefficient at the ground surface

α = fill height-dependent reduction factor

For the site class B rock foundation,

$$\alpha = 1.20*(1+0.01H[(0.5\beta)-1]) \quad \text{(Eq. 3.4)}$$

If the fill height is greater than 100 feet, H can be assumed to be 100 in Equation 3.4.

$$\beta = 1 \text{ second PSa/PGA} \quad \text{(Eq. 3.5)}$$

where 1 second Psa is predicted from GMPEs models.

K_h is suggested to be in the range of $0.5k_{av}$ to $1.0\ k_{av}$. Table 3.16 shows the values of k_h when amplification is considered.

Table 3.16. Horizontal seismic coefficients of each controlling aftershock earthquake with amplification effect.

Controlling Aftershock PGA	α	Amplification (GERD, 2012)	k_h		
			0.5	0.75	1.0
0.16	0.2453	2.67	0.05	0.08	0.10
0.18	0.2807	2.63	0.07	0.10	0.13
0.22	0.1663	2.57	0.05	0.07	0.09

k_h values of the Uttaradit controlling aftershock from tables 3.15 and 3.16 generally matched. The background aftershock produces lower 1 second Psa values, which results in a lower amplification effect on the k_h. Considering the existing data and both methods of estimation, the reasonable range of aftershock k_h analyzed in this research is 0.05 to 0.1.

CHAPTER 4

DEVELOPMENT OF MODEL

This research uses GeoStudio 2020's SEEP/W and SLOPE/W to analyze the slope stability of SRK Dam in case of rapid drawdown and aftershock loading.

SRK Dam's geometry is plotted onto the program according to the as-built maximum section drawing of the dam in the 2-D analysis. The crest elevation does not include camber. Fig. 4.1 shows the 2D geometry of SRK Dam in GeoStudio.

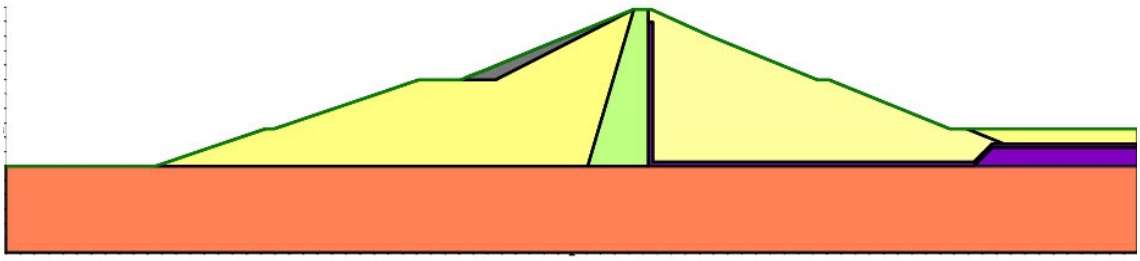

Fig. 4.1 SRK Dam geometry in GeoStudio.

SEEP/W is used to achieve the seepage condition through the dam. The analysis type is steady-state with the water level at full normal retention level of +162 m MSL. The materials are defined as presented in table 4.1.

The model mesh is set to a quads and triangles pattern. An element size of 1 m is used for the element in the area subjected to changes in water level and seepage condition, such as the upper part of upstream fill and the core. The downstream fill element is 3x3 and the foundation element is 6x6 as shown in Fig. 4.2.

Table 4.1. Material definitions in SEEP/W.

Material	Region Color	Material model	Saturated k_x (m/s)	Anisotropy K_y'/k_x'
Core		Saturated/Unsaturated	$4x10^{-7}$	0.25
Upstream fill		Saturated/Unsaturated	$1.6x10^{-6}$	0.1
Downstream fill		Saturated/Unsaturated	$1.6x10^{-6}$	0.1
Drain		Saturated	$5.0x10^{-4}$	1
Riprap		Saturated/Unsaturated	0.01	1
Foundation		Saturated	$1x10^{-10}$	1

The boundary condition on the upstream slope is set as 162 m constant water total head.

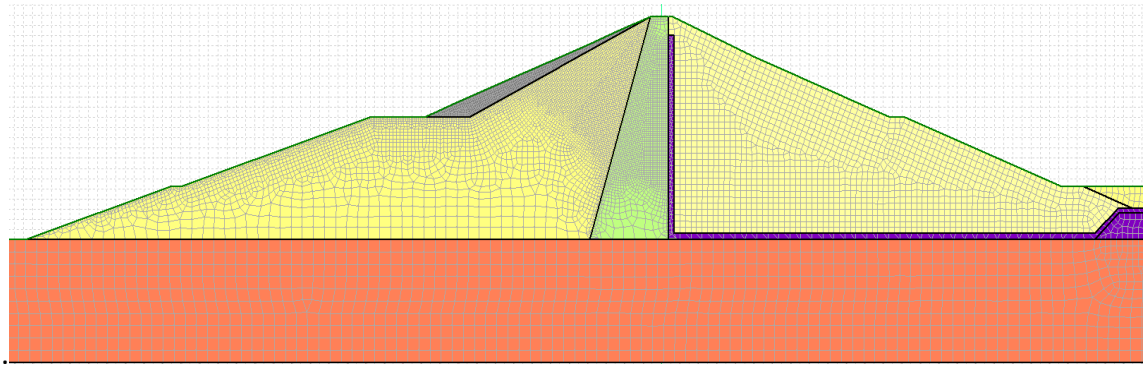

Fig. 4.2 SRK Dam model mesh.

In SLOPE/W, the analysis type is Spencer with Staged Rapid Drawdown analysis (Duncan et al. 1990), with settings as shown in Fig. 4.3. This setting only allows piezometric lines as pore water pressure conditions.

The slip surface setting is as follows. The direction of movement for upstream analysis is right to left and for downstream analysis is left to right. The slip surface option is entry and exit. The entry range is set to always include at least some part of

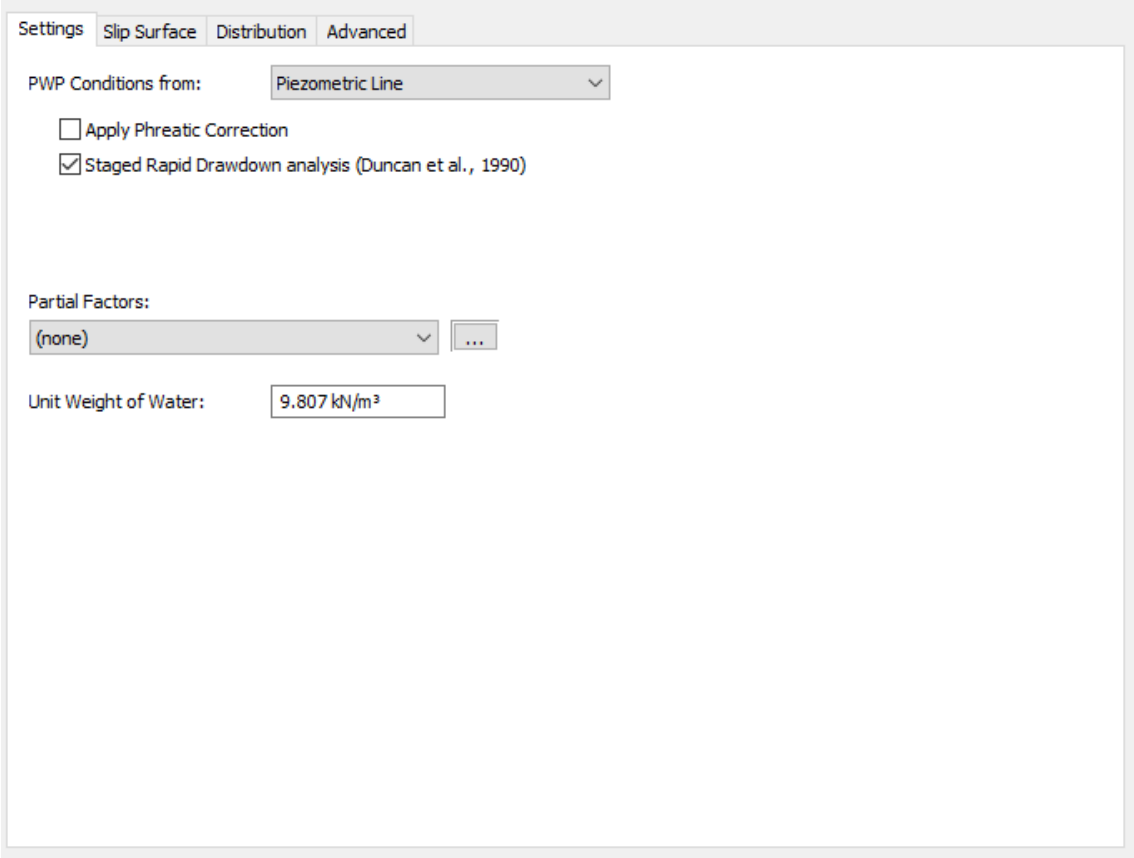

Fig. 4.3 Setting in SLOPE/W for rapid drawdown and seismic loading analysis.

the dam crest because such failures will decrease the height of the crest and increase the risk of dam overtopping. The exit range for the upstream slope analysis is set in two modes. The two possible failure surfaces, as mentioned in section 3.2.2, are shallow failures and deep failures. The minimum slip surface depth is set to 7 m.

The 0 point of the X-axis is set at the centerline of the dam crest. The Y-coordinates are the elevation above mean sea level as in SRK Dam as-built drawing.

The initial entry and exit range of the shallow failures on the upstream slope is set as shown in Fig. 4.4 and 4.5. The next step is solving for the critical slip surface to estimate the entry and exit points of the failure. The entry and exit ranges are then

narrowed down and the number of increments is increased to achieve a more precise and accurate factor of safety for the critical slip surface. This process is repeated until the safety factor value is within 0.01 of the previous step's value.

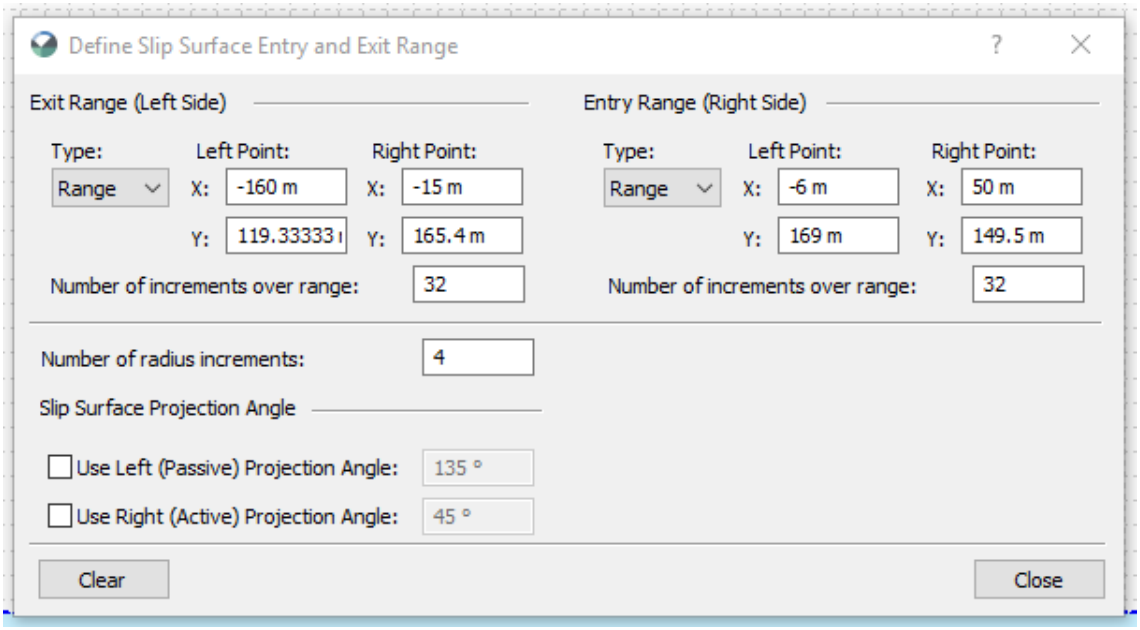

Fig. 4.4 Setting of the initial entry and exit range of shallow failure mode on the upstream slope.

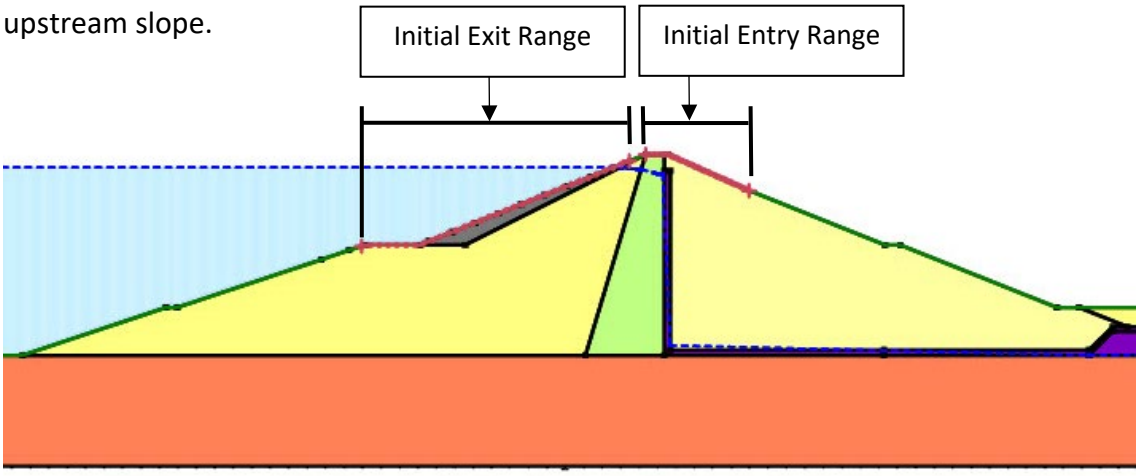

Fig. 4.5 Range of entry and exit on SRK Dam Model for shallow failure surface on the upstream slope.

The initial entry and exit range of the deep failures on the upstream slope is set as shown in Fig. 4.6 and 4.7. The initial entry point range is the same used in the shallow failure analysis. The exit range is set at the upstream toe area so that the failure would include the majority of the slope and tangent to the foundation. The entry and exit ranges are narrowed down and the number of increments is increased until the safety factor value is within 0.01 of the previous step's value.

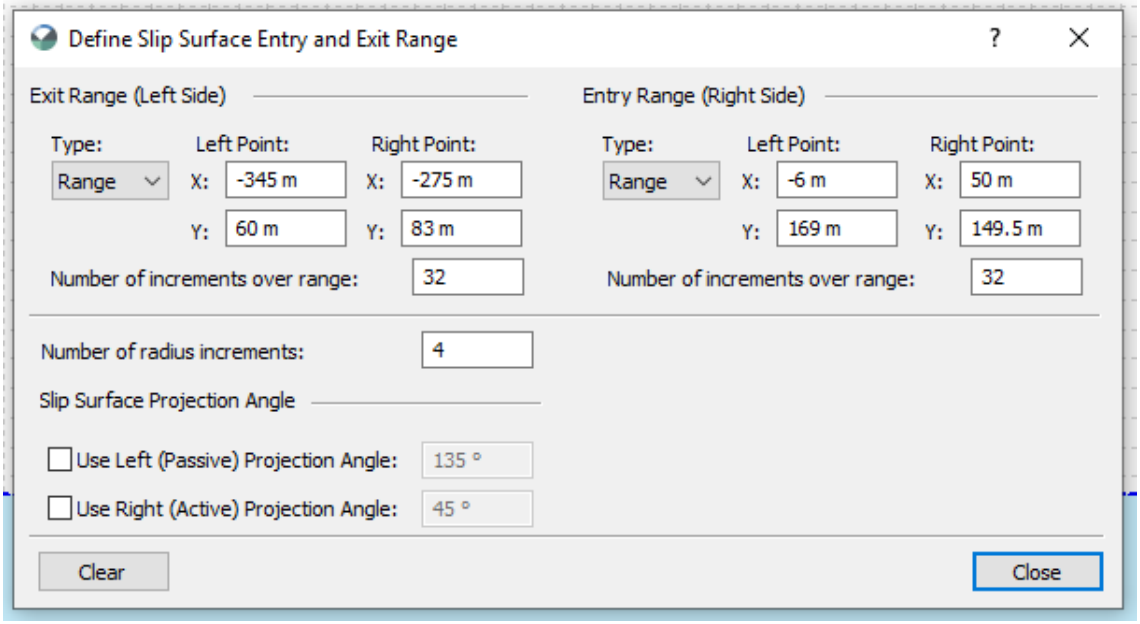

Fig. 4.6 Setting of the initial entry and exit range of deep failure surface on the upstream slope.

The initial entry and exit range of the failures on the downstream slope is set as shown in Fig. 4.8 and 4.9. The downstream side is not affected by the water level drawdown, and therefore the exit range is not limited to the shallow or deep failure surface. The process of narrowing the entry and exit range and increasing the number of increments is the same used in the upstream analysis.

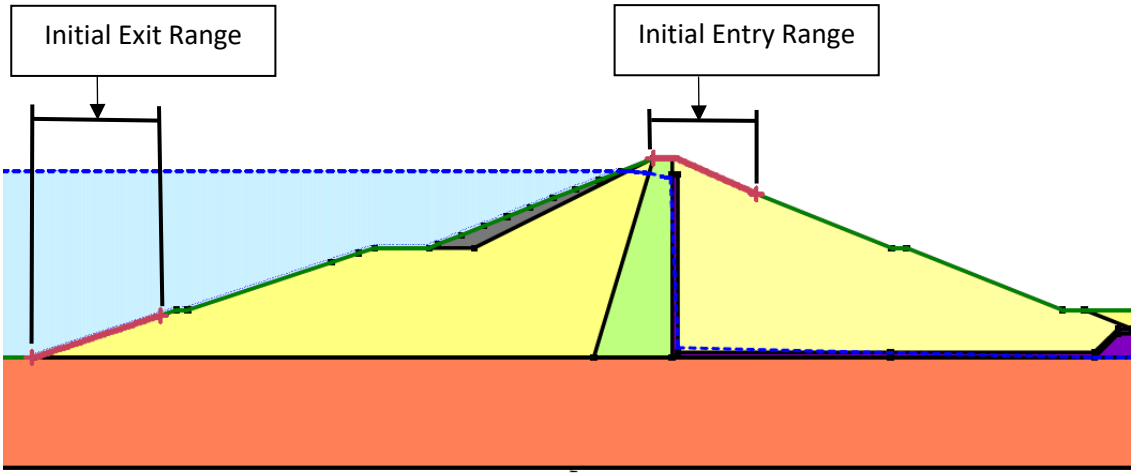

Fig. 4.7 Range of initial entry and exit on SRK Dam Model for deep failure surface on the upstream slope.

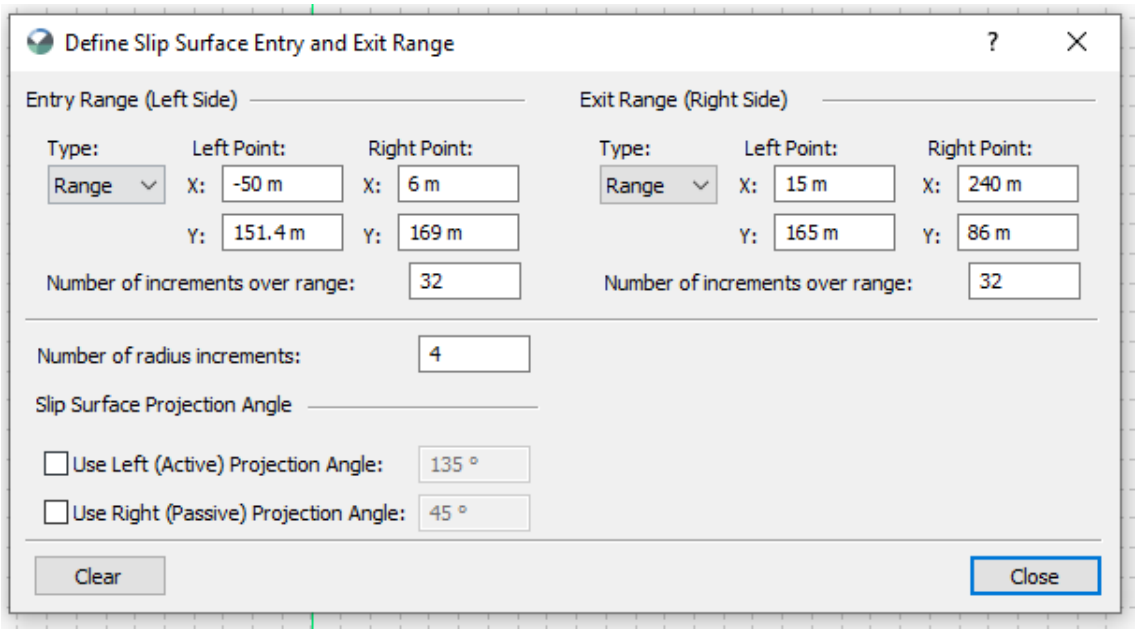

Fig. 4.8 Setting of the initial entry and exit range of failure on the downstream slope.

The material properties in SLOPE/W are as presented in table 4.2.

In this research scenario, the horizontal seismic coefficient (k_h) of the largest aftershock is in the range of 0.05 to 0.08 according to Båth's law. K_h may reach 0.1 if the aftershock is larger than expected. The value for k_h in these research analyses are 0,

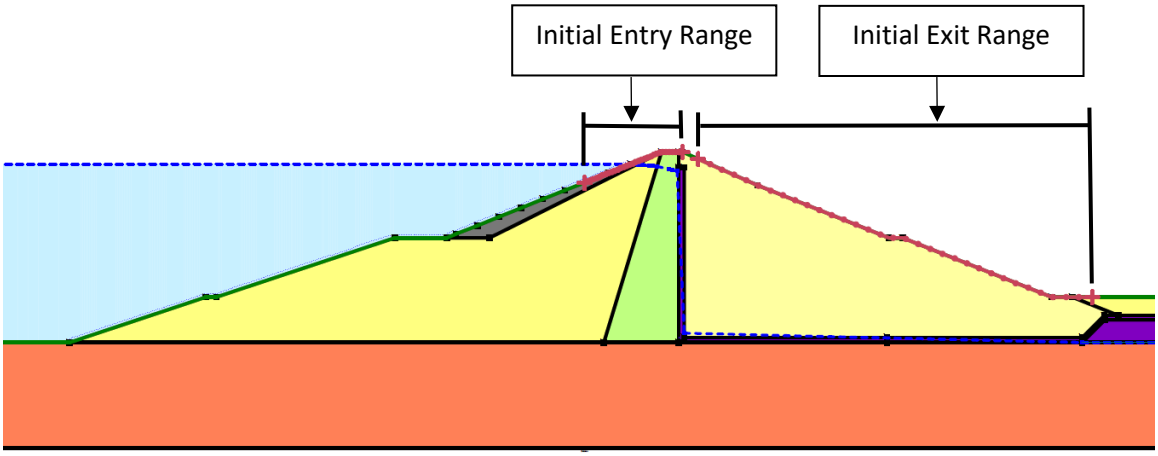

Fig. 4.9 Range of initial entry and exit on SRK Dam Model for failure on the downstream slope.

Table 4.2 Material definitions in SLOPE/W.

Material	Region Color	Material model	Basic			R Envelope*	
			Unit Weight (kN/m^3)	c' (kPa)	ϕ' (°)	c (kPa)	ϕ (°)
Core		Mohr-Coulomb	20	7.5	32	35	17
Upstream fill		Mohr-Coulomb	20	7.5	32	35	17
Downstream fill		Mohr-Coulomb	20	7.5	32	35	17
Drain		Mohr-Coulomb	20	7.5	32	35	17
Riprap		Mohr-Coulomb	22	0	45	5	44
Foundation		Bedrock (impenetrable)	-	-	-	-	-

* Undrained strength parameters

0.025, 0.0375, 0.05, 0.0625, 0.075, 0.10, 0.15, 0.20, and 0.30. Larger seismic coefficients were included to make this research applicable to other dams in more seismically active regions.

The levels of drawdown in this analysis are from 0 to 50 m with 5-meter, at 5-meter interval. The maximum drawdown of SRK Dam is 20 meters. The larger levels are

included to make this research applicable to other dams with more drastic drawdown level.

CHAPTER 5

ANALYSIS AND RESULTS

5.1 Corrections for Upstream Slope Analysis

5.1.1 Pore Water Pressure Condition

One of the limitations of Staged Rapid Drawdown analysis in SLOPE/W is that only piezometric line can be used as the pore water pressure (PWP) condition. There is no option to use the result from SEEP/W analysis. The piezometric line is traced as closely as possible from the result of SEEP/W seepage analysis. The factor of safety (FS) results from the two PWP conditions are expected to differ. In order to determine the discrepancy and solve for the correction equations, the following condition is set up to compare the results in FS: water level is at 162 m and analysis mode is "Staged Pseudo-static analysis: Undrained Strengths (Duncan et al., 1990)."

For the upstream shallow failure mode and deep failure mode, the results are as shown in tables 5.1 and 5.2 respectively. The ratio is calculated by the FS of the PWP: SEEP/W result analysis divided by the FS of the PWP: Piezometric line analysis.

Table 5.1. Factors of safety from the analyses using the result of SEEP/W analysis and piezometric line as pore water pressure condition (shallow failure surface).

k_h	Factor of Safety		Ratio
	PWP: SEEP/W Result	PWP: Piezometric Line	
0.00	2.08	1.82	1.143
0.025	1.87	1.63	1.143
0.0375	1.77	1.55	1.143
0.05	1.69	1.48	1.143
0.0625	1.62	1.41	1.144
0.075	1.55	1.35	1.143
0.10	1.42	1.24	1.144
0.15	1.23	1.07	1.145
0.20	1.08	0.943	1.146
0.30	0.871	0.757	1.151

Table 5.2. Factors of safety from the analyses using the result of SEEP/W analysis and piezometric line as pore water pressure condition (deep failure surface).

k_h	Factor of Safety		Ratio
	PWP: SEEP/W Result	PWP: Piezometric Line	
0.00	2.25	1.89	1.188
0.025	1.95	1.64	1.188
0.0375	1.83	1.54	1.188
0.05	1.72	1.45	1.188
0.0625	1.63	1.37	1.189
0.075	1.54	1.30	1.188
0.10	1.39	1.17	1.189
0.15	1.17	0.985	1.189
0.20	1.01	0.849	1.190
0.30	0.792	0.665	1.191

From tables 5.1 and 5.2, it is clear that the factors of safety from the analysis using the SEEP/W result PWP condition is higher than that from the analysis using the piezometric line. Furthermore, the ratio from the deep failure surface is higher than the shallow failure surface. This increase is expected since the amount of seepage in the deep failure surface is more than the shallow, and therefore the ratio should be greater.

The factors of safety from the piezometric line analysis are plotted against the ratios (Fig. 5.1) and the curve fitted to achieve the correction equations (eq. 5.1 and 5.2).

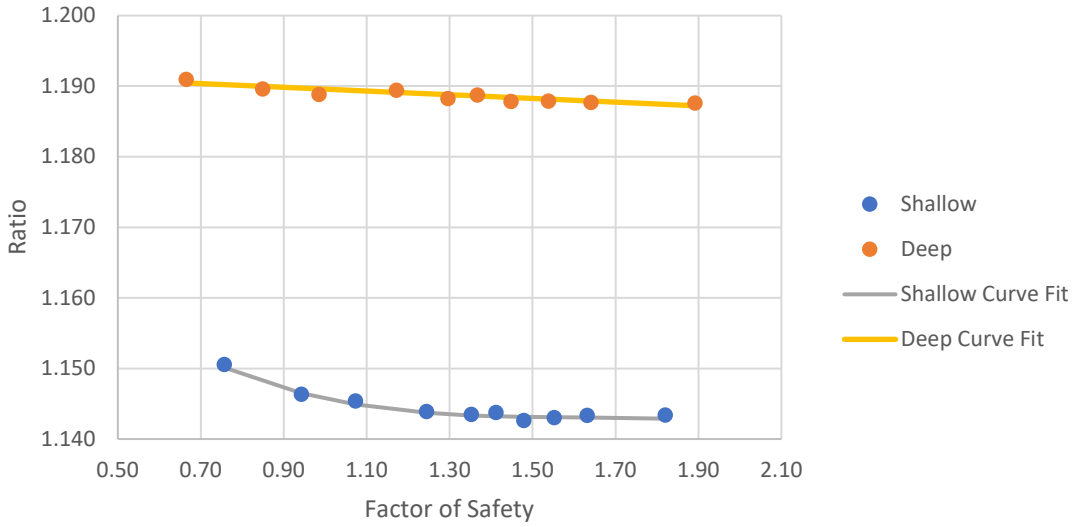

Fig. 5.1 Factor of safety of the piezometric line analysis vs. PWP: SEEP/W result to PWP: Piezometric Line factor of safety ratio.

Shallow Failure Mode FS Correction =

$$1.1895 - 0.08617*FS + 0.053536*FS^2 - 0.011133*FS^3 \quad \text{(Eq. 5.1)}$$

Deep Failure Mode FS Correction = $1.1922 - 0.0026284*FS$ (Eq. 5.2)

5.1.2 Initial Condition

The other limitation of Staged Rapid Drawdown analysis in SLOPE/W is that the horizontal seismic coefficient (k_h) is applied in the first stage of the analysis, which does not represent the initial condition of the scenario. In the "Staged Pseudo-static analysis: Undrained Strengths (Duncan et al., 1990)" analysis mode, the k_h is not applied in the

first stage and is therefore more accurate. The following analyses were performed to compare the results in FS between the two analysis modes: water level is at 162 m and piezometric line is used as PWP.

The results for the upstream shallow failure surface and deep failure surface are as shown in tables 5.3 and 5.4 respectively. The ratio is calculated by the FS of the Staged Pseudo-static analysis divided by the FS of the Staged Rapid Drawdown analysis.

Table 5.3. Factors of safety from the staged pseudo-static analysis and staged rapid drawdown analysis (shallow failure surface).

k_h	Factor of Safety		Ratio
	Staged Pseudo-static analysis	Staged Rapid Drawdown analysis	
0.00	1.82	1.84	0.991
0.025	1.63	1.64	0.995
0.0375	1.55	1.56	0.997
0.05	1.48	1.48	0.999
0.0625	1.41	1.41	1.001
0.075	1.35	1.35	1.004
0.10	1.24	1.23	1.008
0.15	1.07	1.05	1.019
0.20	0.943	0.908	1.039
0.30	0.757	0.699	1.083

From tables 5.3 and 5.4, there is a discrepancy in FS between the two modes of analysis. The maximum difference is 8% for $k_h = 0.3$ in shallow failure mode, followed by 7.5% $k_h = 0.15$ and 0.2 in deep failure mode. In the k_h range particularly relevant to this research (0.05–0.1), the difference does not exceed 5.2%. These ratios will be used as correction in the next stage of analysis. The k_h is plotted against the ratio as shown in Fig 5.2.

Table 5.4. Factors of safety from the staged pseudo-static analysis and staged rapid drawdown analysis (deep failure surface).

k_h	Factor of Safety		Ratio
	Staged Pseudo-static analysis	Staged Rapid Drawdown analysis	
0.00	1.89	1.91	0.991
0.025	1.64	1.67	0.983
0.0375	1.54	1.57	0.977
0.05	1.45	1.49	0.970
0.0625	1.37	1.42	0.965
0.075	1.30	1.35	0.958
0.10	1.17	1.24	0.947
0.15	0.985	1.07	0.925
0.20	0.849	0.918	0.925
0.30	0.665	0.691	0.962

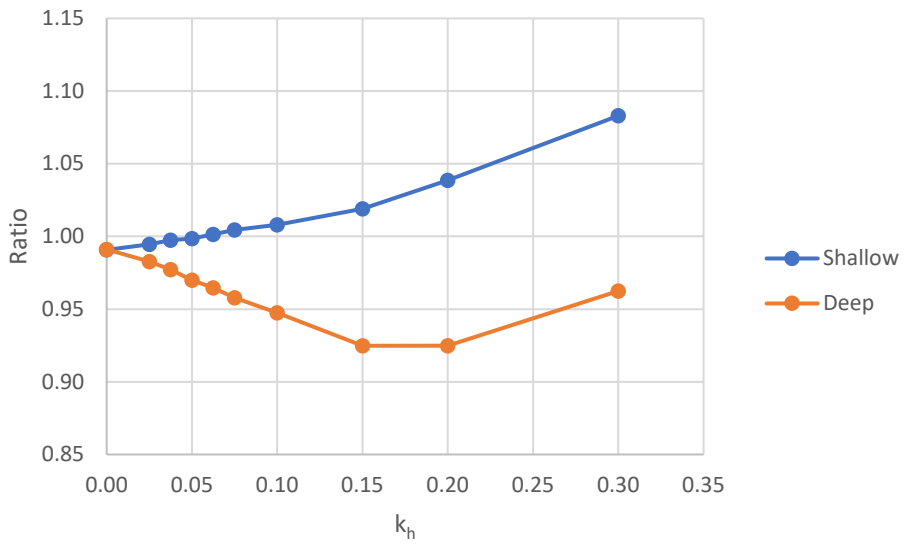

Fig. 5.2 k_h vs. staged pseudo-static analysis to staged rapid drawdown analysis factor of safety ratio.

No corrections are required for the downstream failure mode because there is no significant seepage on the downstream side.

5.2 Staged Rapid Drawdown Analysis

The levels of drawdown in this analysis are from 0 to 50 m, at 5 m intervals. Each level is analyzed using the "Staged Rapid Drawdown analysis (Duncan et al., 1990)" settings with horizontal seismic coefficients of 0, 0.025, 0.0375, 0.05, 0.0625, 0.075, 0.10, 0.15, 0.20, and 0.30. This process is to achieve the critical slip surface and the factor of safety in each condition for all three modes of slope failure (upstream shallow failure, upstream deep failure, and downstream failure). The abovementioned corrections are applied to the factors of safety to attain the most accurate value possible. Tables 5.5, 5.6, and 5.7 show the results of the analyses. Fig. 5.3 and 5.4 show the plot of k_h vs. factors of safety for shallow failure and deep failure respectively.

Table 5.5. Factors of safety for upstream shallow failure surface in each drawdown level and horizontal seismic coefficient.

k_h	Factors of Safety for Each Drawdown Level (Shallow Failure)										
	0m	5m	10m	15m	20m	25m	30m	35m	40m	45m	50m
0.00	2.10	1.90	1.71	1.56	1.46	1.37	1.29	1.23	1.19	1.18	1.18
0.025	1.87	1.70	1.56	1.45	1.34	1.26	1.20	1.15	1.11	1.10	1.11
0.0375	1.77	1.63	1.50	1.39	1.30	1.22	1.16	1.12	1.08	1.07	1.08
0.05	1.69	1.56	1.44	1.34	1.25	1.18	1.12	1.09	1.05	1.05	1.05
0.0625	1.61	1.49	1.39	1.30	1.22	1.15	1.09	1.05	1.03	1.02	1.03
0.075	1.55	1.44	1.34	1.25	1.18	1.12	1.06	1.03	1.01	1.00	1.01
0.10	1.42	1.33	1.25	1.17	1.11	1.05	1.01	0.97	0.96	0.96	0.96
0.15	1.23	1.16	1.10	1.04	0.99	0.95	0.91	0.88	0.87	0.87	0.87
0.20	1.08	1.03	0.98	0.94	0.90	0.86	0.83	0.81	0.79	0.79	0.79
0.30	0.87	0.84	0.81	0.78	0.75	0.73	0.71	0.69	0.69	0.68	0.68

Table 5.6. Factors of safety for upstream deep failure surface in each drawdown level and horizontal seismic coefficient.

k_h	Factors of Safety for Each Drawdown Level (Deep Failure)										
	0m	5m	10m	15m	20m	25m	30m	35m	40m	45m	50m
0.00	2.27	2.18	2.10	2.02	1.94	1.86	1.79	1.71	1.63	1.57	1.52
0.025	1.95	1.89	1.83	1.77	1.70	1.64	1.58	1.53	1.47	1.42	1.37
0.0375	1.83	1.77	1.72	1.67	1.61	1.56	1.51	1.46	1.41	1.36	1.31
0.05	1.72	1.67	1.63	1.58	1.53	1.48	1.44	1.39	1.35	1.30	1.26
0.0625	1.62	1.59	1.54	1.50	1.46	1.42	1.37	1.33	1.29	1.25	1.21
0.075	1.54	1.51	1.47	1.43	1.40	1.35	1.32	1.28	1.24	1.21	1.17
0.10	1.39	1.37	1.34	1.31	1.28	1.25	1.22	1.18	1.15	1.12	1.09
0.15	1.17	1.16	1.14	1.12	1.10	1.07	1.05	1.03	1.01	0.99	0.96
0.20	1.01	1.00	0.98	0.97	0.95	0.93	0.92	0.90	0.89	0.87	0.85
0.30	0.79	0.78	0.78	0.77	0.76	0.75	0.74	0.73	0.72	0.71	0.70

Table 5.7. Factors of safety for downstream failure surface in each horizontal seismic coefficient.

k_h	Factors of Safety
0	1.74
0.025	1.62
0.0375	1.57
0.05	1.52
0.0625	1.48
0.075	1.43
0.10	1.35
0.15	1.21
0.20	1.09
0.30	0.909

The downstream slope factors of safety are not affected by the drawdown level.

The general shapes of the slip surface for upstream shallow failure, upstream deep failure, and downstream failure are as shown in Fig. 5.5, 5.6, and 5.7 respectively.

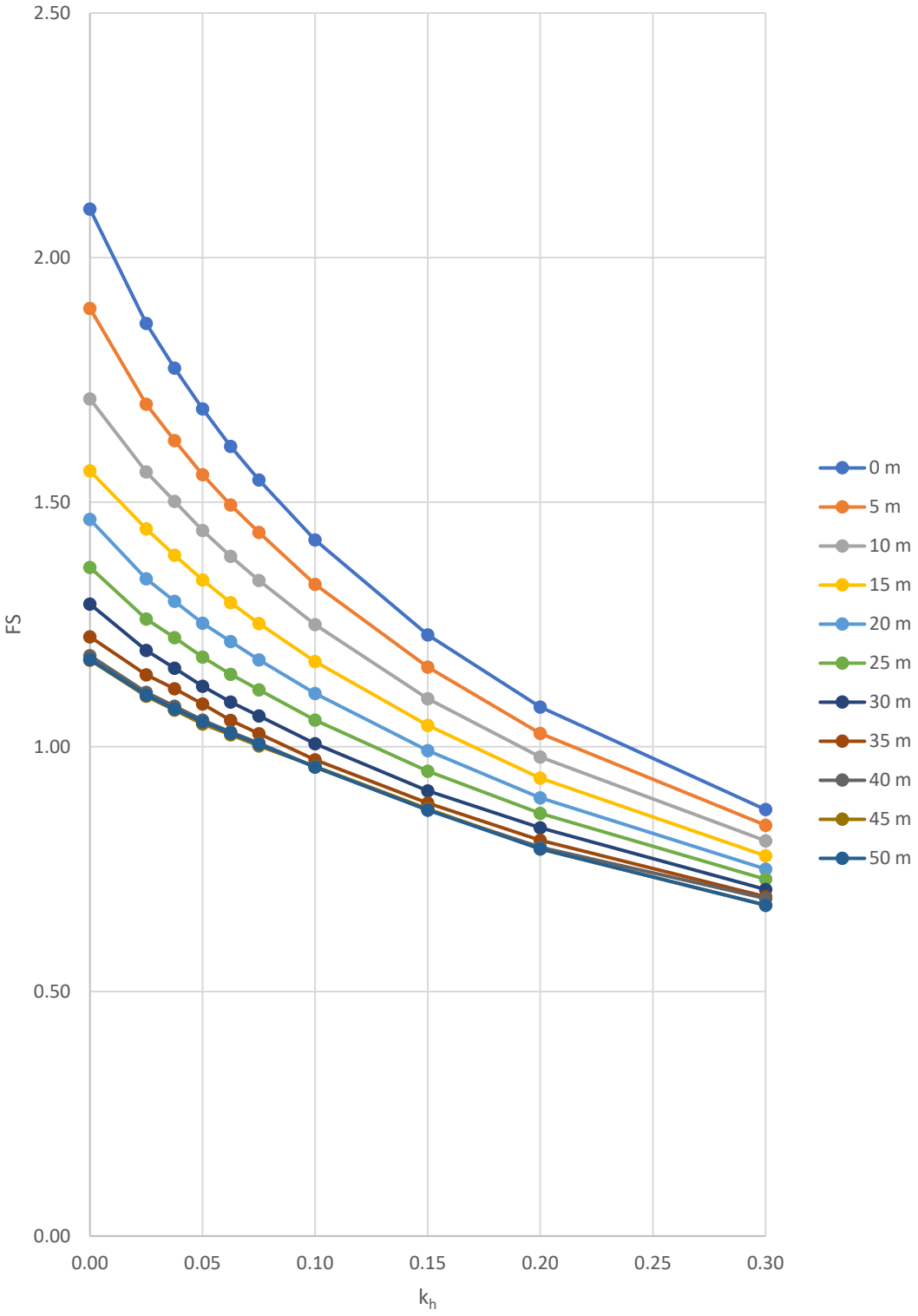

Fig. 5.3 k_h vs. factor of safety for shallow failure in each depth of drawdown.

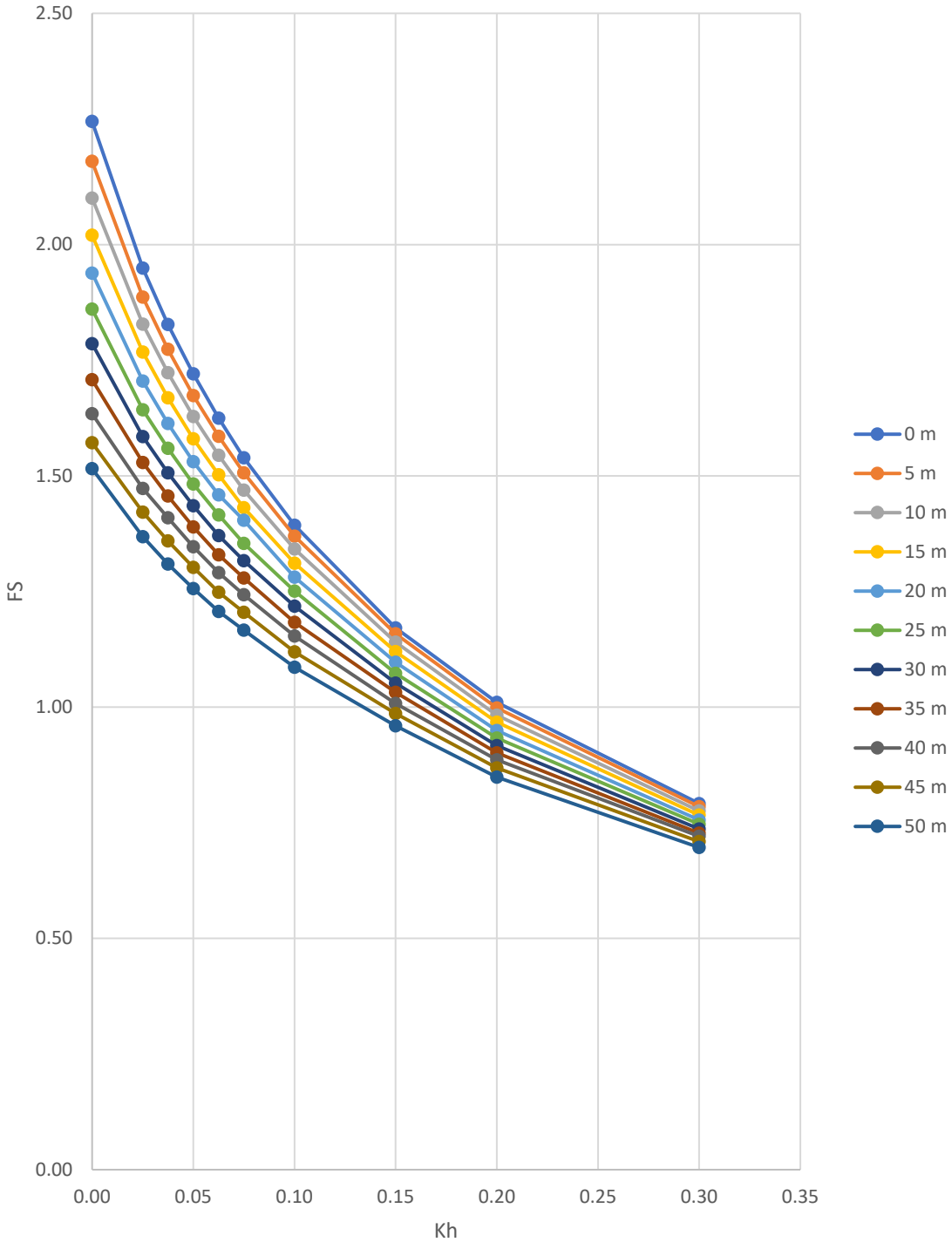

Fig. 5.4 k_h vs. factor of safety for deep failure in each depth of drawdown.

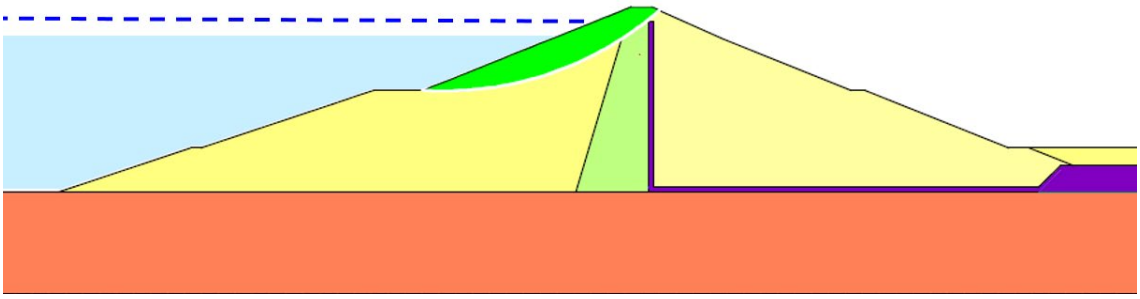

Fig. 5.5 Slip surface of typical upstream shallow failure for 10 m drawdown and k_h = 0.05.

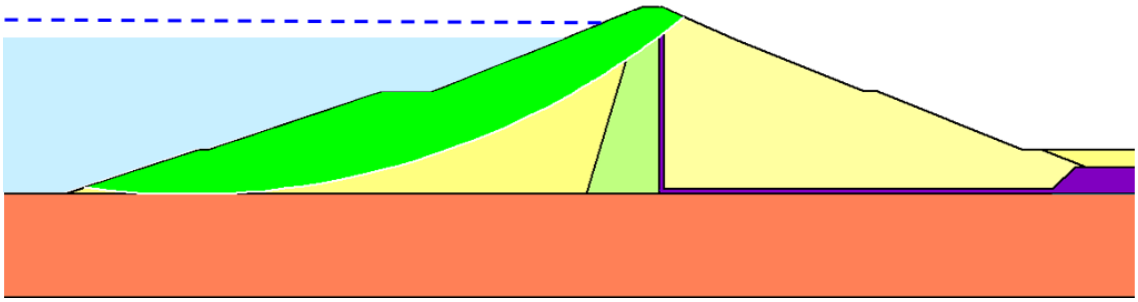

Fig. 5.6 Slip surface of typical upstream deep failure for 10 m drawdown and k_h = 0.05.

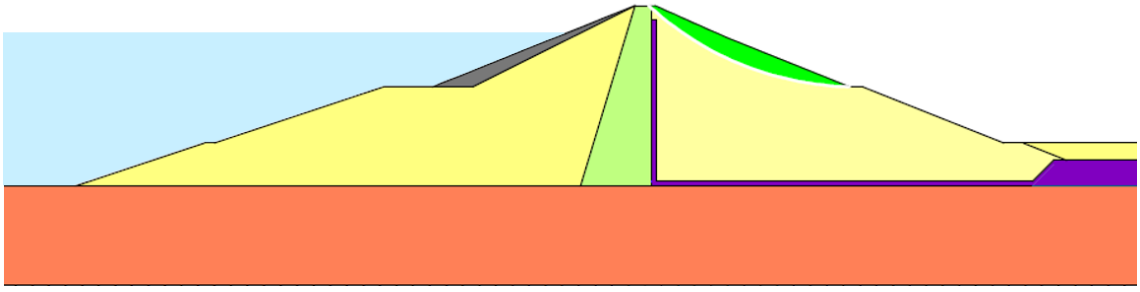

Fig. 5.7 Slip surface of typical downstream failure for k_h = 0.05.

The upstream slope factors of safety can be presented in two ways: each drawdown level and each seismic coefficient value. Fig. 5.8–5.18 show the plot of k_h vs. factors of safety for each level of drawdown for the upstream slope.

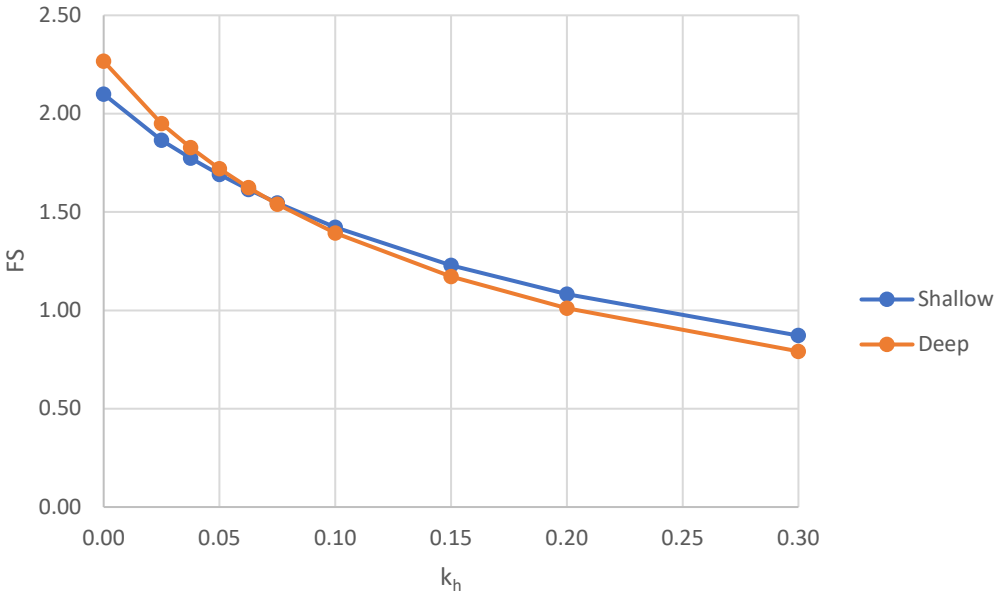

Fig. 5.8 k_h vs. factors of safety for 0 m drawdown (upstream slope).

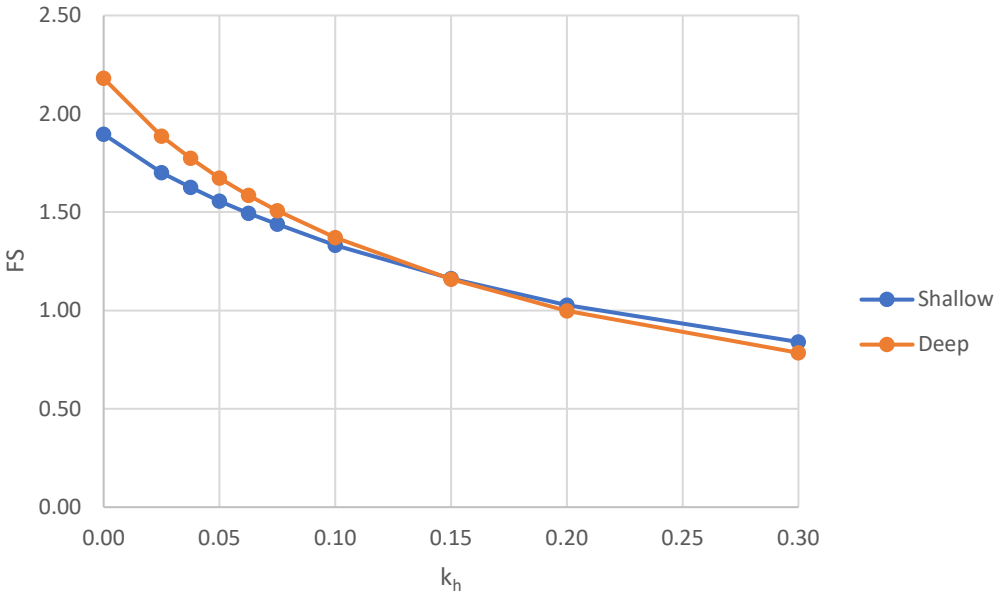

Fig. 5.9 k_h vs. factors of safety for 5 m drawdown (upstream slope).

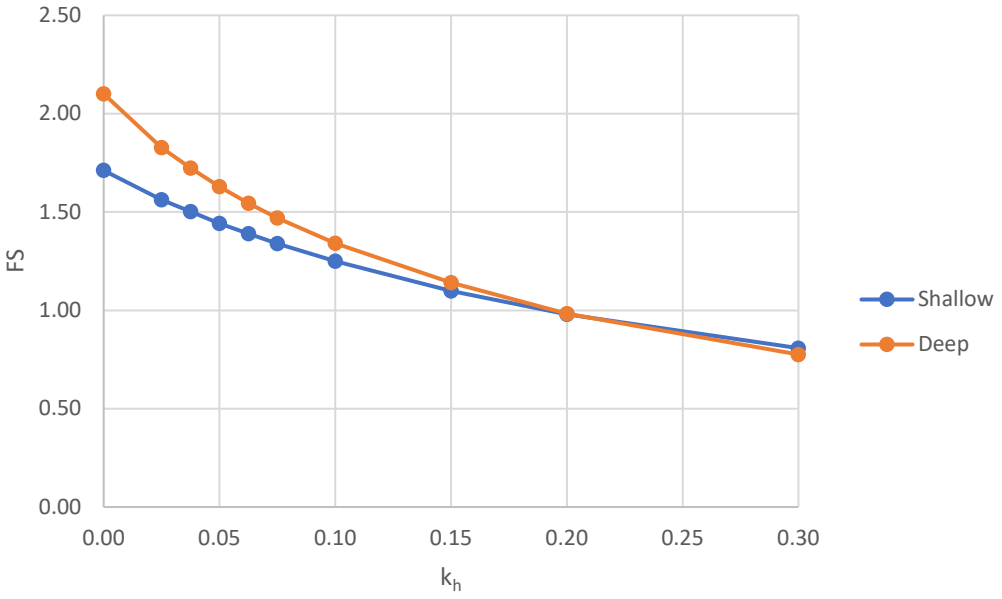

Fig. 5.10 k_h vs. factors of safety for 10 m drawdown (upstream slope).

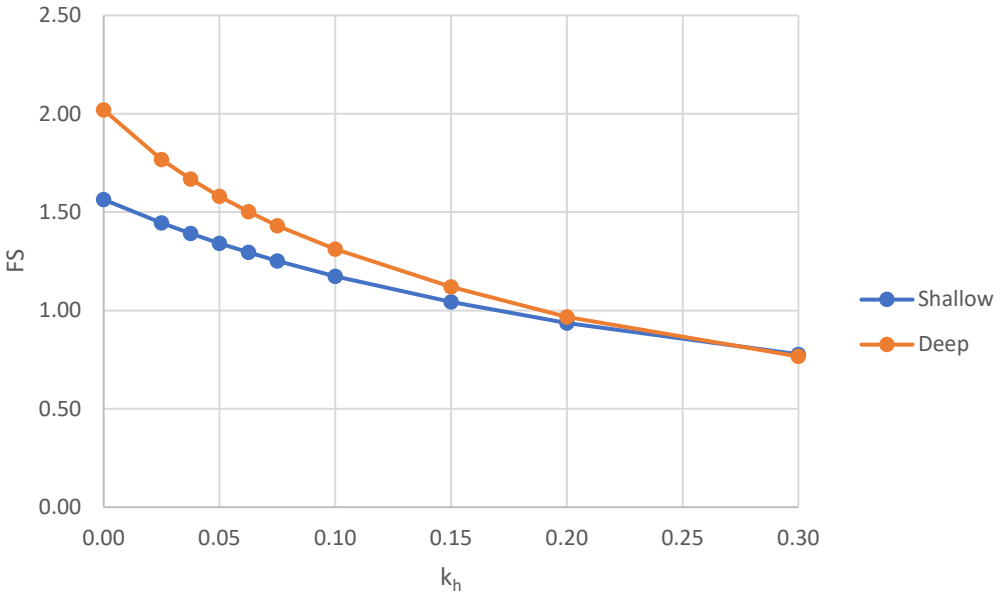

Fig. 5.11 k_h vs. factors of safety for 15 m drawdown (upstream slope).

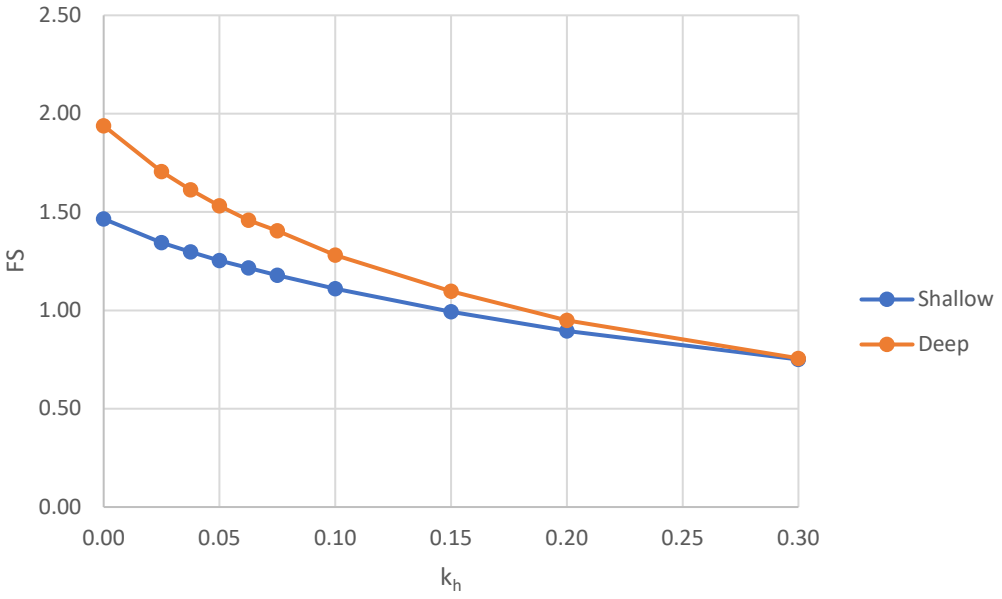

Fig. 5.12 k_h vs. factors of safety for 20 m drawdown (upstream slope).

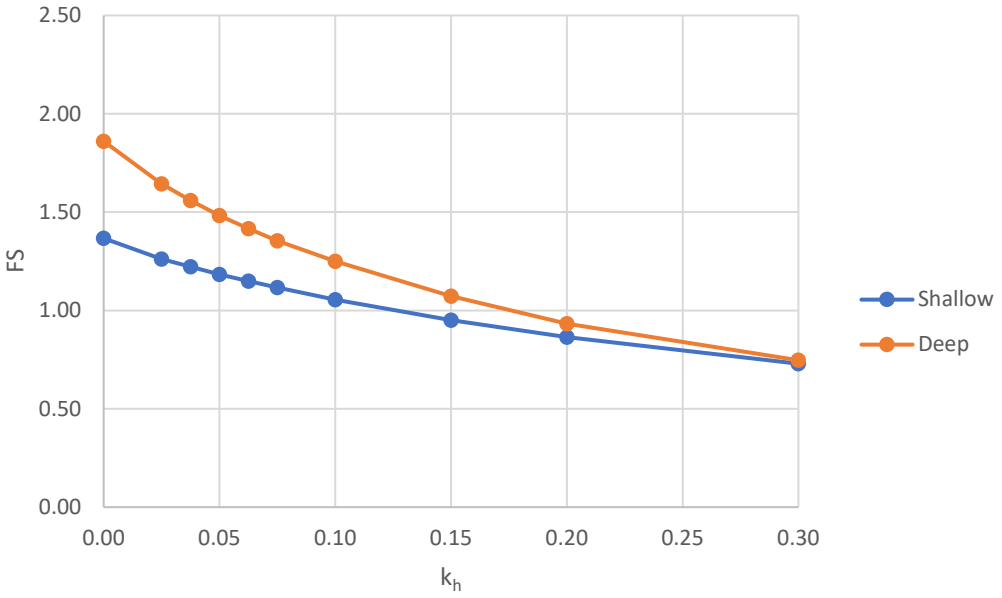

Fig. 5.13 k_h vs. factors of safety for 25 m drawdown (upstream slope).

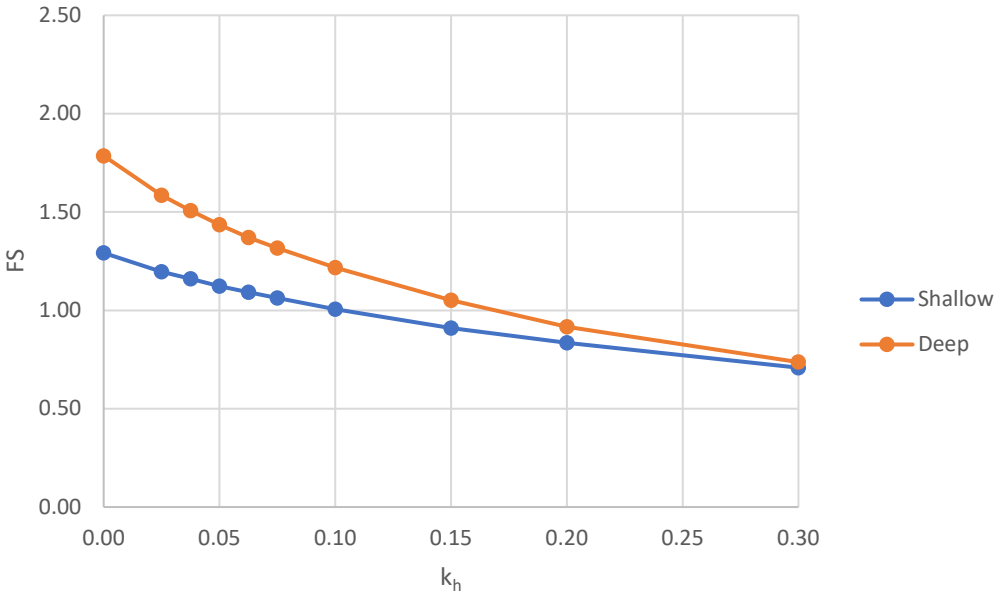

Fig. 5.14 k_h vs. factors of safety for 30 m drawdown (upstream slope).

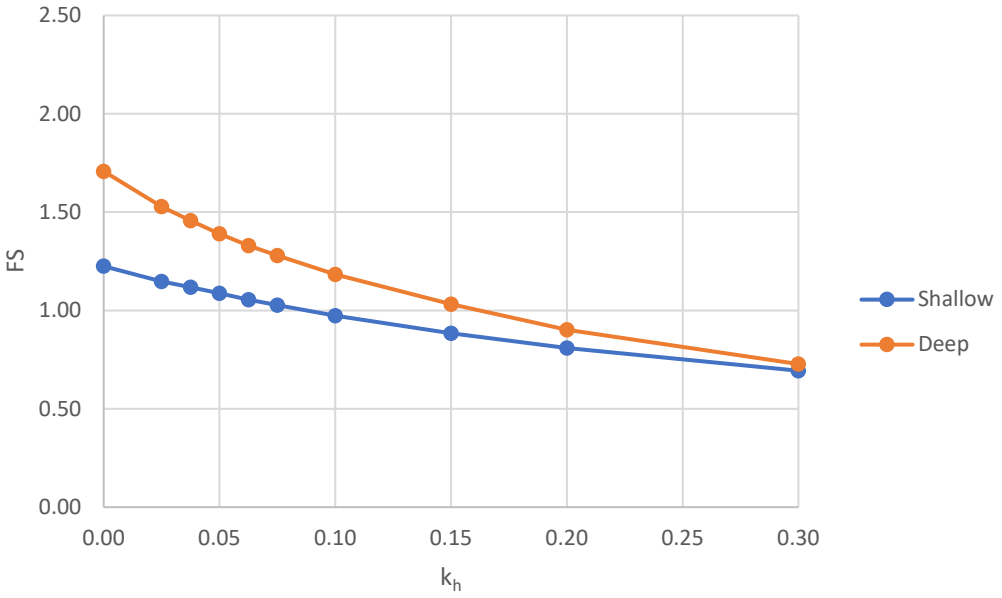

Fig. 5.15 k_h vs. factors of safety for 35 m drawdown (upstream slope).

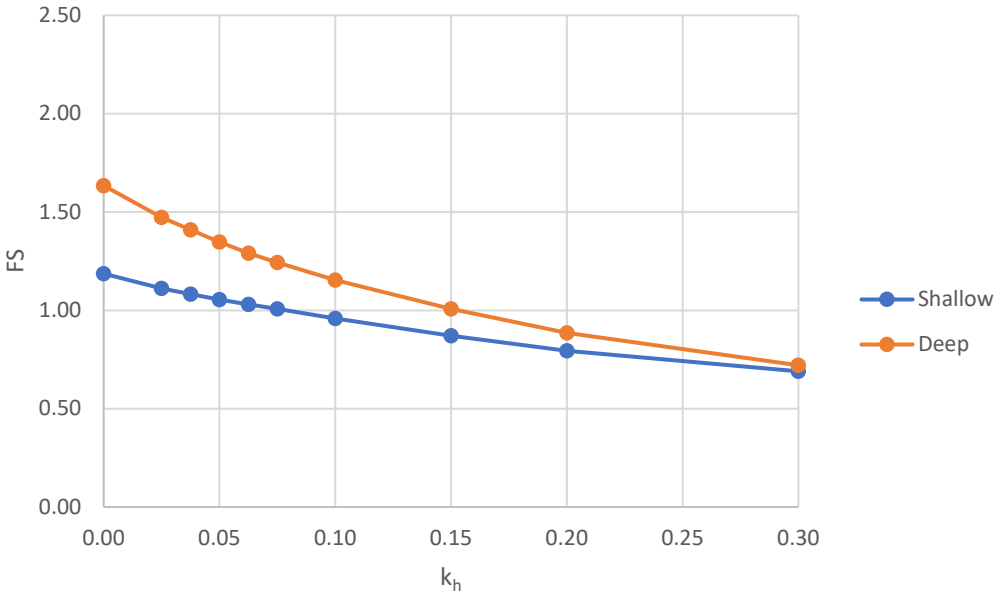

Fig. 5.16 k_h vs. factors of safety for 40 m drawdown (upstream slope).

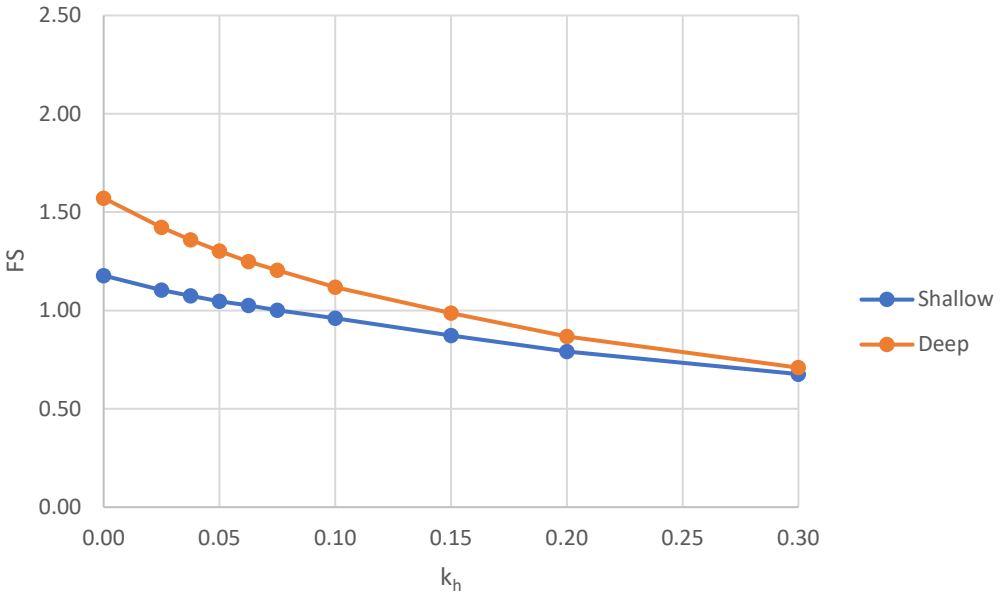

Fig. 5.17 k_h vs. factors of safety for 45 m drawdown (upstream slope).

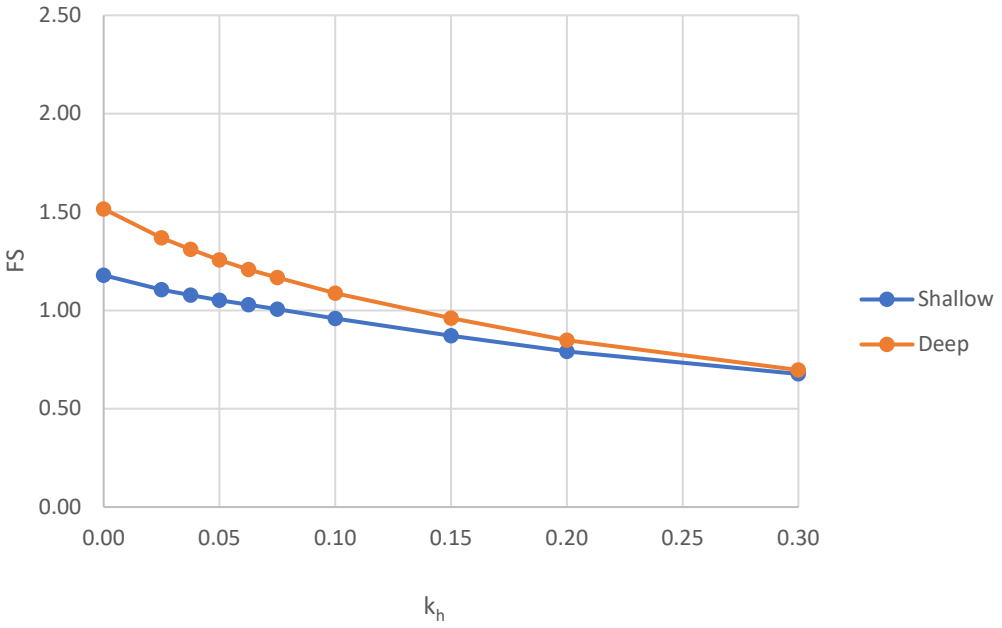

Fig. 5.18 k_h vs. factors of safety for 50 m drawdown (upstream slope).

From Fig. 5.8–5.18, shallow failure has the critical factor of safety for most scenarios. The exceptions are those in the lesser depths of drawdown level with large k_h (0 m drawdown with 0.10–0.30 k_h, 5 m drawdown with 0.20–0.30 k_h, 10 m and 15 m drawdown with 0.03 k_h). In those cases, the differences are not significant. It is reasonable to conclude that for each level of drawdown at SRK Dam, upstream shallow failure is the critical failure mode. Furthermore, the seismic coefficient which represents the earthquake shaking has an impact on the factor of safety. Fig. 5.8–5.18 show that as the k_h value increases, the FS value decreases.

The results can be analyzed by presenting them according to each seismic coefficient value. Fig. 5.19–5.28 show the plot of levels of drawdown vs. factors of safety for each seismic coefficient.

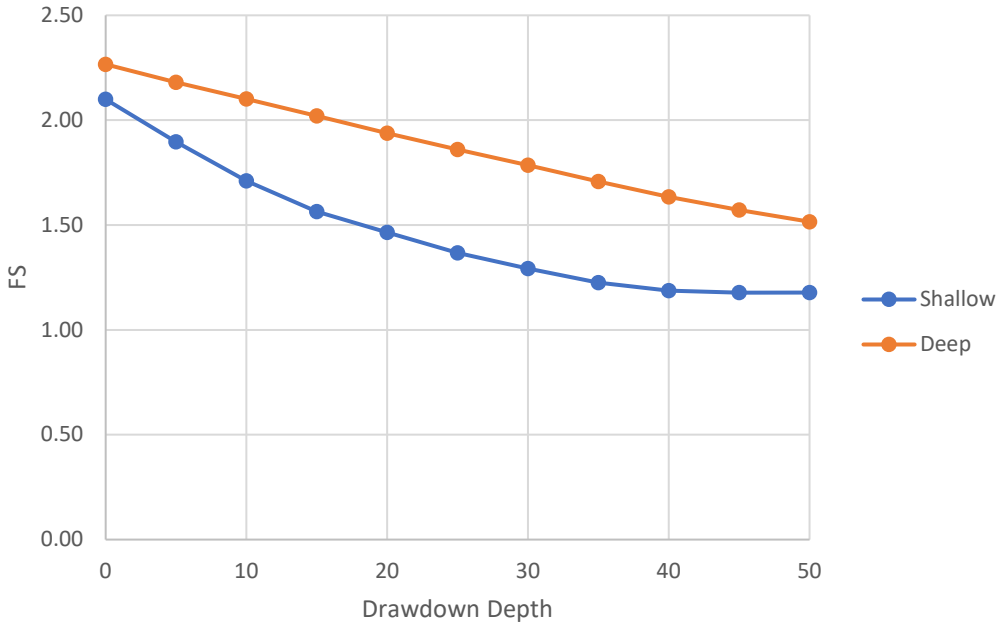

Fig. 5.19 Level of drawdown vs. factors of safety for k_h = 0 (upstream slope).

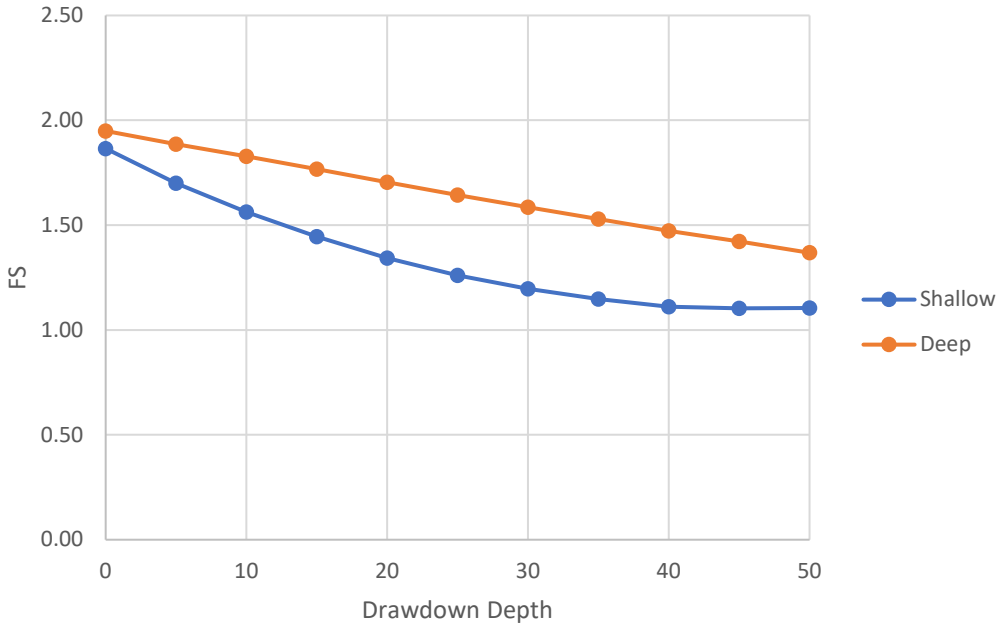

Fig. 5.20 Level of drawdown vs. factors of safety for k_h = 0.025 (upstream slope).

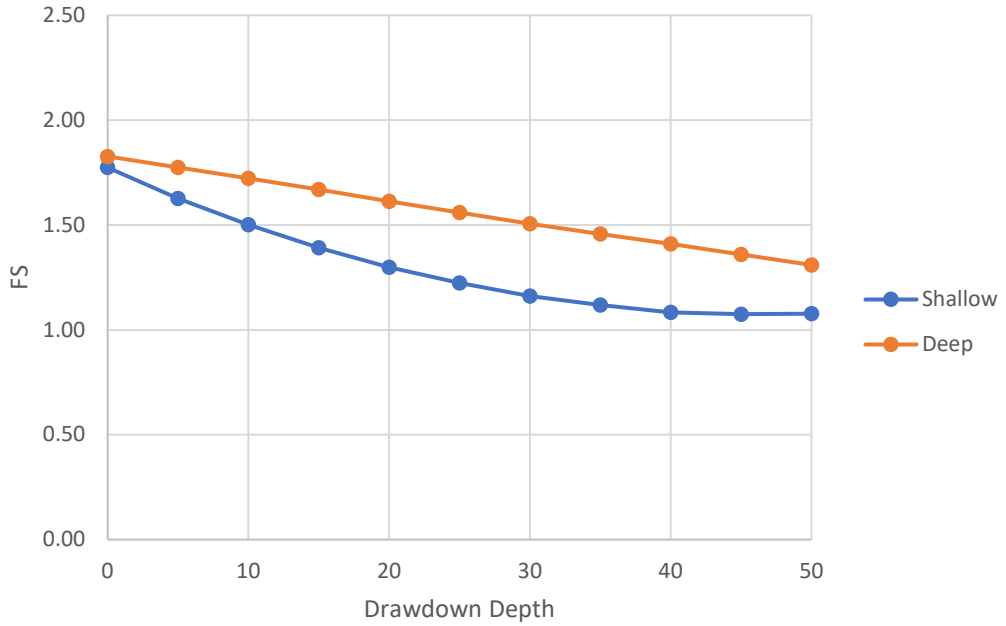

Fig. 5.21 Level of drawdown vs. factors of safety for k_h = 0.0375 (upstream slope).

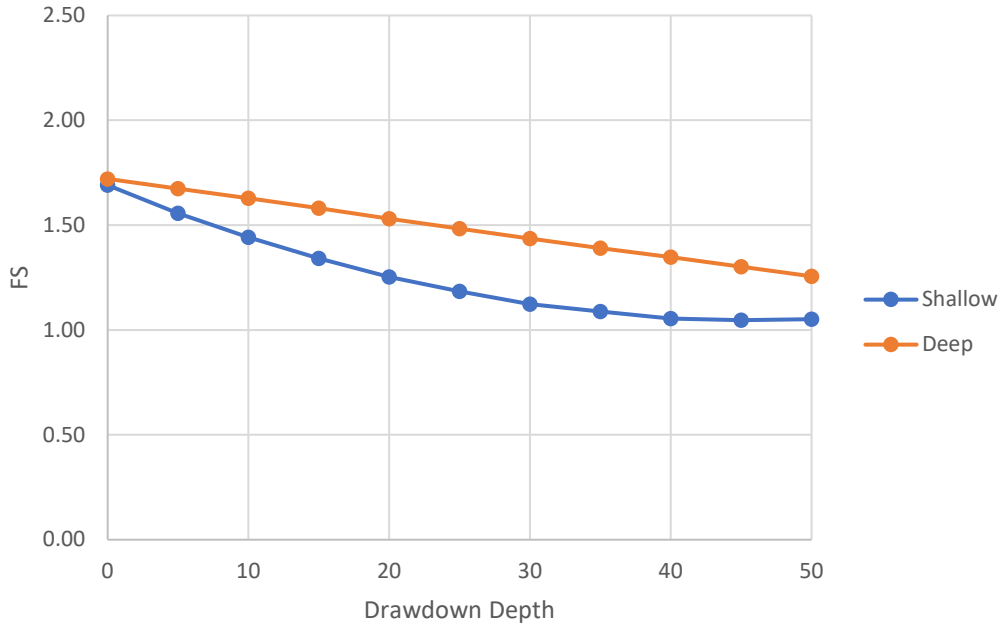

Fig. 5.22 Level of drawdown vs. factors of safety for k_h = 0.05 (upstream slope).

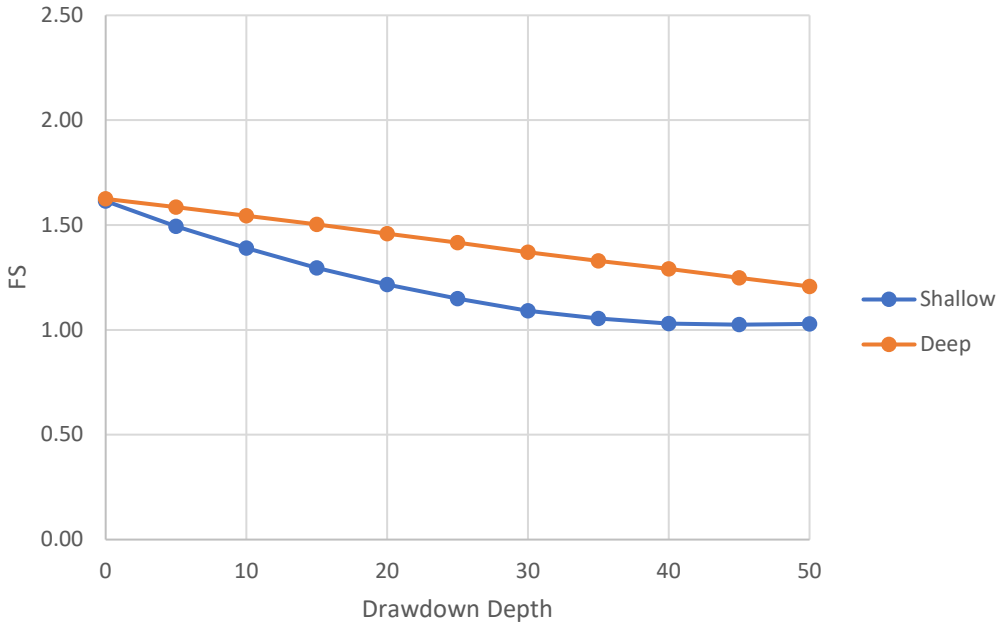

Fig. 5.23 Level of drawdown vs. factors of safety for k_h = 0.0625 (upstream slope).

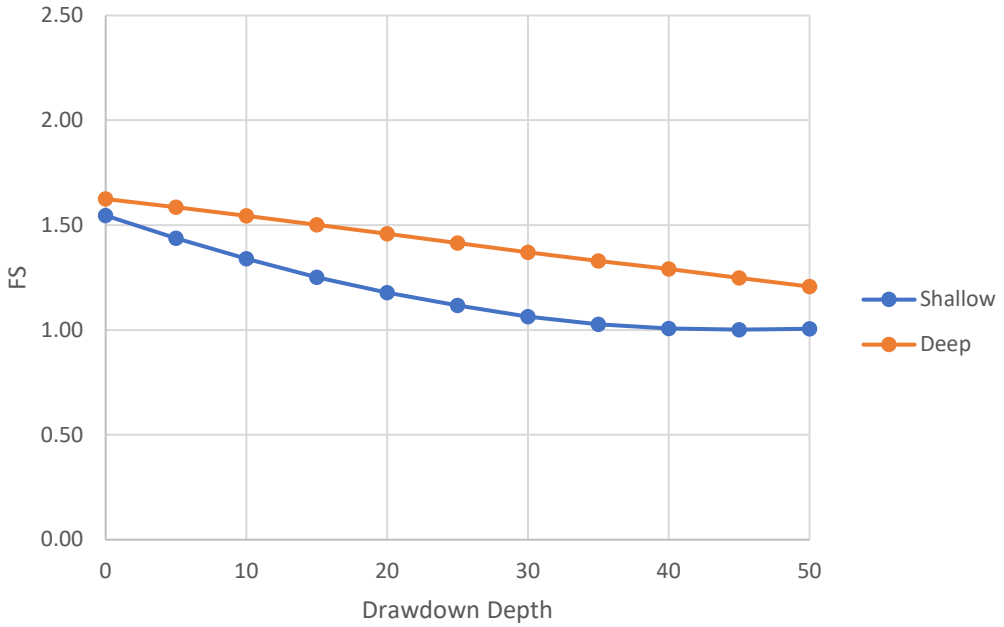

Fig. 5.24 Level of drawdown vs. factors of safety for k_h = 0.075 (upstream slope).

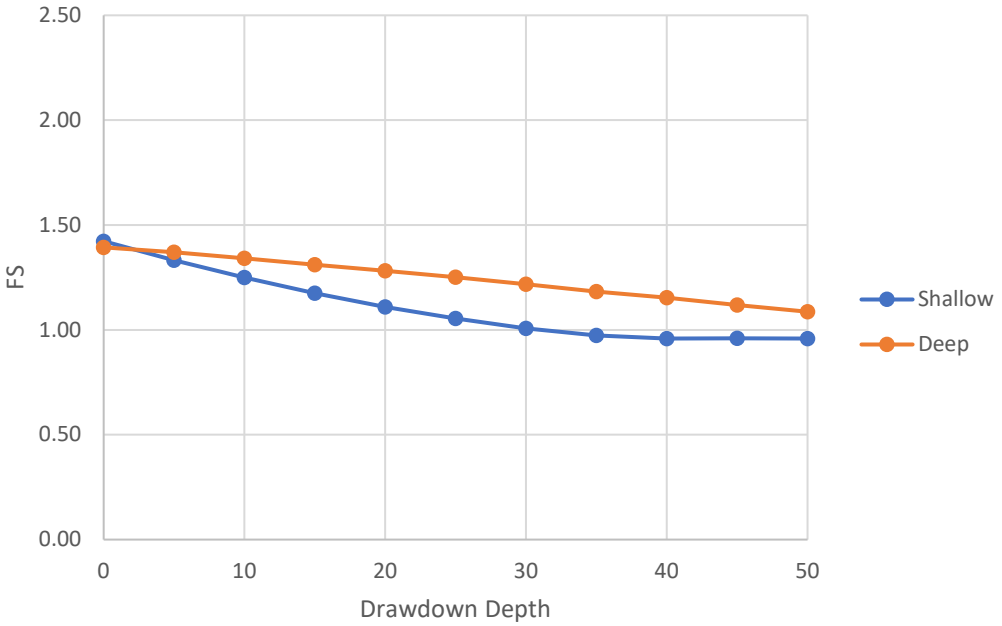

Fig. 5.25 Level of drawdown vs. factors of safety for k_h = 0.1 (upstream slope).

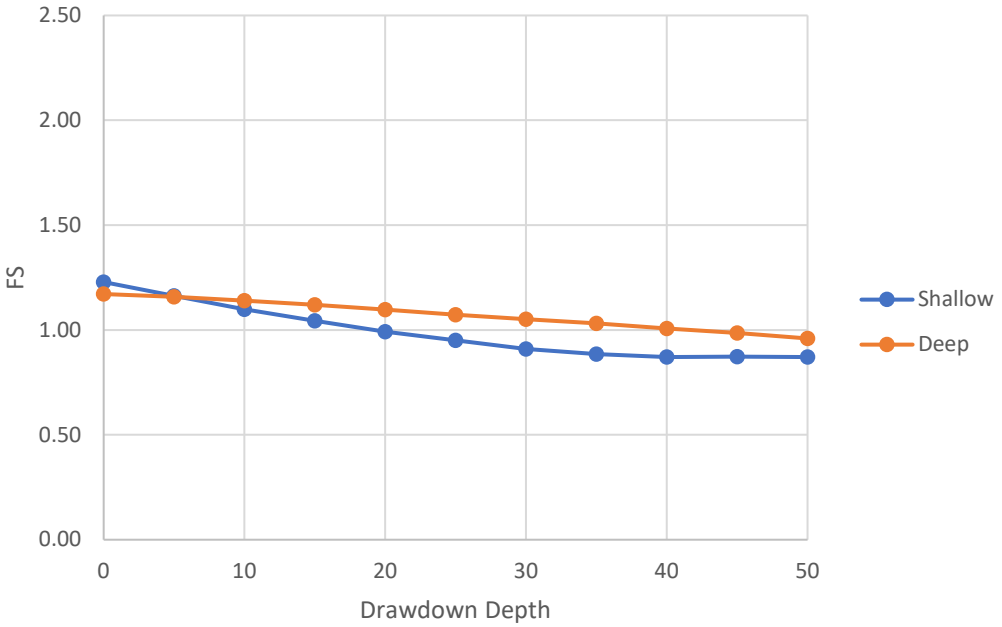

Fig. 5.26 Level of drawdown vs. factors of safety for k_h = 0.15 (upstream slope).

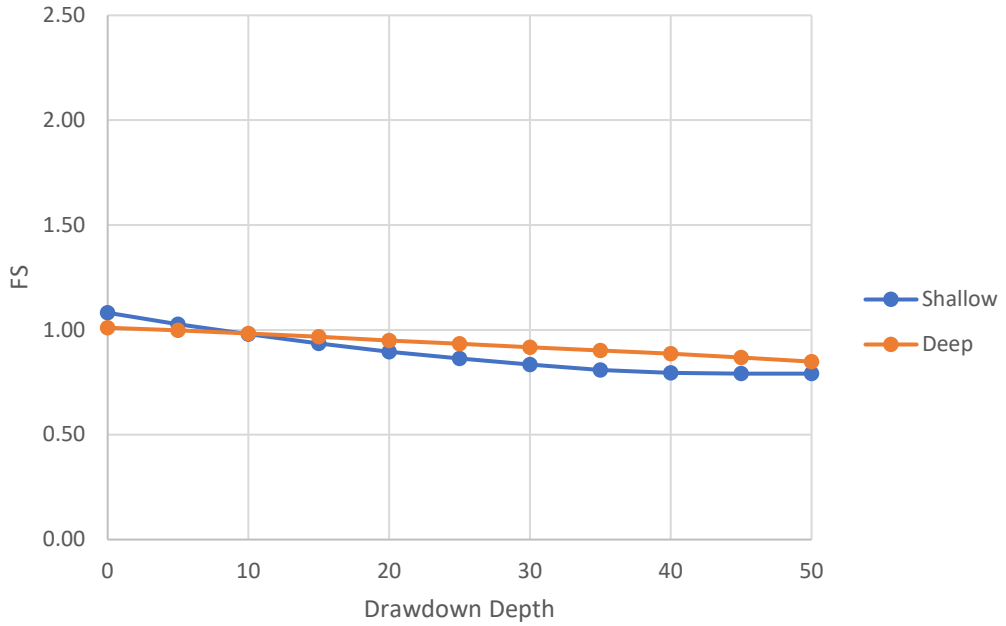

Fig. 5.27 Level of drawdown vs. factors of safety for k_h = 0.20 (upstream slope).

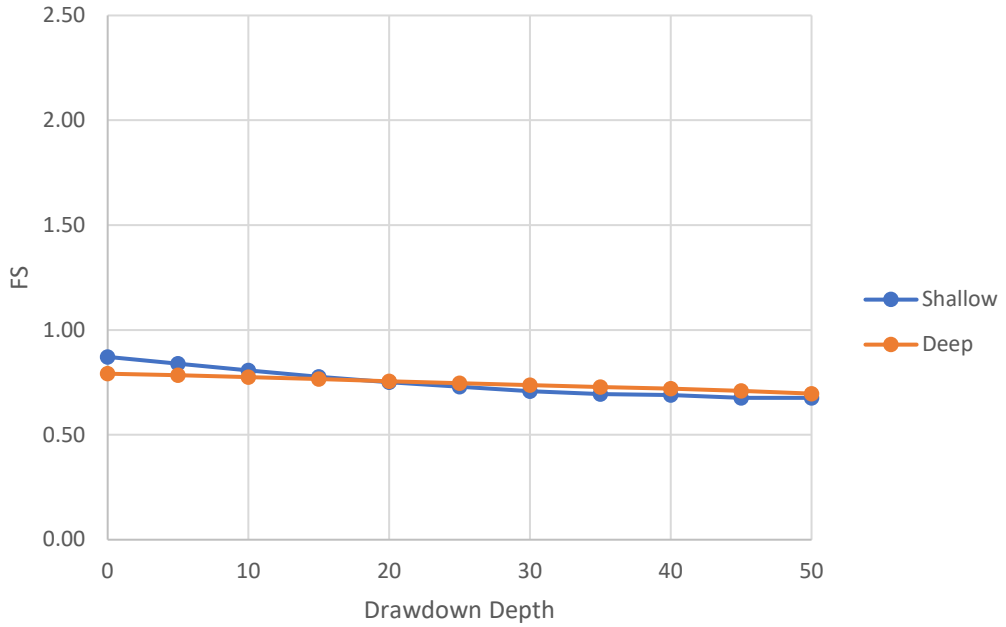

Fig. 5.28 Level of drawdown vs. factors of safety for k_h = 0.30 (upstream slope).

From Fig. 5.19–5.28, the majority of critical FS are those of shallow failure surface. The exceptions are those in the higher k_h with lower drawdown depths. The FS for shallow failure surface level out at 40–50 m because the upstream +120m MSL berm is the controlling factor. The differences in FS values of shallow and deep failure decrease as the seismic coefficient increases. Notably in the case of k_h = 0.30, the FS from both failure modes virtually match for all drawdown depths. It is important to also recognize that increased depth of drawdown results in decreased factors of safety. Overall, the shallow slip surface is the critical failure for each horizontal seismic coefficient analysis.

A visible damage on the dam crest will likely prompt dam operators to lower the reservoir level. A tension crack with a depth of 3 m is put into the model to simulate the damage that maybe cause by a main shock on the dam crest as shown in Fig. 5.29. This analysis is to determine the crack's effect on slope stability

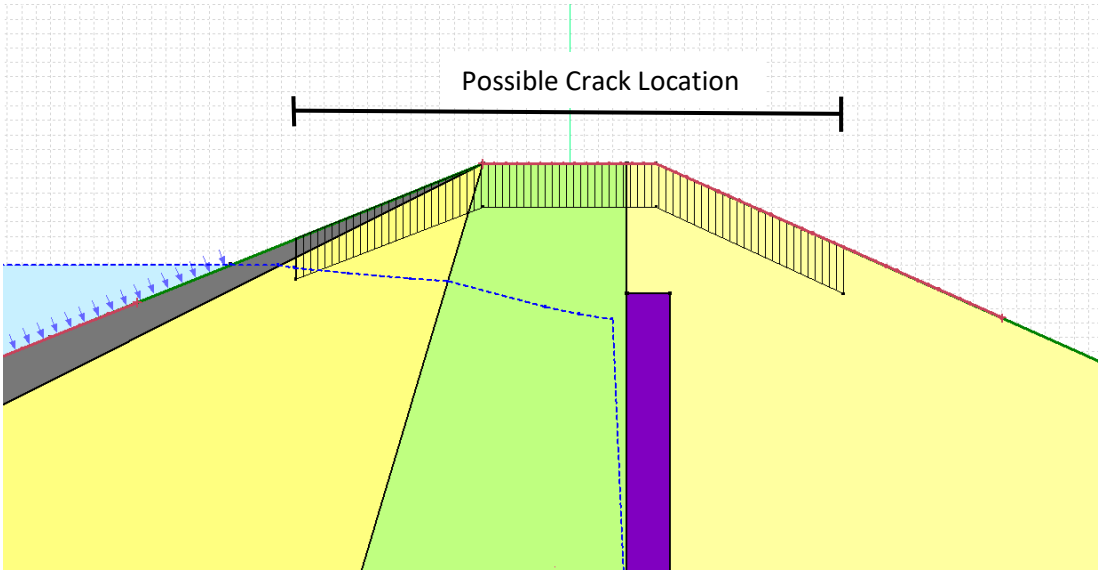

Fig. 5.29 Range of possible tension crack location on the dam model in GeoStudio.

The slope stability results from the model with and without tension crack for 0 m drawdown are compared in table 5.8.

Table 5.8. Upstream shallow failure analysis results of SRK dam with tension crack and without tension crack for 0 m drawdown depth.

k_h	Factor of Safety	
	Without Tension Crack	With Tension Crack
0	2.099	2.104
0.025	1.865	1.867
0.0375	1.774	1.775
0.05	1.691	1.692
0.0625	1.614	1.615
0.075	1.546	1.547
0.10	1.423	1.423
0.15	1.229	1.230
0.20	1.082	1.081
0.30	0.872	0.862

The slope stability results from the model with and without tension crack for k_h = 0.05 are compared in table 5.9.

Table 5.9. Upstream shallow failure analysis results of srk dam with tension crack and without tension crack for k_h = 0.05.

Drawdown (m)	Factor of Safety	
	Without Tension Crack	With Tension Crack
0	1.691	1.692
5	1.556	1.557
10	1.442	1.444
15	1.341	1.340
20	1.253	1.253
25	1.184	1.183
30	1.124	1.124
35	1.088	1.083
40	1.055	1.057

A typical slip surface for a dam model with tension crack is shown in Fig. 5.30.

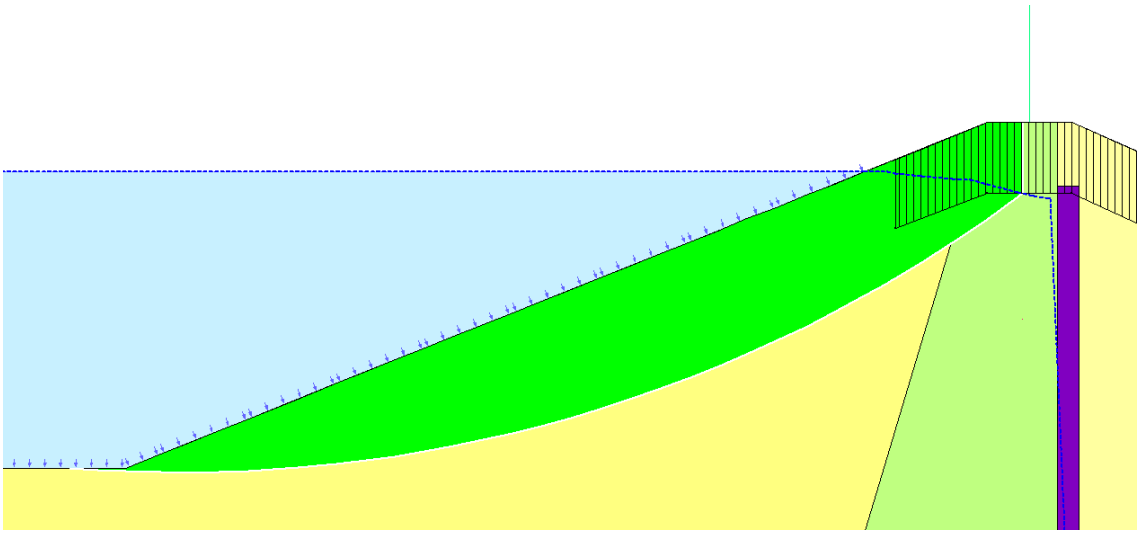

Fig. 5.30 Typical slip surface for dam model with tension crack line on the crest.

While the entry point is mainly controlled by the tension crack line, the overall shape of the slip surface remains the same. Moreover, the safety factor values remain largely the same as the model without the tension crack, with minor differences in the third digit. Therefore, it can be concluded that the 3 m tension crack has little to no effect on the analysis.

5.3 Time for Drawdown at SRK Dam

The above analysis of drawdown covers a wide range of depths but has not yet accounted for time. As calculated in section 3.2.2, the times for SRK Dam materials to be considered 50% drained are 4–20 days for shallow failure and 35–177 days for deep failure. From Fig. 3.9, the maximum possible drawdown depths with the initial reservoir water level of +162 m MSL are shown in table 5.10.

Table 5.10. SRK maximum possible drawdown depth for each rapid drawdown time.

Days	Maximum Possible Drawdown (m)
4	3
20	11
35	20
177	58*

* 58 m of drawdown is when the water level reaches the dead storage

In theory, the reservoir can be drawn down to the dead storage at +104 m MSL. However, in practice there are a number of constraints that do not allow such drastic release of water. As mentioned in section 3.2.3, maximum drawdown is 20 m.

5.4 Results

As discussed in chapter 4, the horizontal seismic coefficient of the largest controlling aftershock is in the range of 0.05 to 0.1. Table 5.11 presents the factors of safety for shallow failure within the mentioned k_h range. Fig. 5.27 shows the plot of drawdown depths vs. factors of safety for shallow failure with k_h = 0.05, 0.0625, 0.075, and 0.1.

For the upstream shallow slip surface, the maximum drawdown depth within the rapid drawdown period is 3–11 m. From table 5.11, the factors of safety in the drawdown range of 0–15 m are all higher than 1.1, which is the minimum required FS for rapid drawdown shallow failures.

Factors of safety for deep failure in the same k_h range are presented in table 5.12. Fig. 5.32 shows the plot of drawdown depths vs. factors of safety for deep failure with k_h = 0.05, 0.0625, 0.075, and 0.1.

Table 5.11. Factors of safety for upstream shallow failure with k_h = 0.05, 0.0625, 0.075, and 0.1.

Drawdown (m)	Factor of Safety			
	k_h = 0.05	k_h = 0.0625	k_h = 0.075	k_h = 0.1
0	1.69	1.61	1.55	1.42
5	1.56	1.49	1.44	1.33
10	1.44	1.39	1.34	1.25
15	1.34	1.30	1.25	1.17
20	1.25	1.22	1.18	1.11
25	1.18	1.15	1.12	1.05
30	1.12	1.09	1.06	1.01
35	1.09	1.05	1.03	0.97
40	1.05	1.03	1.01	0.96
45	1.05	1.02	1.00	0.96
50	1.05	1.03	1.01	0.96

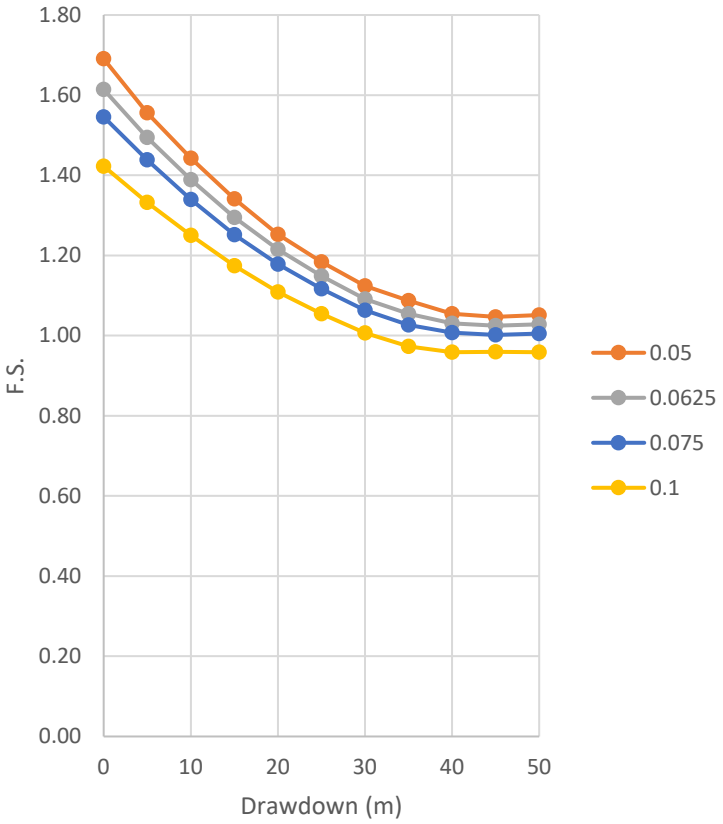

Fig. 5.31 Drawdown depths vs. factors of safety for shallow failure with kh = 0.05, 0.0625, 0.075, and 0.1.

Table 5.12. Factors of safety for upstream deep failure with k_h = 0.05, 0.0625, 0.075, and 0.1.

Drawdown (m)	Factor of Safety			
	k_h = 0.05	k_h = 0.0625	k_h = 0.075	k_h = 0.1
0	1.72	1.62	1.54	1.39
5	1.67	1.59	1.51	1.37
10	1.63	1.54	1.47	1.34
15	1.58	1.50	1.43	1.31
20	1.53	1.46	1.40	1.28
25	1.48	1.42	1.35	1.25
30	1.44	1.37	1.32	1.22
35	1.39	1.33	1.28	1.18
40	1.35	1.29	1.24	1.15
45	1.30	1.25	1.21	1.12
50	1.26	1.21	1.17	1.09

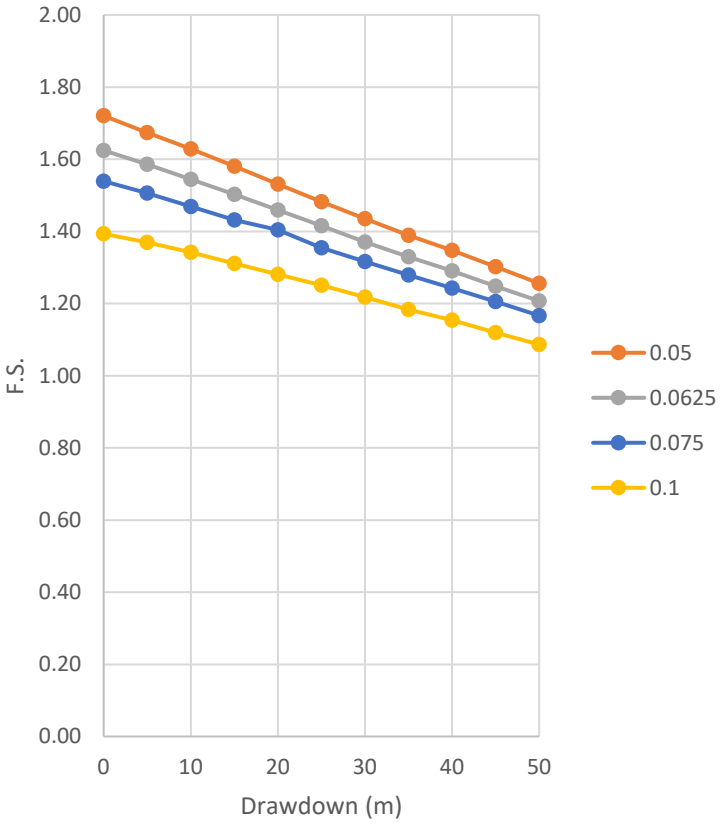

Fig. 5.32 Drawdown depths vs. factors of safety for deep failure with k_h = 0.05, 0.0625, 0.075, and 0.1.

For the upstream deep slip surface, the maximum drawdown depths within the rapid drawdown period is 20 m. From table 5.12, the factors of safety in the drawdown range of 0–20 m are all higher than 1.3, which is the minimum required FS for rapid drawdown deep failures.

The factors of safety for downstream slope in the 0.05–0.1 k_h range are 1.35 and above, as shown in table 5.13. The minimum factor of safety for the downstream slope in case of earthquake is 1.1–1.2.

Table 5.13. Factors of safety of downstream slope with k_h = 0.05, 0.0625, 0.075, and 0.1.

k_h	Factor of Safety
0.05	1.52
0.0625	1.48
0.075	1.43
0.1	1.35

CHAPTER 6

SUMMARY AND CONCLUSIONS

Rapid drawdown and seismic loading both threaten the stability of dams. The main objective of this thesis is to identify if the event of rapid drawdown and earthquake aftershock loading at the same time should be included in risk assessment for embankment dams. Sirikit Dam is used in the analyses. The model was developed in GeoStudio to analyze for the critical factor of safety in various cases of drawdown depths and seismic loadings.

SRK Dam geometry is plotted in the program according to the as-built drawing. The materials descriptions and properties used are a combination of existing data, reasonable estimation, Stark and Hussain's (2013) empirical correlation for drained fully softened secant friction angle, and engineering judgment. The maximum rate of drawdown for SRK reservoir is calculated using the maximum capacity of all water-releasing structures and the minimum rate of reservoir inflow. The time for the dam materials to drain after drawdown is calculated using the first step of the multi-stage rapid drawdown analysis proposed by Duncan, Wright, and Wong (1990). The times for drainage for shallow failure are 4–20 days, which has the maximum drawdown depth in the range of 3–11 m. For deep failure, times for drainage are 35–177 days, with maximum drawdown of 20–58 m. However, the practical level of drawdown based on historical data is 20 m, which can be achieved in 35 days at the quickest. The effect of rapid drawdown is only applicable for the upstream slope.

The seismicity data of the two active faults in the nearby area are from the U.S. Geological Survey (2007), Department of Mineral Resources of Thailand (2011), and Seismological Bureau, Meteorological Department of Thailand (2017). From these data, the maximum moment magnitude of each earthquake source is estimated using Wells and Coppersmith's (1994) empirical relationships between moment magnitude and surface rupture length. Using Båth's (1965) law, the largest aftershock magnitude is estimated. Furthermore, aftershock magnitudes larger than what Båth's law predicts are also considered. Maximum peak ground acceleration (PGA) values are estimated from aftershock magnitudes using the NGA-West2 Ground Motion Prediction Equations (GMPEs) model. Horizontal seismic coefficients are determined and applied in the SLOPE/W slope analysis.

There are some limitations of the GeoStudio functions that causes the resulting factor of safety to be lower than it should be. Therefore, corrections are developed by performing analyses with the same settings and applied to rapid drawdown with seismic coefficient analysis.

The analyses are performed with a range of drawdown from 0 m to 50 m with 5 m intervals. The seismic coefficients are 0, 0.025, 0.0375, 0.05, 0.0625, 0.075, 0.1, 0.15, 0.20, and 0.30. The stability analysis results of the possible rapid drawdown and aftershock scenario for SRK Dam is shown in tables 6.1, 6.2, and 6.3.

The minimum factor of safety for rapid drawdown shallow failure is 1.1. From table 6.1, all factors of safety for SRK Dam's upstream slope are larger than the

Table 6.1. Factors of safety for upstream shallow failure.

Drawdown (m)	Factor of Safety			
	k_h = 0.05	k_h = 0.0625	k_h = 0.075	k_h = 0.1
0	1.69	1.61	1.55	1.42
5	1.56	1.49	1.44	1.33
10	1.44	1.39	1.34	1.25
15	1.34	1.30	1.25	1.17

Table 6.2. Factors of safety for upstream deep failure.

Drawdown (m)	Factor of Safety			
	k_h = 0.05	k_h = 0.0625	k_h = 0.075	k_h = 0.1
0	1.72	1.62	1.54	1.39
5	1.67	1.59	1.51	1.37
10	1.63	1.54	1.47	1.34
15	1.58	1.50	1.43	1.31
20	1.53	1.46	1.40	1.28

Table 6.3. Factors of safety for downstream failure.

Factor of Safety			
k_h = 0.05	k_h = 0.0625	k_h = 0.075	k_h = 0.1
1.52	1.48	1.43	1.35

requirement. For deep failure, the minimum factor of safety is 1.3. From table 6.2, SRK Dam also meets the requirement. The downstream slope, which is not affected by rapid drawdown, has a minimum factor of safety requirement for seismic shaking of 1.2. From table 6.3, SRK downstream slope has a greater factor of safety than the requirement. In conclusion, this research analysis shows that SRK Dam is safe from the largest possible rapid drawdown and aftershock loading at the same time. Additionally, the result does not suggest any modifications to the current large earthquake emergency plan.

However, it is important to note that the data and materials properties used in this research are from reports by others. Reasonable assumptions based upon

geotechnical principles and engineering judgement were made to achieve suitable parameters for the analyses. Further laboratory and field investigation of geometry and material properties are required achieve more accurate factors of safety.

From tables 6.1 and 6.2, the critical slip surface is the shallow failure for all cases. However, the factors of safety for deep failure are not much larger than those for shallow. The deep slip surface is an arguably more dangerous mode of failure. In field conditions, there may be some factors that cause deep failure to mobilize before shallow failure can occur. Therefore, deep failure should always be included in stability analysis of dams even though it may not be the critical mode of failure.

In each level of drawdown depth, the factor of safety decreases as the seismic coefficient increases. Similarly, in each seismic coefficient value, the factor of safety decreases as the drawdown depth increases. It can be concluded that drawdown condition and seismic condition have effects on each other.

Because of the size of the dam and its reservoir, lowering the water level in practice is a slow process. It is very unlikely for SRK Dam to experience rapid drawdown and strong aftershock shaking at the same time. However, the water level of smaller embankment dams can fluctuate significantly. Rapid drawdown coupled with aftershock earthquake loading can be a significant failure mode for smaller dams. Therefore, this mode of failure should be considered for all embankment dams.

Further research may be performed on the actual probability of rapid drawdown and aftershock, scenarios with different initial water level and outflow rate, and the effect of deformation on the dam.

References

Anderson, D. G., Martin, G. R., Lam, I., and Wang, J. N. 2008. "Retaining walls." *Seismic analysis and design of retaining walls, buried structures, slopes, and embankments.* Washington, DC: National Academies Press. 68–95.

Båth, M. 1965. "Lateral inhomogeneities of the upper mantle." *Tectonophysics,* 2 (6), 483–514. https://doi.org/10.1016/0040-1951(65)90003-X.

Bozorgnia, Y., Abrahamson, N. A., Atik, L. A., Ancheta, T. D., Atkinson, G. M., Baker, J. W., Baltay, A., Boore, D. M., Campbell, K. W., Chiou, B. S.-J., Darragh, R., Day, S., Donahue, J., Graves, R. W., Gregor, N., Hanks, T., Idriss, I. M., Kamai, R., Kishida, T., … Youngs, R. 2014. "NGA-West2 research project." *Earthq. Spectra*, 30 (3), 973–987. https://doi.org/10.1193/072113EQS209M

Chandler, R. J., and Skempton, A. W. 1974. "The design of permanent cutting slopes in stiff fissured clays." *Géotechnique*, 24 (4), 457–466. https://doi.org/10.1680/geot.1974.24.4.457.

Civil Maintenance Division, Electricity Generating Authority of Thailand. 2003. *SRK Dam spillway manual.*

Das, B. M. and Sivakugan, N. 2019. "Geotechnical properties of soil." *Principles of foundation engineering,* 9th Ed., Boston, MA: Cengage. 8–67.

Department of Mineral Resources. 2011. *แผ่นดินไหวกับประเทศไทย [Earthquakes and Thailand].*

Department of Mineral Resources. 2016. Active fault zones in Thailand. Accessed March 29, 2021. http://www.dmr.go.th/main.php?filename=fault_en.

Duncan, J. M., Wright, S. G., and Wong, K. S. 1990. "Slope stability during rapid drawdown." In Vol. 2 of *Proc., H. Bolton Seed Memorial Symp.*, 253–272.

Duncan, J. M., Wright, S. G., and Brandon, T. L. 2014. *Soil strength and slope stability,* 2nd Ed., Hoboken, NJ: Wiley.

Earthquake Observation Division, Thai Meteorological Department. n.d. Accessed March 24, 2021. https://earthquake.tmd.go.th/.

Geotechdata. (n.d.). Geotechnical parameters. Accessed March 24, 2021. http://www.geotechdata.info/parameter.

Geotechnical Engineering Research and Development Center, Department of Civil Engineering, Faculty of Engineering, Kasetsart University. 2012. *Stability analysis of SRK Dam under seismic loading report.*

Holtz, R. D., Kovacs, W. D., and Sheahan, T. C. 2013. *An introduction to geotechnical engineering*, 2nd Ed., Upper Saddle River, NJ: Prentice Hall.

Kramer, S. L. 1996. "Seismic hazard analysis." *Geotechnical earthquake engineering*. Upper Saddle River, NJ: Prentice Hall.

Lowe, J. and Karafiath, L. 1960. "Stability of earth dams upon drawdown." In Vol. 2 of *Proc. 1st Pan Am. Conf. Soil Mech. Found. Eng.*, 537–552.

Marcuson, W. F., III. 1981. "Moderator's report for session on 'Earth dams and stability of slopes under dynamic loads.'" In Vol. 3 of *Proc. Int. Conf. on Recent Adv. in Geotech. Earthq. Eng. Soil Dyn*. 1175.

Mesri, G. and Abdel-Ghaffar, M. E. M. 1993. "Cohesion intercept in effective stress-stability analysis." *J. Geotech. Eng.* 119 (8). 1229–1249.

PEER Center. (n.d.). Global Ground Motion Prediction Equations Program. Accessed March 11, 2021. https://apps.peer.berkeley.edu/globalgmpe/home/.

Power, M., Chiou, B., Abrahamson, N., Bozorgnia, Y., Shantz, T., and Roblee, C. 2019. "An overview of the NGA Project." *Earthq. Spectra*, 24 (1), 3–21. https://doi.org/10.1193/1.2894833.

Royal Irrigation Department of Thailand. 1975. *Sirikit Dam report*. Denver, CO: Engineering Consultants.

Seismological Bureau, Meteorological Department. 2017. *Characteristics of seismicity patterns in the Thailand-Laos-Myanmar border region.* Bangkok, Thailand. Accessed March 24, 2021. https://earthquake.tmd.go.th/documents/file/seismo-doc-1492664958.pdf.

Shcherbakov, R. and Turcotte, D. L. 2004. "A modified form of Bath's Law." *B. Seismol. Soc. Am.*, 94, 1968–1975. https://doi.org/10.1785/012003162.

Shcherbakov, R., Turcotte, D., and Rundle, J. 2005. "Aftershock statistics." *Pure Appl. Geophys.,* 162, 1051–1076. https://doi.org/10.1007/s00024-004-2661-8.

Skempton, A. W. (1970). "First time slides in overconsolidated clays." *Géotechnique*, 20 (3), 320–324.

Skempton, A. W. 1977. “Slope stability of cuttings in brown London clay.” In Vol. 3 of *Proc. 9th Int. Conf. Soil Mech. Found. Eng.*, 261–270.

Stark, T. D., Choi, H., and McCone, S. 2005. “Drained shear strength parameters for analysis of landslides.” *J. Geotech. Geoenviron. Eng.,* 131 (5), 575–588.

Stark, T. D. and Hussain, M. (2013). “Empirical correlations: Drained shear strength for slope stability analyses.” *J. Geotech. Geoenviron. Eng.,* 139 (6), 853–862.

Terzaghi, K., Peck, R. B., and Mesri, G. 1996. *Soil mechanics in engineering practice*, 3rd Ed., Upper Saddle River, NJ: Prentice Hall.

U.S. Army Corps of Engineers. 2003. “Design criteria.” *Engineering and design: Slope stability,* Washington, DC, 3-2. Accessed March 24, 2021. https://www.publications.usace.army.mil/Portals/76/Publications/EngineerManuals/EM_1110-2-1902.pdf.

U.S. Department of Interior, Bureau of Reclamation. 2014. “Seepage.” *Design Standards No. 13, Embankment Dams*. Accessed March 24, 2021. https://www.usbr.gov/tsc/techreferences/designstandards-datacollectionguides/finalds-pdfs/DS13-8.pdf.

Petersen, M., Harmsen, S., Mueller, C., Haller, K., Dewey, J., Luco, N., Crone, A., Lidke, D., and Rukstales, K. 2007. *Documentation for the Southeast Asia Seismic Hazard Maps.* Reston, VA: U.S. Geological Survey, U.S. Department of the Interior.

Wells, D., and Coppersmith, K. 1994. “New empirical relationships among magnitude, rupture length, rupture width, rupture area, and surface displacement.” *B. Seismol. Soc. Am.,* 84 (4), 974-1002.

APPENDIX

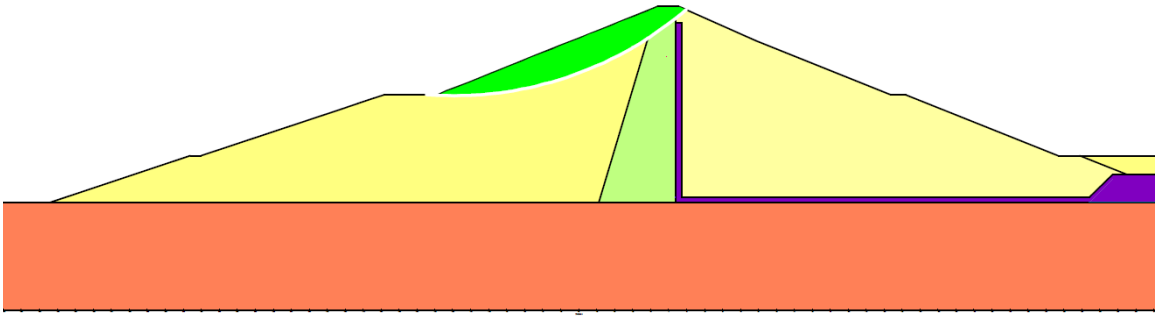

Fig A.1 Slip surface of upstream shallow failure with 0 m. drawdown and k_h = 0.05.

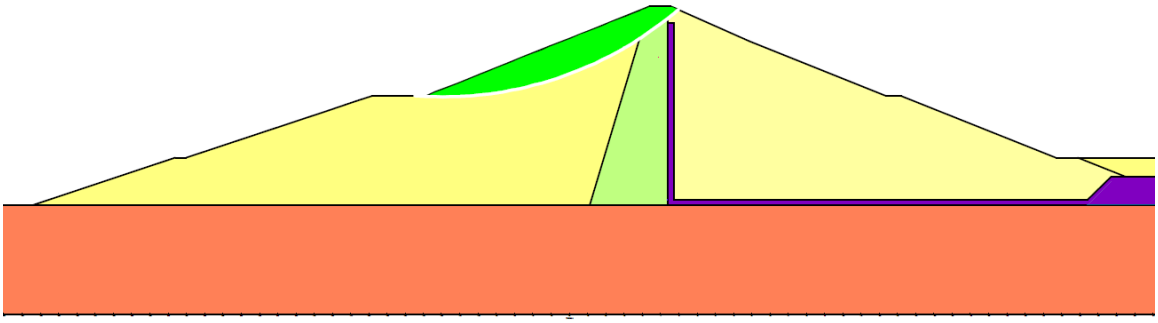

Fig A.2 Slip surface of upstream shallow failure with 0 m. drawdown and k_h = 0.0625.

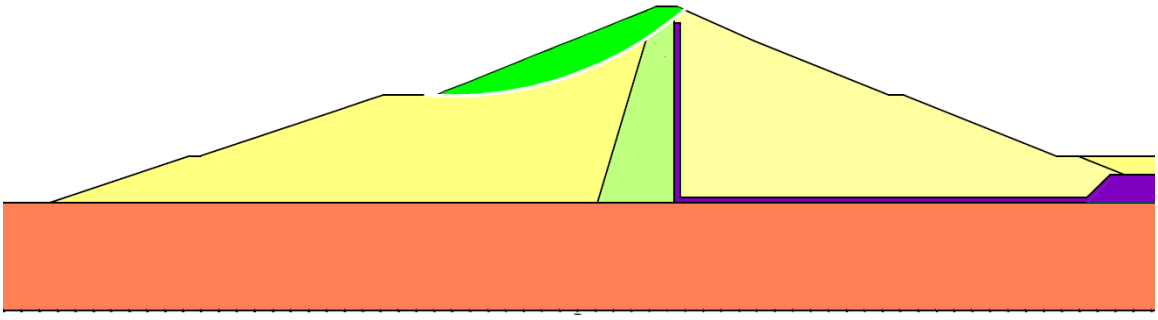

Fig A.3 Slip surface of upstream shallow failure with 0 m. drawdown and k_h = 0.075.

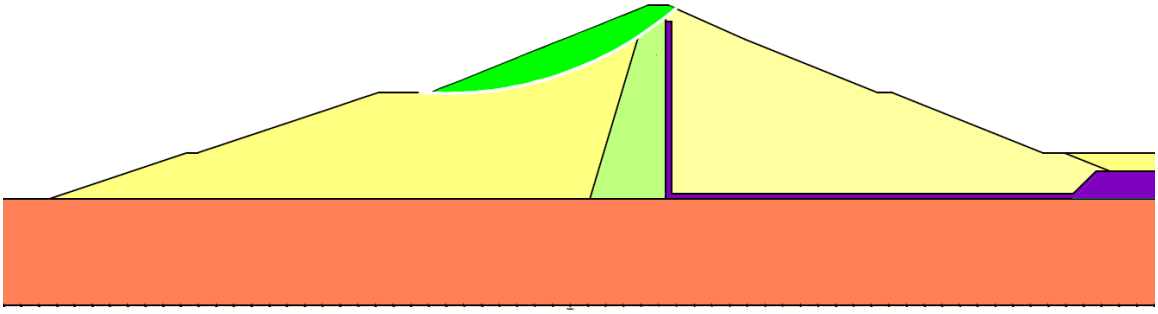

Fig A.4 Slip surface of upstream shallow failure with 0 m. drawdown and k_h = 0.10.

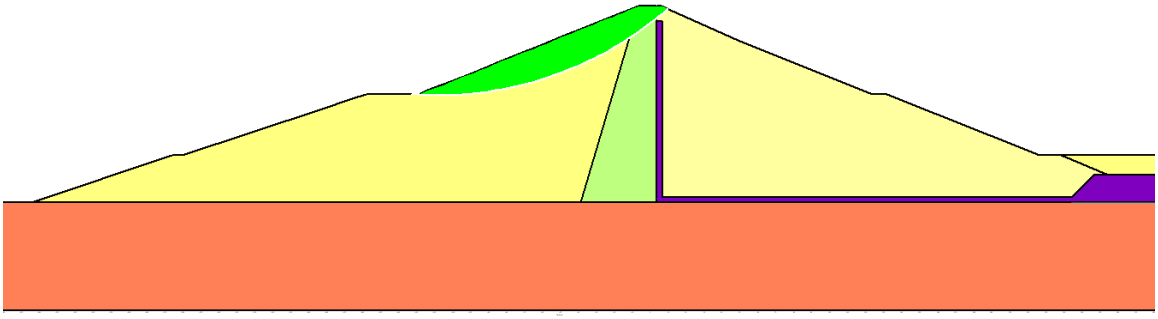

Fig A.5 Slip surface of upstream shallow failure with 5 m. drawdown and k_h = 0.05.

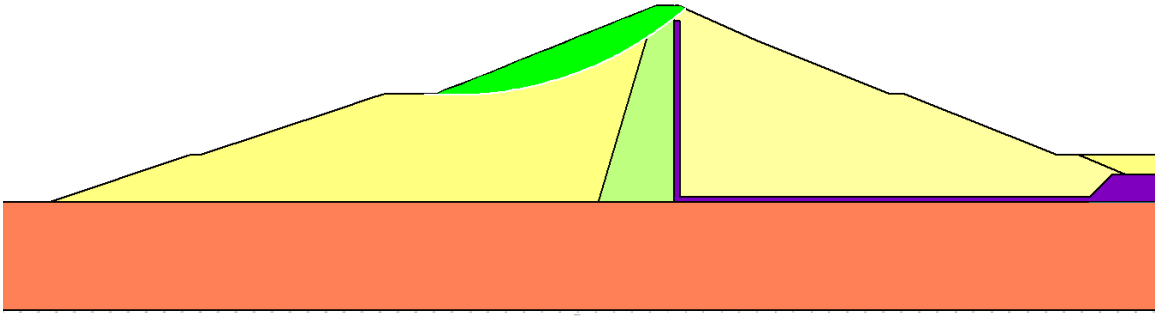

Fig A.6 Slip surface of upstream shallow failure with 5 m. drawdown and k_h = 0.0625.

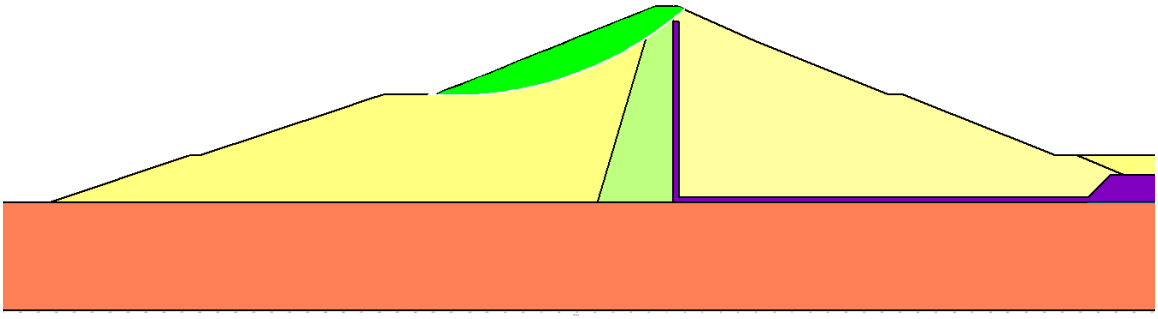

Fig A.7 Slip surface of upstream shallow failure with 5 m. drawdown and k_h = 0.075.

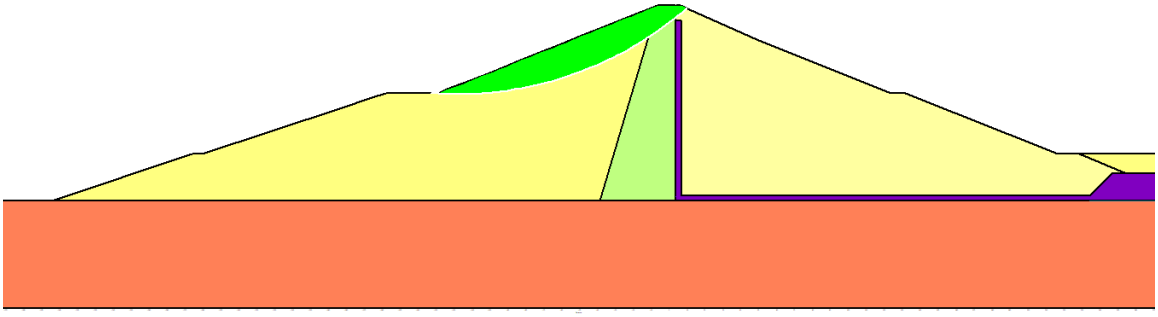

Fig A.8 Slip surface of upstream shallow failure with 5 m. drawdown and k_h = 0.10.

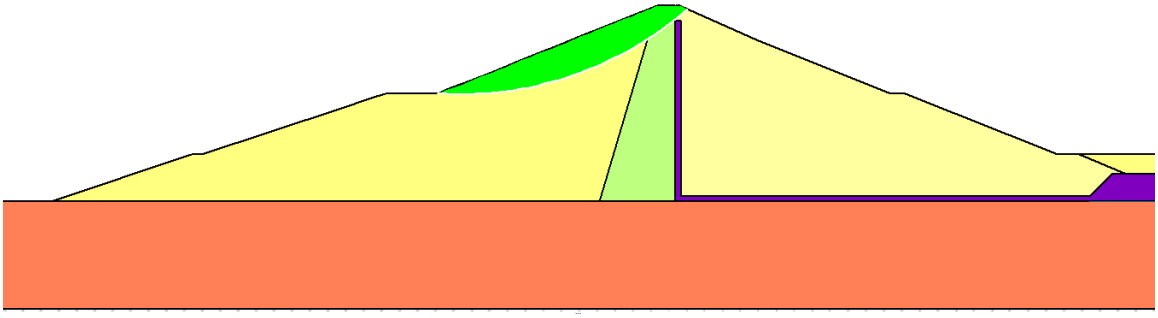

Fig A.9 Slip surface of upstream shallow failure with 10 m. drawdown and k_h = 0.05.

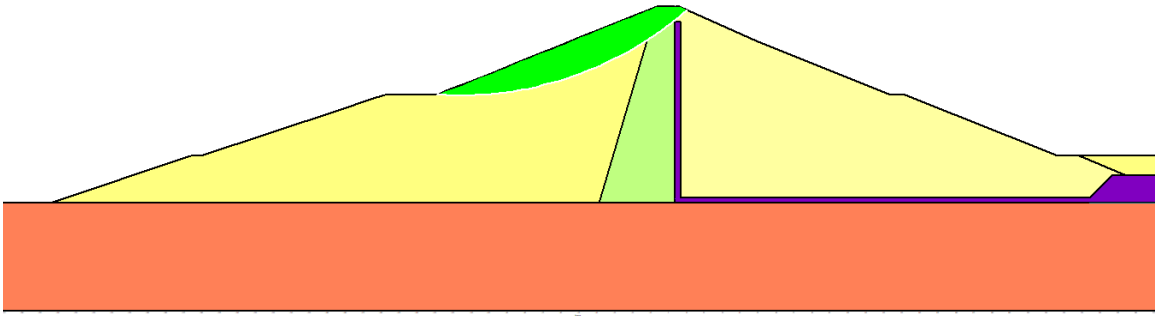

Fig A.10 Slip surface of upstream shallow failure with 10 m. drawdown and kh = 0.0625.

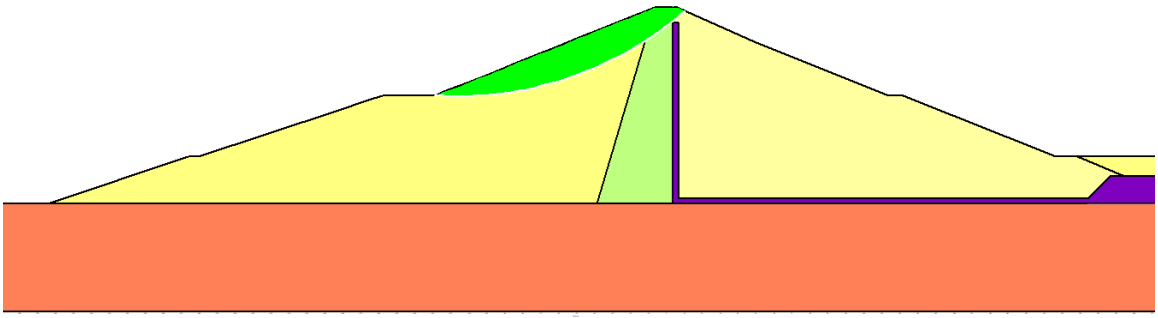

Fig A.11 Slip surface of upstream shallow failure with 10 m. drawdown and k_h = 0.075.

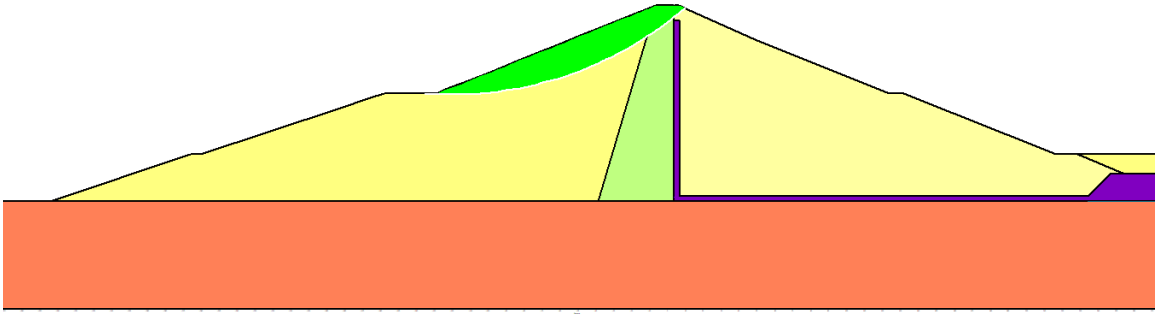

Fig A.12 Slip surface of upstream shallow failure with 10 m. drawdown and k_h = 0.10.

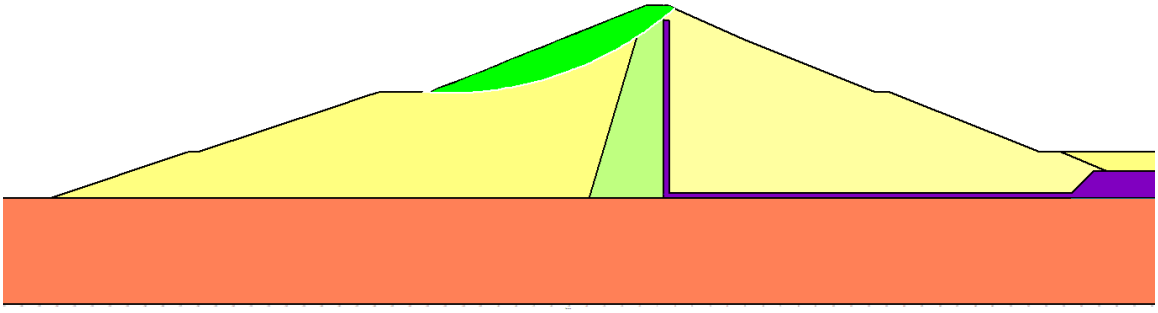

Fig A.13 Slip surface of upstream shallow failure with 15 m. drawdown and k_h = 0.05.

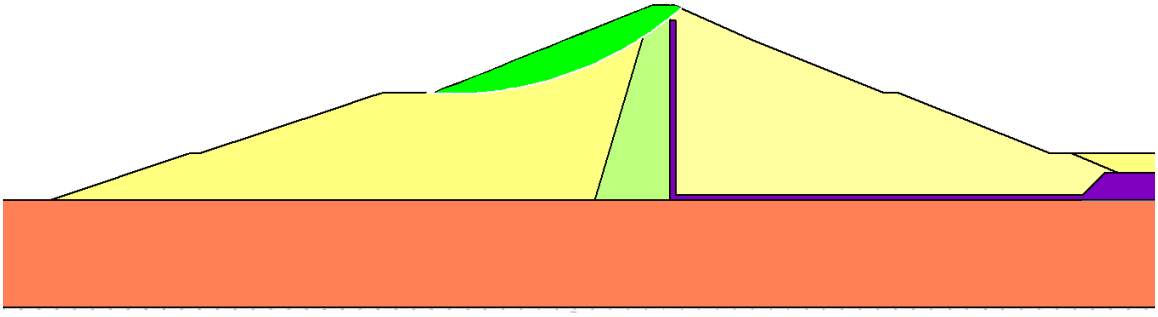

Fig A.14 Slip surface of upstream shallow failure with 15 m. drawdown and k_h = 0.0625.

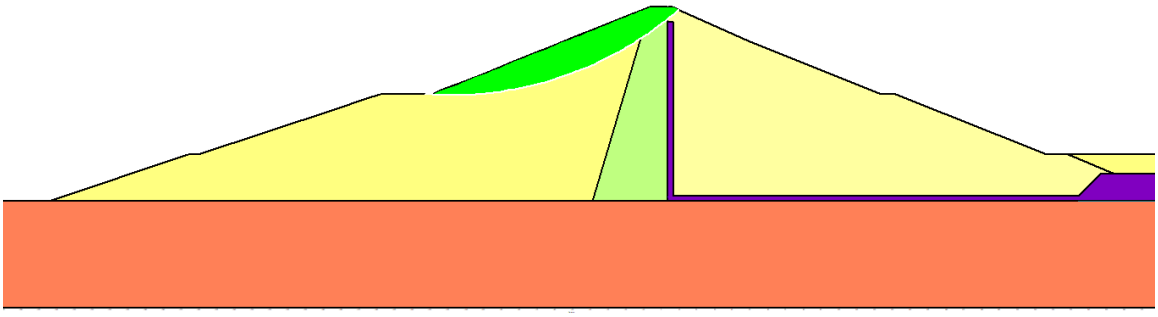

Fig A.15 Slip surface of upstream shallow failure with 15 m. drawdown and k_h = 0.075.

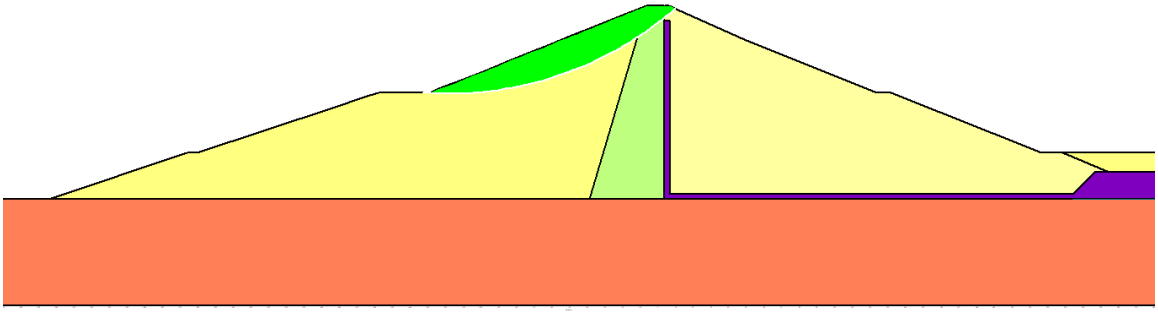

Fig A.16 Slip surface of upstream shallow failure with 15 m. drawdown and k_h = 0.10.

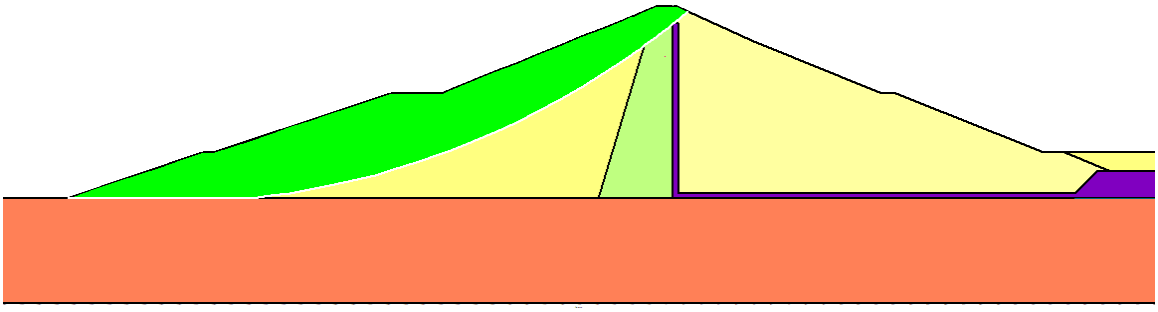

Fig A.17 Slip surface of upstream deep failure with 0 m. drawdown and k_h = 0.05.

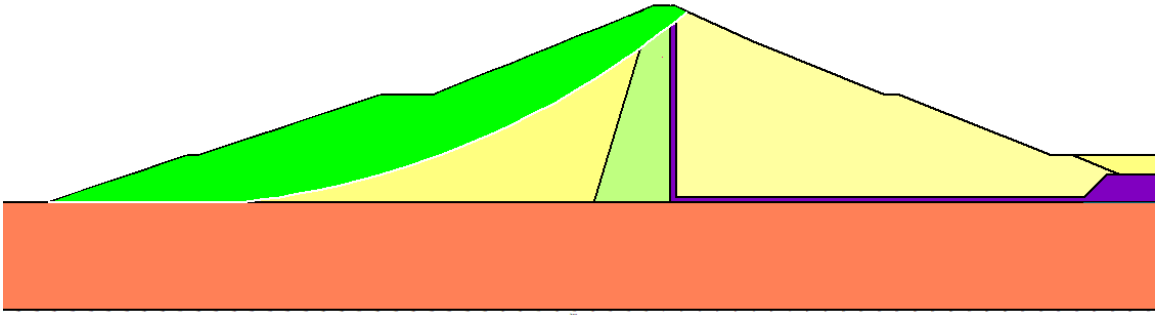

Fig A.18 Slip surface of upstream deep failure with 0 m. drawdown and k_h = 0.0625.

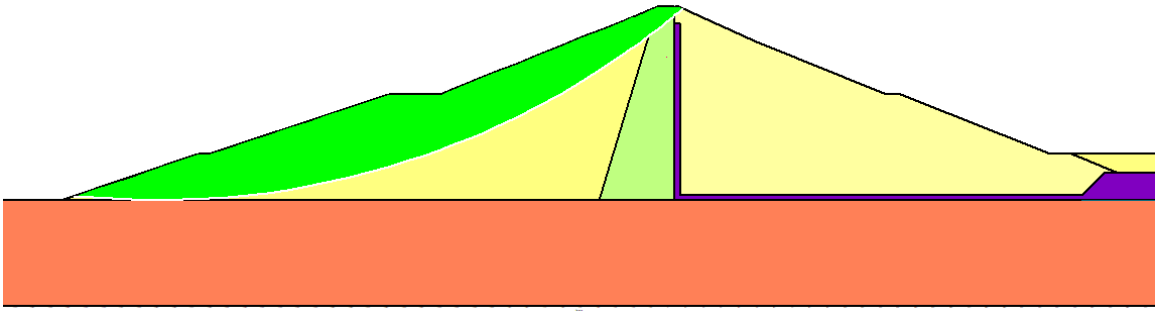

Fig A.19 Slip surface of upstream deep failure with 0 m. drawdown and k_h = 0.075.

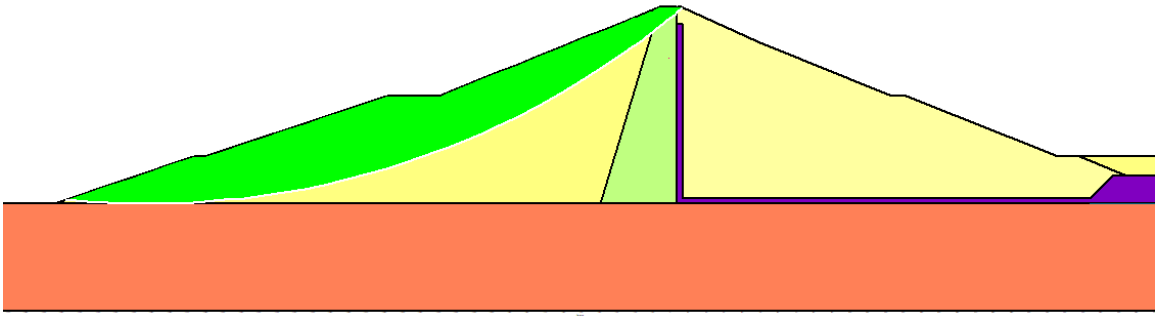

Fig A.20 Slip surface of upstream deep failure with 0 m. drawdown and k_h = 0.10.

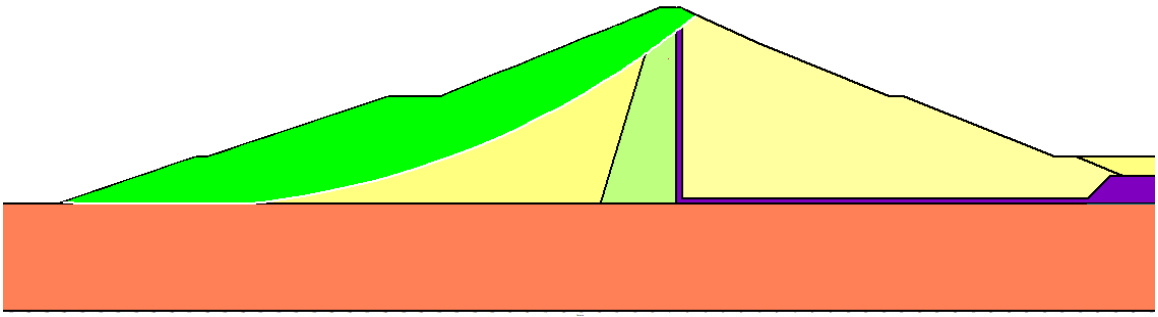

Fig A.21 Slip surface of upstream deep failure with 5 m. drawdown and k_h = 0.05.

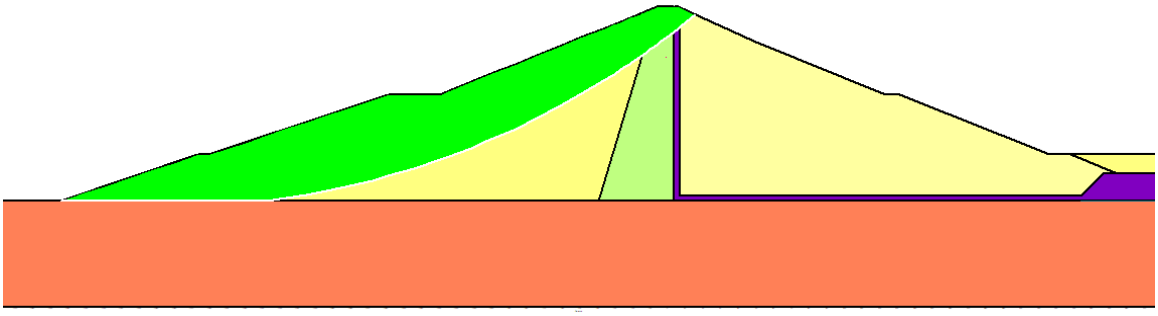

Fig A.22 Slip surface of upstream deep failure with 5 m. drawdown and k_h = 0.0625.

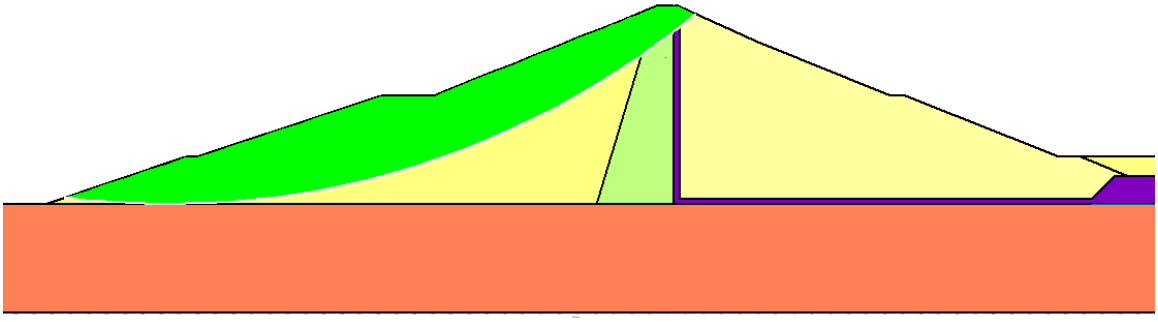

Fig A.23 Slip surface of upstream deep failure with 5 m. drawdown and k_h = 0.075.

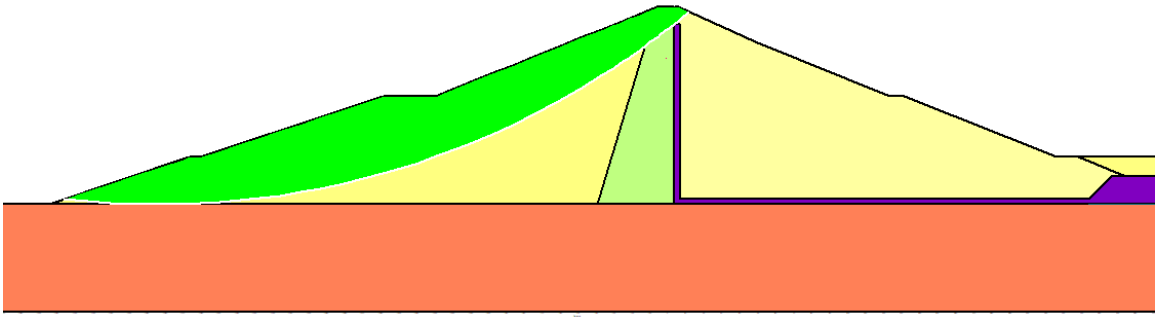

Fig A.24 Slip surface of upstream deep failure with 5 m. drawdown and k_h = 0.10.

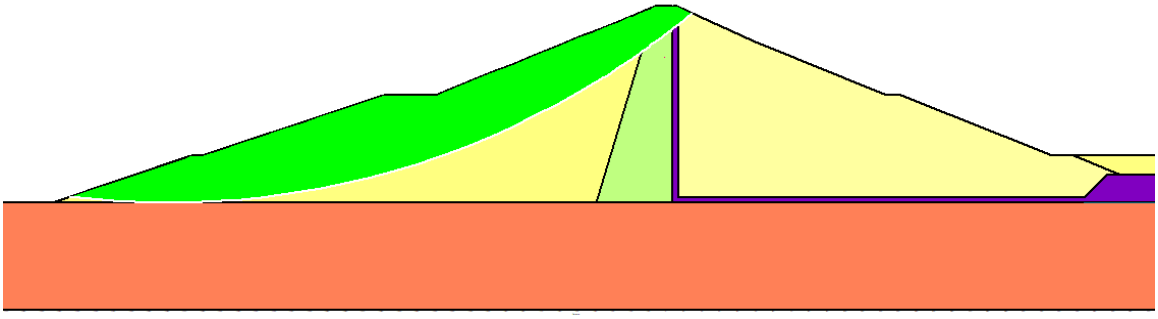

Fig A.25 Slip surface of upstream deep failure with 10 m. drawdown and k_h = 0.05.

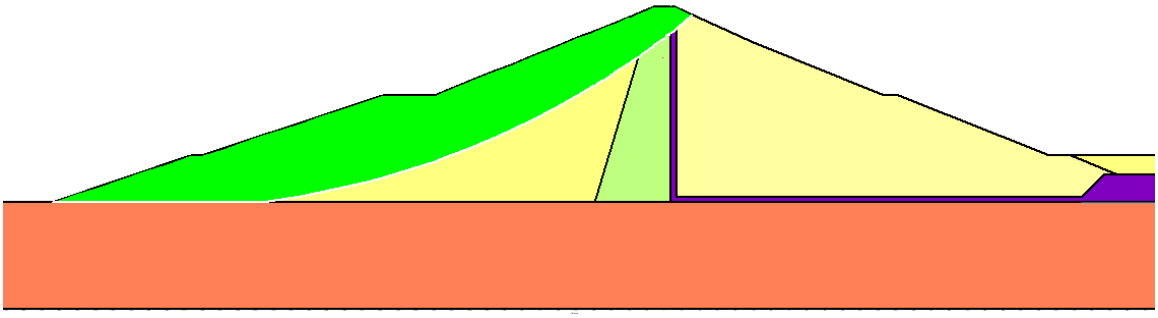

Fig A.26 Slip surface of upstream deep failure with 10 m. drawdown and k_h = 0.0625.

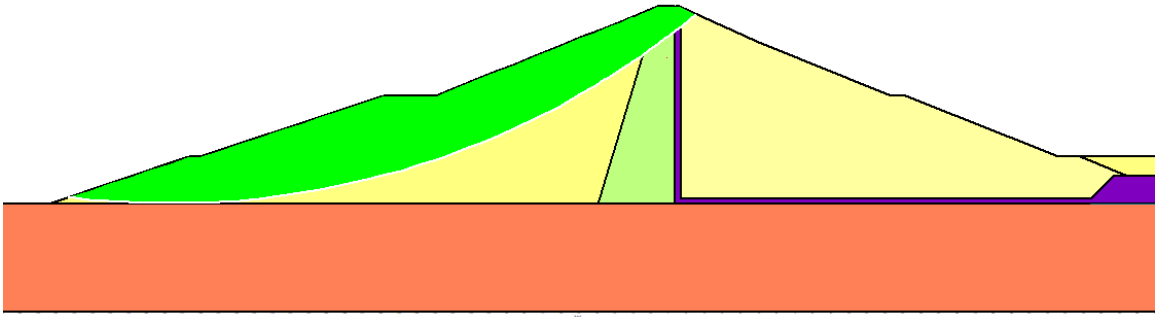

Fig A.27 Slip surface of upstream deep failure with 10 m. drawdown and k_h = 0.075.

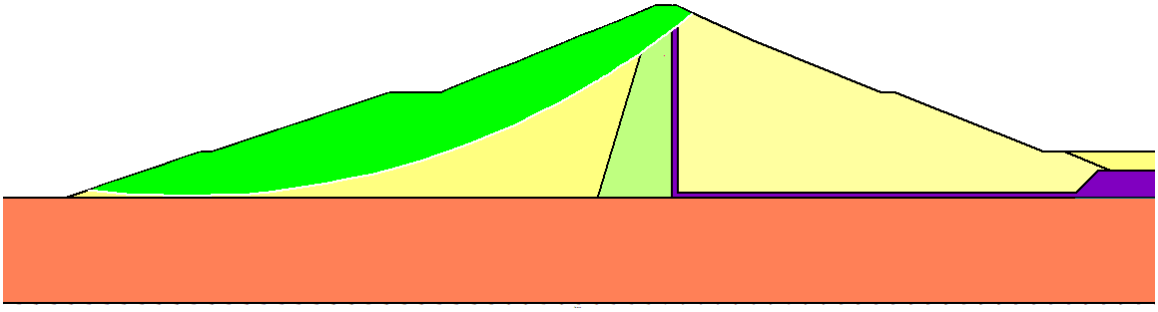

Fig A.28 Slip surface of upstream deep failure with 10 m. drawdown and k_h = 0.10.

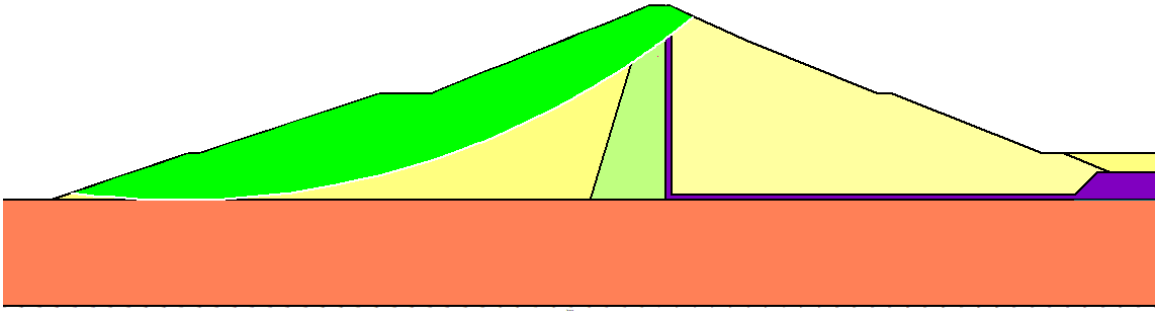

Fig A.29 Slip surface of upstream deep failure with 15 m. drawdown and k_h = 0.05.

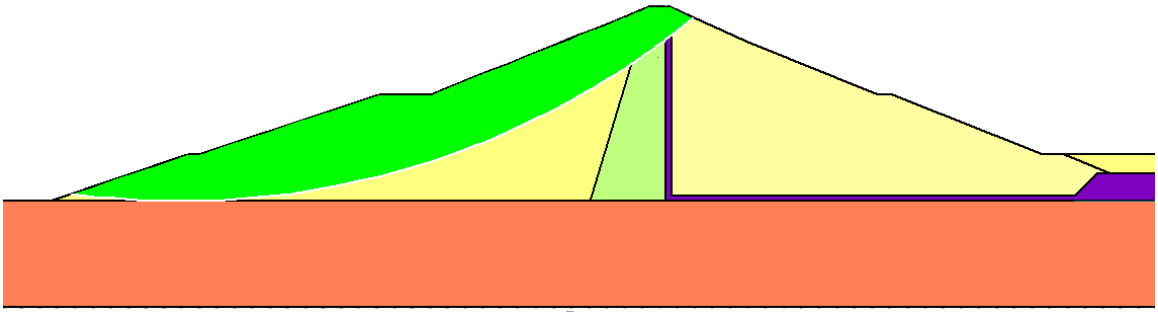

Fig A.30 Slip surface of upstream deep failure with 15 m. drawdown and k_h = 0.0625.

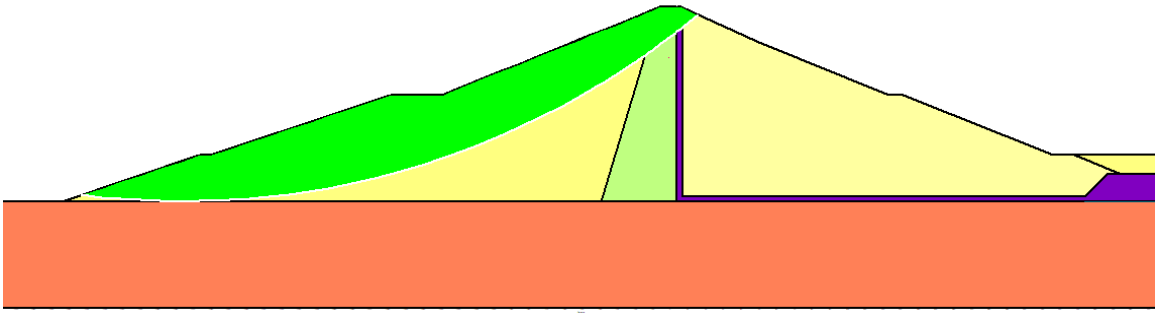

Fig A.31 Slip surface of upstream deep failure with 15 m. drawdown and k_h = 0.075.

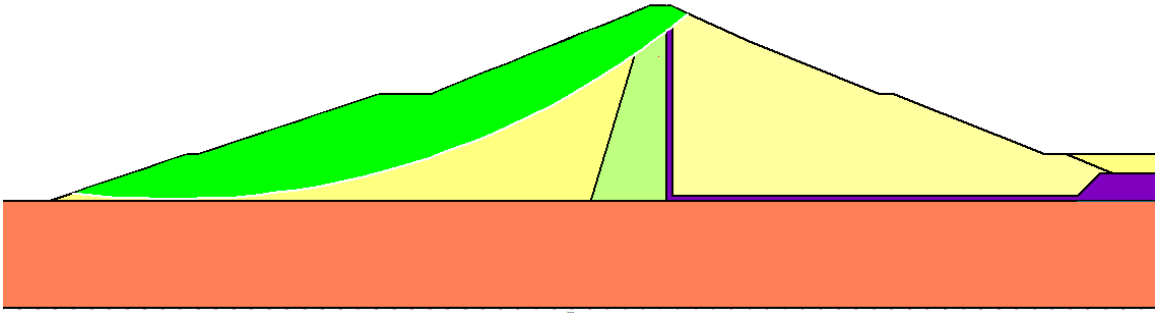

Fig A.32 Slip surface of upstream deep failure with 15 m. drawdown and k_h = 0.10.

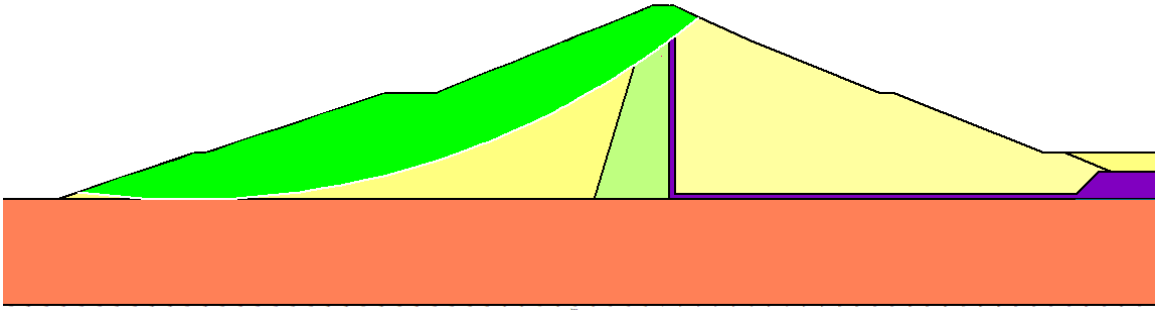

Fig A.33 Slip surface of upstream deep failure with 20 m. drawdown and k_h = 0.05.

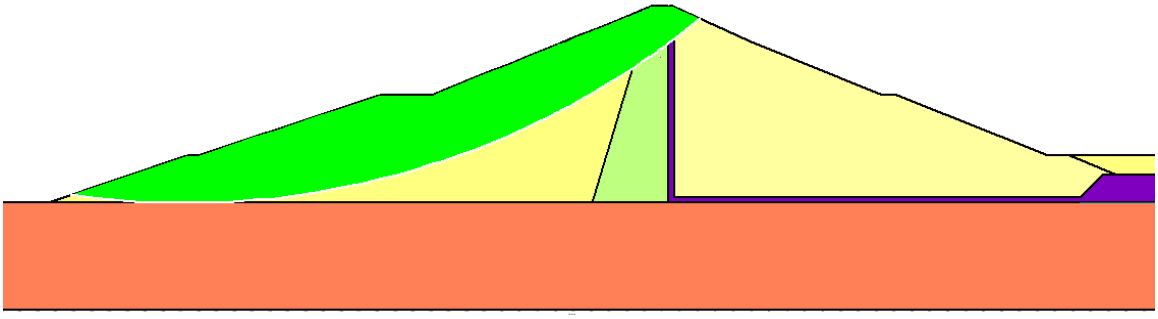

Fig A.34 Slip surface of upstream deep failure with 20 m. drawdown and k_h = 0.0625.

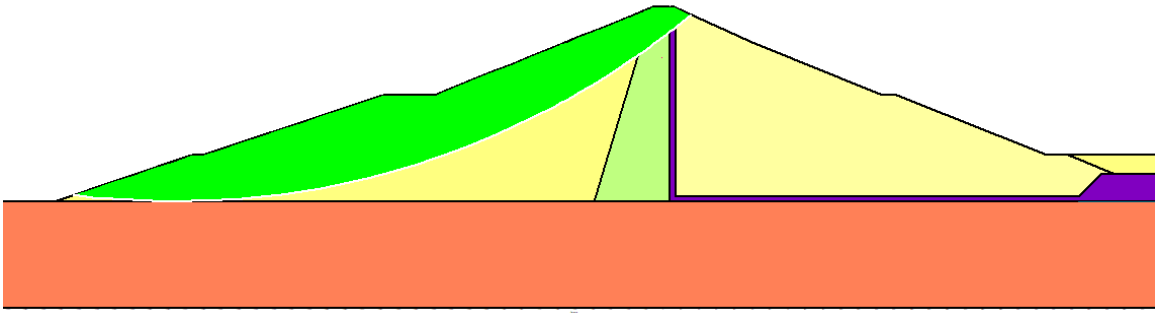

Fig A.35 Slip surface of upstream deep failure with 20 m. drawdown and k_h = 0.075.

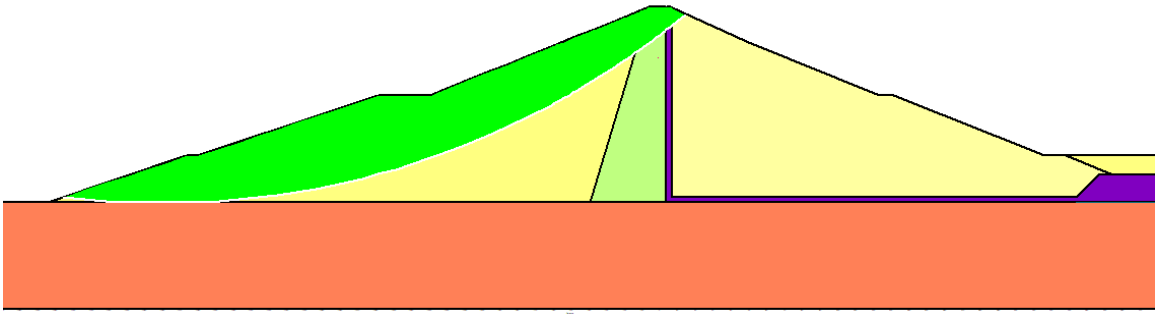

Fig A.36 Slip surface of upstream deep failure with 20 m. drawdown and k_h = 0.10.

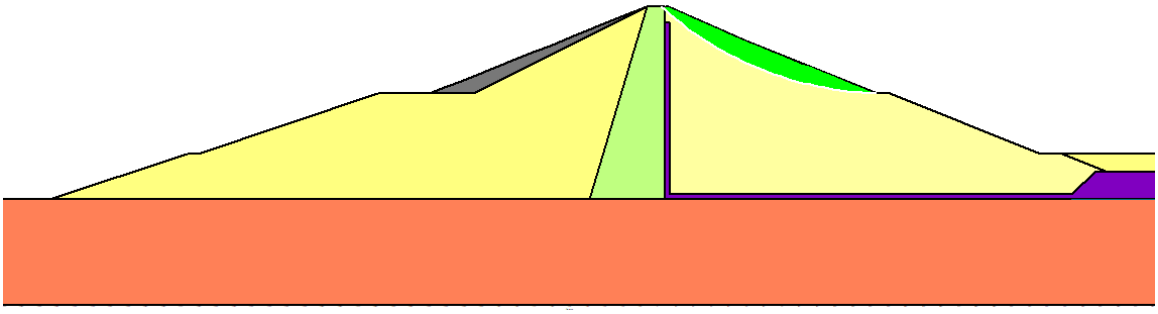

Fig A.37 Slip surface of downstream failure with k_h = 0.05.

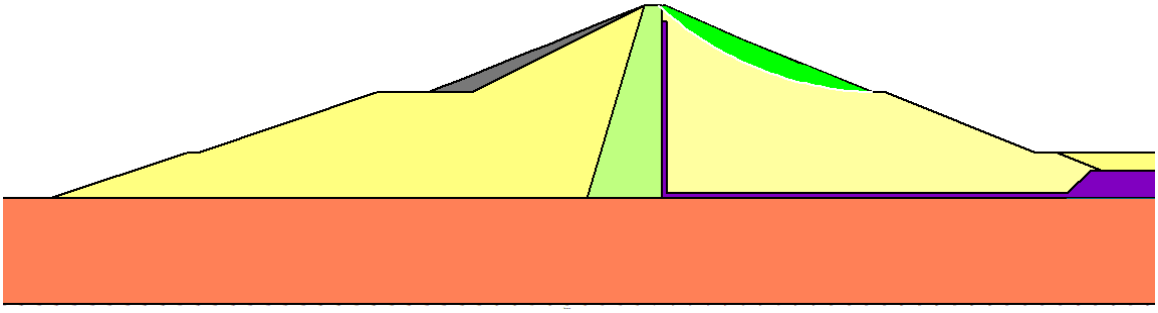

Fig A.38 Slip surface of downstream failure with k_h = 0.0625.

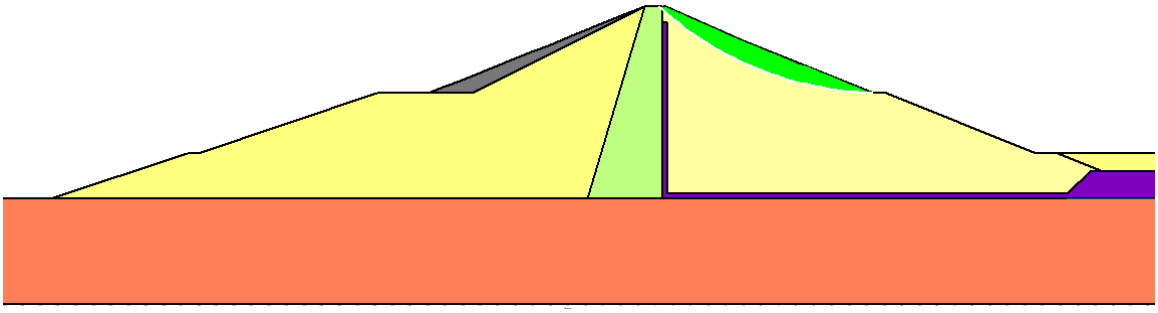

Fig A.39 Slip surface of downstream failure with k_h = 0.075.

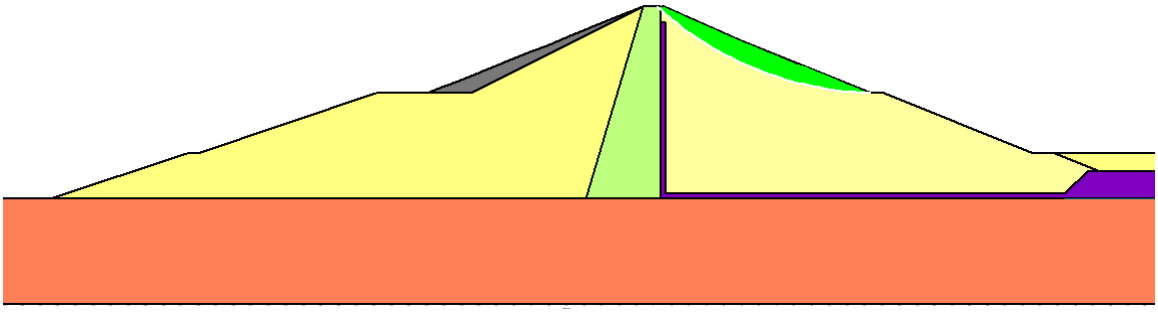

Fig A.40 Slip surface of downstream failure with k_h = 0.10.